Paul

NUREG/CR–5807
KEI No. 1721

Improvements in Motor Operated Gate Valve Design and Prediction Models for Nuclear Power Plant Systems

SBIR Phase I Final Report
September 1990–April 1991

Prepared by
J. K. Wang, M. S. Kalsi

Kalsi Engineering, Inc.

Prepared for
U.S. Nuclear Regulatory Commission

AVAILABILITY NOTICE

Availability of Reference Materials Cited in NRC Publications

Most documents cited in NRC publications will be available from one of the following sources:

1. The NRC Public Document Room, 2120 L Street, NW., Lower Level, Washington, DC 20555
2. The Superintendent of Documents, U.S. Government Printing Office, P.O. Box 37082, Washington, DC 20013-7082
3. The National Technical Information Service, Springfield, VA 22161

Although the listing that follows represents the majority of documents cited in NRC publications, it is not intended to be exhaustive.

Referenced documents available for inspection and copying for a fee from the NRC Public Document Room include NRC correspondence and internal NRC memoranda; NRC bulletins, circulars, information notices, inspection and investigation notices; licensee event reports; vendor reports and correspondence; Commission papers; and applicant and licensee documents and correspondence.

The following documents in the NUREG series are available for purchase from the GPO Sales Program: formal NRC staff and contractor reports, NRC-sponsored conference proceedings, international agreement reports, grant publications, and NRC booklets and brochures. Also available are regulatory guides, NRC regulations in the *Code of Federal Regulations*, and *Nuclear Regulatory Commission Issuances*.

Documents available from the National Technical Information Service include NUREG-series reports and technical reports prepared by other Federal agencies and reports prepared by the Atomic Energy Commission, forerunner agency to the Nuclear Regulatory Commission.

Documents available from public and special technical libraries include all open literature items, such as books, journal articles, and transactions. *Federal Register* notices, Federal and State legislation, and congressional reports can usually be obtained from these libraries.

Documents such as theses, dissertations, foreign reports and translations, and non-NRC conference proceedings are available for purchase from the organization sponsoring the publication cited.

Single copies of NRC draft reports are available free, to the extent of supply, upon written request to the Office of Administration, Distribution and Mail Services Section, U.S. Nuclear Regulatory Commission, Washington, DC 20555.

Copies of industry codes and standards used in a substantive manner in the NRC regulatory process are maintained at the NRC Library, 7920 Norfolk Avenue, Bethesda, Maryland, for use by the public. Codes and standards are usually copyrighted and may be purchased from the originating organization or, if they are American National Standards, from the American National Standards Institute, 1430 Broadway, New York, NY 10018.

NUREG/CR-5807
KEI No. 1721

Improvements in Motor Operated Gate Valve Design and Prediction Models for Nuclear Power Plant Systems

SBIR Phase I Final Report
September 1990–April 1991

Manuscript Completed: July 1991
Date Published: May 1992

Prepared by
J. K. Wang, M. S. Kalsi

W. S. Farmer, NRC Project Manager

Kalsi Engineering, Inc.
745 Park Two Drive
Sugar Land, TX 77478

Prepared for
Division of Engineering
Office of Nuclear Regulatory Research
U.S. Nuclear Regulatory Commission
Washington, DC 20555
NRC FIN L1667

ABSTRACT

This research is aimed at improving the performance of gate valves at nuclear power plants (1) by developing improved predictive models and (2) by identifying design improvements that overcome problems/limitations of the current gate valve designs.

Phase I research is aimed at developing improved operating thrust models for the most common types of gate valves in use at U.S. nuclear power plants. The research completed under Phase I addresses shortcomings in the current motor operated gate valve performance models by investigating localized contact stresses under disc tilting caused by fluid flow, by predicting inertial thrust overshoot, and by providing a comprehensive review of friction/galling data for gate valves. Instrumented valve test data provided by Duke Power Company were used to make limited comparisons with the analytical predictions. The areas that require systematic testing to further refine the predictive models are identified.

TABLE OF CONTENTS

LIST OF FIGURES

ACKNOWLEDGEMENTS

We are grateful to the United States government for the $50,000 funding provided under the Small Business Innovation Research (SBIR) Program which made this research possible. Special thanks are due to William S. Farmer of the NRC for his guidance and encouragement throughout the project.

Duke Power Company and Neal Estep of Duke Power deserve special recognition for giving permission to use their flow loop test data and the results of analyses performed for them.

The authors would like to thank Bobbie Lambert for patiently working through many revisions and for her painstaking attention to detail in preparing this manuscript.

EXECUTIVE SUMMARY

This report documents the results of Phase I research proposed and conducted by Kalsi Engineering, Inc. to improve the operability of motor-operated gate valves in nuclear power plants. Phase I research, funded by the Small Business Innovation Research (SBIR) program, resulted in the following major accomplishments:

- Opening and closing thrust equations for the common types of gate valves used in U.S. nuclear power plants have been developed and documented.

- An analytical methodology to predict inertial thrust overshoot in an MOV gate valve has been developed from first principles. Comparisons against data supplied by Duke Power Company have confirmed that the methodology is sound, and there is good quantitative agreement between analytical predictions and actual test results.

- The results of a comprehensive review of friction and galling data are documented in this report to provide a rational basis for selecting an appropriate coefficient of friction for a given application.

- The concept of *index of contact stress severity* has been introduced to determine whether or not a gate valve will behave predictably under fluid flow forces. Preliminary analysis approaches to calculate localized contact stresses at the disc-to-guide contact and at the disc-to-downstream seat contact under disc tilting conditions have been developed.

- Significant factors that affect the *opening* thrust requirements of a gate valve have been identified, and quantitative methods that can be used to diagnose valve opening problems have been documented.

- Improvements in gate valve designs to make them less sensitive to pressure/thermal transients and external pipe loads have been identified, and some quantitative examples are included to show the degree of improvement achievable.

In summary, the Phase I research has been successful in completing the *preliminary* development of improved gate valve operability models. This can serve as an excellent foundation to continue further analytical and experimental development that is necessary to provide reliable and proven gate valve operability models to the nuclear power industry.

1. INTRODUCTION

1.1. Background

Operability problems with motor operated valves (MOVs) in the U.S. nuclear power plants have been extensively documented in references [1]* through [12]. The Nuclear Regulatory Commission's (NRC) safety concerns regarding the operability of the MOVs were further reinforced by the failure of several gate valves to close within the manufacturer specified thrust requirements under simulated high energy pipe break conditions in the recently conducted NRC tests [4,23]. Even though several of the earlier reports and surveys have described the operability problems in detail [7,8,9], it was the issuance of NRC IE Bulletin 85-03 [1], Generic Letter 89-10 [2], and the recent gate valve tests [4,23] that finally resulted in the industry-wide recognition of the significance of the MOV problems.

Kalsi Engineering, Inc., having been intimately involved in solving valve problems for the utilities for over 13 years, submitted a proposal under the Small Business Innovation Research (SBIR) Program to initiate a systematic research directed at improving the motor operated gate valve designs and operability prediction models. This proposal was selected, thus giving the principal investigators an opportunity to document the key technical approaches that have been developed by Kalsi Engineering, Inc in solving problems and making improvements in the design and performance of MOVs.

1.2. Objectives

The *overall* objectives of Phases I and II of this SBIR project defined by the principal investigators are to improve the operability of the motor operated gate valves in the nuclear power plant safety system by: (1) developing more comprehensive and reliable models for predicting operability; (2) identifying improvements that can overcome the deficiencies observed in the current gate valve designs.

The overall objectives stated above are quite broad and would require extensive analytical research as well as testing to fully accomplish these goals. The more specific objectives under SBIR Phase I funding constraints were limited to: (1) providing closing and opening thrust equations (based on ideal free-body diagrams) for the types of gate valve designs which are in common use in the U.S. nuclear power plants; (2) developing a preliminary analytical methodology to quantitatively assess the effect of fluid flow forces imposed on the disc on the valve performance; (3) developing an analytical model to predict thrust overshoot due to inertia; (4) documenting friction and galling data, including principal investigators' experience, relevant to gate valve operability; (5) documenting factors that affect the gate valve opening thrust requirements; and (6) identifying possible improvements in the gate valve design.

---

* Numbers in brackets denote References listed in Section 7.

1.3. Technical Approach and Summary

The objectives of Phase I research were accomplished by first developing stem thrust requirements for closing and opening the gate valves of several different designs that are in use in the U.S. nuclear power plants: (1) conventional gate using solid, flexible and split wedge designs, (2) parallel (expanding) wedge gates of through-conduit and double-disc design, and (3) parallel slide gate. These results are summarized in Section 2 with detailed derivations included in Appendix A.

An important factor that has not been adequately considered in the gate valve designs by many manufacturers is the effect of fluid flow forces on the disc along the flow direction. In some valve designs, the fluid forces can cause titling of the disc in mid-travel position resulting in localized loading at the edges of the disc guides or between the disc and the downstream seat. As evidenced in the NRC sponsored and other tests [4,21,23], severe damage can occur to the internals of such valve designs by the high fluid flow forces under blowdown conditions. Even though the potential for damage is expected to be considerably lower when these valves are operated under less severe, pumped flow conditions, *quantitative* approaches to predict their performance have not been available.

Section 2 of this report summarizes a preliminary analytical approach that has been developed to estimate the mid-travel disc loads and local contact stresses due to fluid forces at the potential areas of contact. These preliminary local contact stress calculations are based on simplifying assumptions of linear, small displacement elasticity equations. The limitations of this approach and further refinements that are needed in this area are identified. The concept of using these results as an *index of contact stress severity* is introduced, which can be used as a design guide in making comparisons between different valve geometries and loading conditions. To accurately account for non-linear behavior at the contact due to localized yielding and wear, further refinements using large displacement elastic/plastic finite element analysis, as well as systematic testing to obtain empirical correlations over a wide range of parametric conditions are needed.

Another deficiency in predicting the operability of the MOVs has been the lack of analytical techniques to quantify the effect of inertia on the thrust overshoot. Currently, inertial overshoot problems are detected only by MOV testing. The Phase I research overcomes this deficiency by documenting an analytical approach, based on first principles, that has been developed to *quantitatively* predict the inertial overshoot. Results show good comparisons against actual test data provided by Duke Power Company from their flow loop testing [15]. Section 4 and Appendix D present these results.

Coefficient of friction between the disc and seats is one of the dominant factors that determines the overall thrust requirements for gate valves. Even though Stellite hardfacing

has been used for years as a standard overlay material at the seating faces by most valve manufacturers, test data for its coefficient of friction performance span an extremely wide range. This is largely due to the fact that tribological behavior at the sliding contacts in the gate valve is affected by several factors that are not explicitly understood and controlled during valve tests. Section 3 of this report presents a summary of the coefficient of friction and galling data based on the principal investigators' laboratory testing and field experience, with a focus on those factors that have the most impact on the performance of gate valves. Condition of the contact surfaces, e.g. the undetected presence or absence of galling or absorbed contaminant layer of lubricants (even of molecular scale) can account for very large differences in the "apparent" coefficient of friction. Systematic testing using real gate valve internals is needed to determine the onset of galling in local areas of contact, and to determine conditions under which continued cycling results in increases in apparent friction and seizure or stable frictional behavior after local wear.

Lastly, the *opening* thrust requirements for wedge gate valves are influenced by several factors that are not easily quantifiable in actual MOV applications. The unwedging thrust during opening is influenced by the wedging force from the previous closing cycle, external pipe load causing disc pinching, effect of higher pressure trapped in the body cavity resulting in energization of both upstream and downstream discs in some of the gate valve designs, and thermal binding caused by temperature transients. The practical approach to *minimize* the effect of these variables on operability performance has been to bypass the torque switch during the initial portion of the opening stroke, thus making maximum actuator output available. The problems are detected only when the magnitude of these effects exceeds the actuator output. Section 5 and Appendices E and F discuss these factors and present analytical methods that can be employed by the utility engineers and valve manufacturers to detect and eliminate such problems.

In summary, Phase I research has shown that the operability predictions of MOV gate valves can be significantly improved by properly taking into account a number of factors that have been largely ignored in the past. Further analytical refinements and extensive testing are needed to systematically address the areas identified in this report to develop reliable operability prediction models that cover the wide range of variations in the valve designs present at the nuclear power plants.

2. GATE VALVE TYPE, GEOMETRY, AND ITS EFFECT ON OPENING AND CLOSING THRUSTS

There are five different types of gate valves that cover most of the applications in nuclear power plants in the United States. The key features of these designs are shown in Figure 2.1. Variations in the most commonly used gate valves include solid, flexible, and split gates (Figure 2.1a). The two types of parallel expanding wedge gates shown in Figure 2.1b are also used, but their population is smaller. Parallel sliding gate valves shown in Figure 2.1c are relatively uncommon in the United States, but are widely used in European nuclear power plants. The advantages and disadvantages of various design features for these valves are discussed in detail in Reference [13]

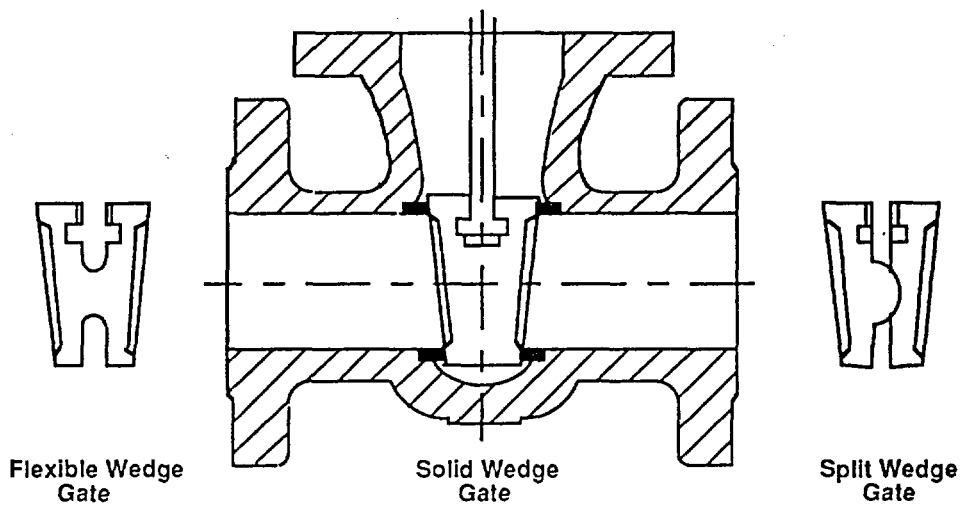

Figure 2.1a
Conventional Solid Wedge, Flexible Wedge, and Split Wedge Gate Valves

As shown in these figures, the designs vary significantly in gate geometries. Other important variations that affect performance are related to gate guide arrangements and their dimensions; clearances at critical locations between gate, guides, and seats; seat contact widths; and materials and surface finish in the disc guide sliding interfaces.

Section 2 presents the gate thrust requirements for the above-described variations in gate geometries. This section also addresses the potential for disc tilting during mid-travel due to fluid forces across the disc. Disc tilting causes localized loading between the disc and the downstream seat, or between the disc and the guides. A preliminary analysis approach to determine the localized contact stresses is presented in this section to determine the loading severity based upon valve design and operating conditions.

Preliminary analyses of localized contact stresses between disc and seats as well as disc and guides used in typical wedge gate valve designs are presented in this section. The preliminary approach presented here needs further analytical refinement and empirical correlations to develop improved predictive models. Detailed derivations of the equations summarized in this section are included in Appendices A, B, and C.

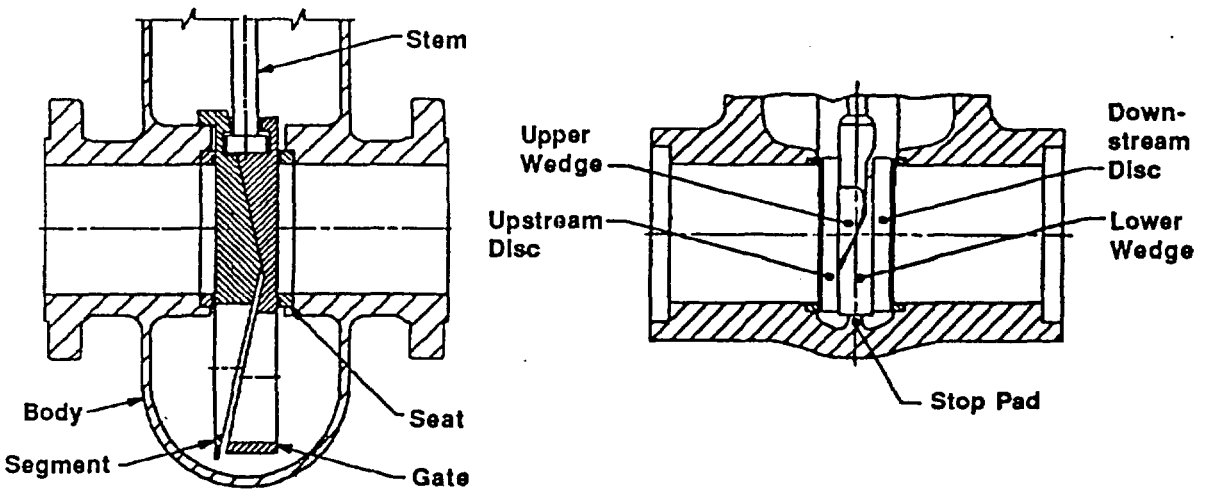

Figure 2.1b
Parallel Expanding Gate Valves

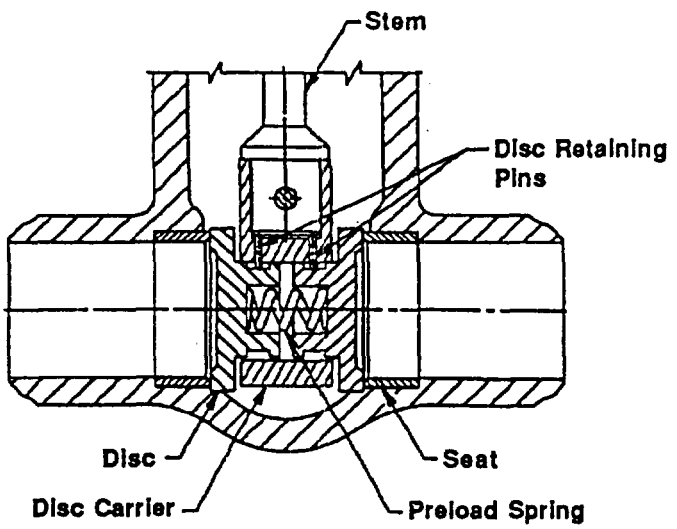

Figure 2.1c
Parallel Sliding Gate Valve

2.1. Stem Thrust for Solid, Flexible, and Split Wedge Gate Valves

Even though there are differences in the performance of solid, flexible, and split wedge gate valves as related to their sensitivity to external piping loads and thermal binding [13], the equations for their stem thrust requirements based upon free body considerations are the same. Subsections 2.1.1 through 2.1.2 summarize the stem thrust requirements to overcome only the differential pressure load across the disc. Subsections 2.1.3 and 2.1.4 give the stem wedging and unwedging thrust requirements to close and open the gate, respectively. The total stem thrust requirements to close and open the gate are provided in Section 2.4, which include other components such as stem packing load, stem rejection force (also referred to as blowout force or piston effect force), and stem and gate weight.

2.1.1. *Closing Stem Thrust to Overcome Gate Differential Pressure*

As shown in Section A.1.1 of Appendix A, the stem thrust at the gate to overcome the differential pressure during closing can be expressed as:

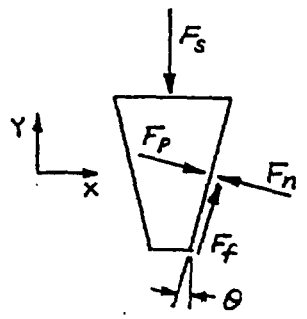

Figure 2.2
Gate Equilibrium Under ΔP Load During Closing

$$F_s = \left(\frac{\mu}{\cos\theta - \mu \sin\theta}\right) F_p \qquad \text{(Eq. 2.1)}$$

where

F_s = stem load at gate, lb

F_p = disc pressure load due to upstream/downstream differential pressure, lb

= ΔP x (effective seat area)

μ = coefficient of friction between gate and seat

θ = 1/2 of gate wedge angle, deg

The disc pressure load, F_p, is the product of ΔP and seat area based on effective disc sealing diameter as discussed further in Section 2.5.

From Equation 2.1 the relationship between the commonly-used term *disc factor* (sometimes called *valve factor*) and coefficient of friction, μ, can be derived:

$$\text{Disc Factor} = \frac{\mu}{\cos\theta - \mu \sin\theta} \qquad \text{(Eq. 2.1a)}$$

For typical wedge gate valves that use a total wedge angle of around 10 degrees (or $\theta = 5°$) and a normal range of coefficients of friction, the difference between the disc factor and the coefficient of friction is practically negligible, as discussed in Section 3.1. The disc factor calculated in the closing direction can be as much as 5 percent higher than the coefficient of friction for typical values of θ and μ that are encountered in practice.

2.1.2. *Opening Stem Thrust to Overcome Disc Differential Pressure*

As derived in Section A.1.2 of Appendix A, stem thrust during opening of a wedge disc against a differential pressure is given by:

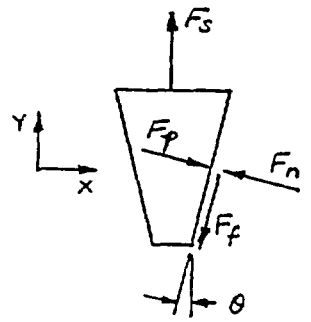

Figure 2.3
Gate Equilibrium Under
ΔP Load During Opening

$$F_s = \left(\frac{\mu}{\cos\theta + \mu \sin\theta} \right) F_p \qquad \text{(Eq. 2.2)}$$

From this one can derive the equivalence between the disc factor in the opening direction and the coefficient of friction:

$$\text{Disc Factor} = \frac{\mu}{\cos\theta + \mu \sin\theta} \qquad \text{(Eq. 2.2a)}$$

The disc factor in the *opening* direction is slightly less than the coefficient of friction for typical ranges of wedge angles and coefficients of friction (within 5 percent of the coefficient of friction), as discussed in Section 3.1.

As stated earlier, the stem force calculated in Equation 2.1 or 2.2 is the force required to overcome the differential pressure resistance only.

2.1.3. *Stem Wedging Load - Closing*

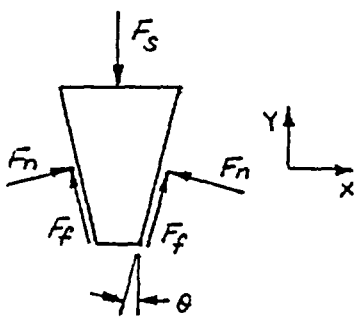

Figure 2.4
Gate Equilibrium under
Wedging Load During Closing

The stem wedging load is related to the normal seat contact force, F_n, as shown in Section A.1.3 of Appendix A:

$$F_s = 2(\sin\theta + \mu \cos\theta) F_n \qquad \text{(Eq. 2.3)}$$

It should be noted that this equation applies to the case when there is no differential pressure across the gate. When differential pressure is present, the stem force F_S in this equation is the net stem force after subtracting the differential pressure load.

In some cases, the limit switch instead of the torque switch is used to stop the disc travel in the closing direction. Where acceptable from the shut-off standpoint, this approach can be used to reduce, and in some cases eliminate, the wedging load, F_n.

2.1.4. *Stem Unwedging Load - Opening*

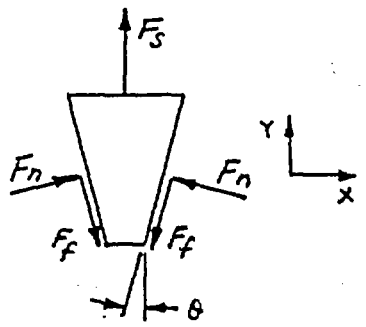

Figure 2.5
Gate Equilibrium under
Unwedging Load During Opening

Section A.1.4 of Appendix A shows that the unwedging load to overcome the seat contact force, F_n, is given by:

$$F_s = 2(\mu \cos\theta - \sin\theta) F_n \qquad \text{(Eq. 2.4)}$$

The seat contact force, F_n, that is to be overcome during the opening cycle is developed by (1) wedging load from the previous closing cycle, including inertia overshoot, (2) external piping loads, or (3) differential thermal effects between the valve body and disc. Section 4 provides an analytical methodology to predict stem thrust due to inertia overshoot, and Section 5 discusses external pipe load and thermal effects that may influence the normal load, F_n.

2.2. Stem Thrust for Parallel Expanding Gate Valves

This Subsection 2.2 summarizes the stem thrust requirements for closing and opening directions for the two types of parallel expanding gate valves shown in Figure 2.1b. The same stem thrust equations apply to both types of parallel expanding gate valves shown in this figure. The typical wedge angle used in the through-conduit type is 15 degrees, and for the double-disc type is 25 degrees. It should be noted that for coefficient of friction of 0.47 (= tan 25°) or less, the 25-degree angle between the wedge surfaces (also referred to as *back angles*) provides a non-locking condition between the wedges.

2.2.1. *Stem Thrust to Overcome Gate Differential Pressure - Closing and Opening*

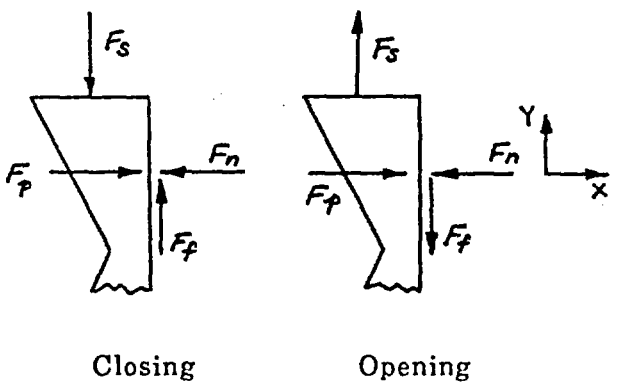

Closing Opening

Figure 2.6
Gate Equilibrium Under ΔP Load During
Closing/Opening

As shown in Section A.2.1 of Appendix A, the following equation applies to both closing and opening stem thrusts to overcome gate frictional force due to ΔP load:

$$F_s = \mu F_p \qquad \text{(Eq. 2.5)}$$

where

μ = coefficient of friction between seat and disc

F_p = disc pressure load due to upstream/downstream differential pressure, lb

= ΔP x (effective seat area)

2.2.2. *Stem Wedging Load - Closing*

The stem wedging load for a parallel expanding gate valve is shown in Section A.2.2 of Appendix A to be given by:

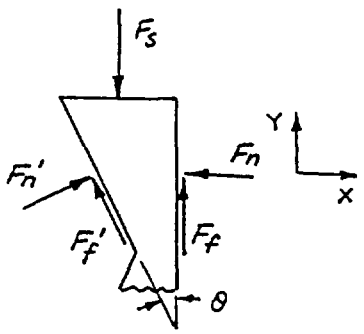

Figure 2.7
Gate Equilibrium Under
Wedging Load During Closing

$$F_s = \left(\mu + \frac{\sin\theta + \mu' \cos\theta}{\cos\theta - \mu' \sin\theta} \right) F_n \qquad \text{(Eq. 2.6)}$$

where

μ = coefficient of friction between seat and disc

μ' = coefficient of friction between wedge faces

θ = parallel gate total wedge angle, deg

F_n = normal force between gate and seat due to wedging, lbs

This equation makes allowance for the fact that the coefficients of friction at the seat-to-disc interface may be different than that at the wedge interface. Typically the seat faces have a finer surface finish and are overlaid with Stellite hard-facing, whereas the wedge faces have a rougher surface finish and are not hard-faced.

If the coefficient of friction at the seat faces and the wedge faces is assumed to be the same, $\mu' = \mu$, and this equation reduces to

$$F_s = \left(\frac{\sin\theta\left(1-\mu^2\right) + 2\mu\cos\theta}{\cos\theta - \mu\sin\theta} \right) F_n \qquad \text{(Eq. 2.6a)}$$

Equation 2.6a shows that the stem load is proportional to the seat contact force, F_n.

2.2.3. *Stem Unwedging Load - Opening*

The stem unwedging load to overcome the seat contact force, F_n, for a parallel expanding gate valve is given by (reference Section A.2.3, Appendix A):

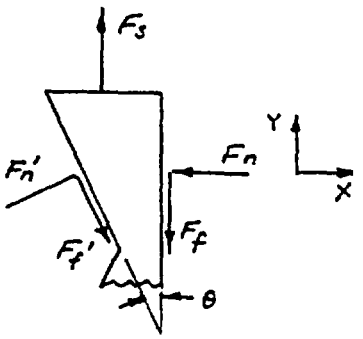

$$F_s = \left(\frac{(\mu\mu' - 1)\sin\theta + (\mu + \mu')\cos\theta}{\cos\theta + \mu'\sin\theta} \right) F_n \qquad \text{(Eq. 2.7)}$$

For $\mu = \mu'$, this equation reduces to:

$$F_s = \left(\frac{\sin\theta\left(\mu^2 - 1\right) + 2\mu\cos\theta}{\cos\theta + \mu\sin\theta} \right) F_n \qquad \text{(Eq. 2.7a)}$$

Figure 2.8
Gate Equilibrium Under Unwedging Load During Opening

As discussed in Section 2.1.4, the seat contact force F_n to be overcome is determined by adding the wedging force from the previous closing cycle to the resultant force from external piping loads and differential thermal expansion loads between the body and disc.

2.3. Stem Loads for Parallel Sliding Gate Valves - Closing and Opening

Most parallel sliding gate valves are equipped with a preloading spring to maintain proper contact and provide a low pressure seal between the disc and seats. As shown in Appendix A, Section A.3.1, the required stem thrust to overcome ΔP and spring load friction can be expressed as:

$$F_s = 2\mu F_{sp} + \mu F_p \qquad \text{(Eq. 2.8)}$$

where F_{sp} = disc spring load, lb

$F_p = \Delta P \times$ (effective seat area), lbs

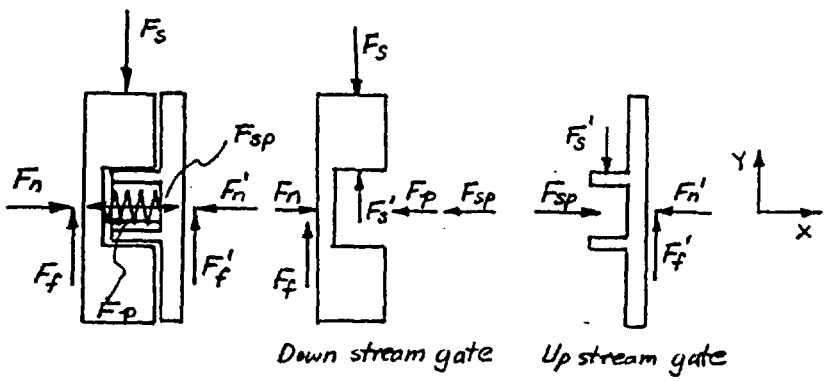

Figure 2.9
Gate Equilibrium Under ΔP Load During Closing

The above equation applies to both closing and opening directions, and the pressure load is applied to the downstream disc only. It should also be noted that, since the seat faces and the disc faces are parallel, there is no wedging or unwedging load associated with this type of design.

2.4. Total Stem Thrust Requirements

The total stem thrust requirements for a gate valve stem can be determined by a summation of all the loads applied to the stem. For stem thrust requirements in the *closing* direction, a summation of the forces yields:

$$\Sigma F = 0$$

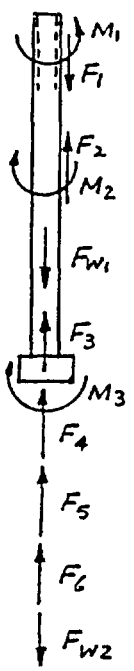

Figure 2.10 Overall Stem Load Equilibrium

$$F_1 = F_2 + F_3 + F_4 + F_5 + F_6 - F_{w1} - F_{w2} \qquad \text{(Eq. 2.9)}$$

where F_1 = required stem thrust for closing, lbs

F_2 = stem packing load, lbs (see Section 8)

F_3 = stem piston load, lbs

$= \pi/4\ d_s^2 \times \Delta P$, where d_s is the stem diameter

F_4 = stem load to overcome gate ΔP as summarized in Sections 2.1 through 2.3 for different types of gate valves, lbs

F_5 = stem wedging load as summarized in Section 2.1 and 2.2, lbs

F_6 = stem torque reaction load, lbs

$$= \frac{M_3}{d}\mu''$$

where $M_3 = M_1 - M_2$ = stem torque from actuator - stem packing torque, in-lbs

μ'' = coefficient of friction at the torque reaction contact surface (usually at the gate guides)

d = moment arm for the torque reaction forces, in.

F_{w1} = stem weight, lbs (often negligible compared to other forces)

F_{w2} = gate weight, lbs (often negligible compared to other forces)

Detailed derivations for each load component are given in Appendix A and summarized in Sections 2.1 through 2.3.

The overall stem force equilibrium for valve *opening* is basically the same with F_1, F_2, F_4, F_5, and F_6 in reverse direction:

$$F_1 = F_2 - F_3 + F_4 + F_5 + F_6 + F_{w1} + F_{w2} \qquad \text{(Eq. 2.10)}$$

2.5. Effective Gate Sealing Diameter

The pressure loads calculated in the previous sections are computed based on the gate differential pressure multiplied by the effective pressure area. The pressure area depends on the effective sealing diameter, d_s. It is an imaginary diameter that seals the upstream high pressure from leaking into the downstream seat inside diameter. The higher upstream pressure surrounds the upstream side of the gate and the downstream side of the gate up to the effective sealing diameter. The area inside the sealing diameter, d_s, on the downstream side of the disc is considered exposed to the lower downstream pressure.

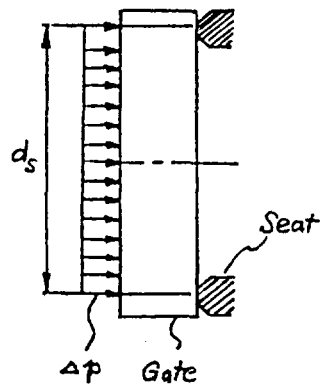

Figure 2.11
Effective Gate Sealing Diameter

Based on this definition of effective sealing diameter, d_s, the pressure load on the gate can be expressed as:

$$F_p = \Delta P \left(\frac{\pi}{4} d_s^2 \right) \qquad \text{(Eq. 2.11)}$$

Without actual testing, the sealing diameter estimate can be based on engineering judgement considering the differences in various designs and experience. The key factors that influence the sealing diameter are discussed below:

- ***Disc stiffness.*** Elastic deflection of the gate under a differential pressure load creates a higher local contact stress closer to the seat inside diameter as shown in Figure 3.1. This tends to bias the effective sealing diameter towards the seat I.D. The high local contact stress keeps the higher pressure fluid from leaking to the lower pressure on the downstream side. The disc flexibility effect usually is more pronounced on large size gates.

- ***Seat edges.*** The seat edges at the inside and outside diameters are usually chamfered. The intersections between chamfers and seat faces are normally rounded and polished to remove sharp edges. The actual operation of a valve under differential pressure also causes localized wear or yielding of the seat edges (especially on the inside diameter) under high local contact stresses. This can result in some increase of the effective sealing diameter above the seat inside diameter.

- ***Uneven seat contact.*** Disc and seat deflections under pressure usually result in uneven circumferential seat contact due to their uneven stiffness and support, as shown in Figure 3.1. This uneven seat contact pressure distribution also affects the equivalent sealing diameter used in the pressure load calculation.

The exact contribution of all of these factors on the effective seat diameter is hard to quantify without testing. In the absence of additional data, the following simple approach has been found to be adequate, and is recommended:

- Use the mean seat diameter for a narrow seat:

$$d_s = 1/2 \text{ (Seat I.D. + Seat O.D.)} \qquad \text{(Eq. 2.12a)}$$

- Use a sealing diameter closer to the seat inside diameter for a wide seat. An approximation sometimes used for wide seat faces is

$$d_s = \text{Seat I.D.} + 1/3 \text{ (Seat O.D. - Seat I.D.)} \qquad \text{(Eq. 2.12b)}$$

It is not uncommon to see seat I.D. being used as the effective sealing diameter in some cases, with the objective of determining a *conservative* coefficient of friction value, as in the case of KWU-Siemens data presented in Section 3.5. In using any of the coefficient of friction data to predict operating forces in other gate valves, it is important to use the same assumptions regarding the effective sealing diameter that were used in reducing the test data. This is sometimes overlooked, thus adding unnecessary conservatism.

2.6. Disc Tilting Due to Fluid Flow

During valve closing, the disc moves into the flow stream and interrupts the steady flow. The projection of the disc into the flow stream behaves like a blunt body in the flow stream and is subjected to fluid dynamic forces along the flow direction. As the disc advances, it increases the flow path resistance, thus resulting in an increase in differential pressure load on the disc. Although the actual pressure distribution on the disc in mid-travel position is difficult to accurately quantify without computational fluid dynamic analysis or instrumented valve testing, it is certain that the resulting fluid dynamic force will push the disc in the downstream direction. In some gate valve designs, this fluid force tends to cause tilting of the disc during mid-travel. The magnitude of this force depends upon the flow rate and hence the differential pressure across the disc. A tilted disc sliding under a high differential pressure load in mid-travel position (such as encountered during downstream pipe rupture) can develop high local contact stresses in the valve components. As observed in the NRC-sponsored high energy pipe break tests [4,23,25], severe galling can occur in disc guide slots, disc guides, and/or seat faces depending upon guide clearances and other specific features of the individual valve design. Under pump flow conditions, the magnitude of the pressure drop across the disc is significantly lower than that experienced under blowdown conditions related to a downstream pipe rupture.

The effect of flow on disc closing was analyzed for a 4-inch Borg-Warner flex wedge gate valve tested at Duke Power Company's flow loop[1]. Several key factors that affect disc tilting are discussed and quantified in this section using available valve and flow data. This analysis shows how the internal parts of this 4-inch gate valve interact during opening or closing under differential pressure. The design details of disc guide length, guide strength, clearances, and corner radii can significantly affect the valve performance, as discussed in the following analysis. The analysis also points out the need for better quantification of gate loads in the mid-travel position. Appendix B includes detailed calculations and procedures used in the analysis of the 4-inch Borg-Warner valve. Additional description of this valve and the testing that was done on it by Duke Power are given in Section 3.4 of this report. A description of the analysis and key conclusions is given below.

2.6.1. *Estimating Flow-Induced Load on Disc in Mid-Travel Position*

The fluid flow forces to which the disc is subjected during closing or opening of the valve have not been addressed adequately in many gate valve designs. This section presents a simplified approach to estimating the fluid dynamic force imposed on the disc during closing under typical pump flow conditions.

For gate valves, the average flow resistance coefficient as a function of disc opening from a number of gate valve designs is derived in Appendix B based on References 30 and 31. The results are shown in Figure 2.12.

---

1 J. K. Wang and M. S. Kalsi. *Valve Factor Analysis for 4- and 6-inch Borg Warner Flex Wedge Gate Valves*, proprietary report for Duke Power Company, KEI Document No. 1646, April 1990.

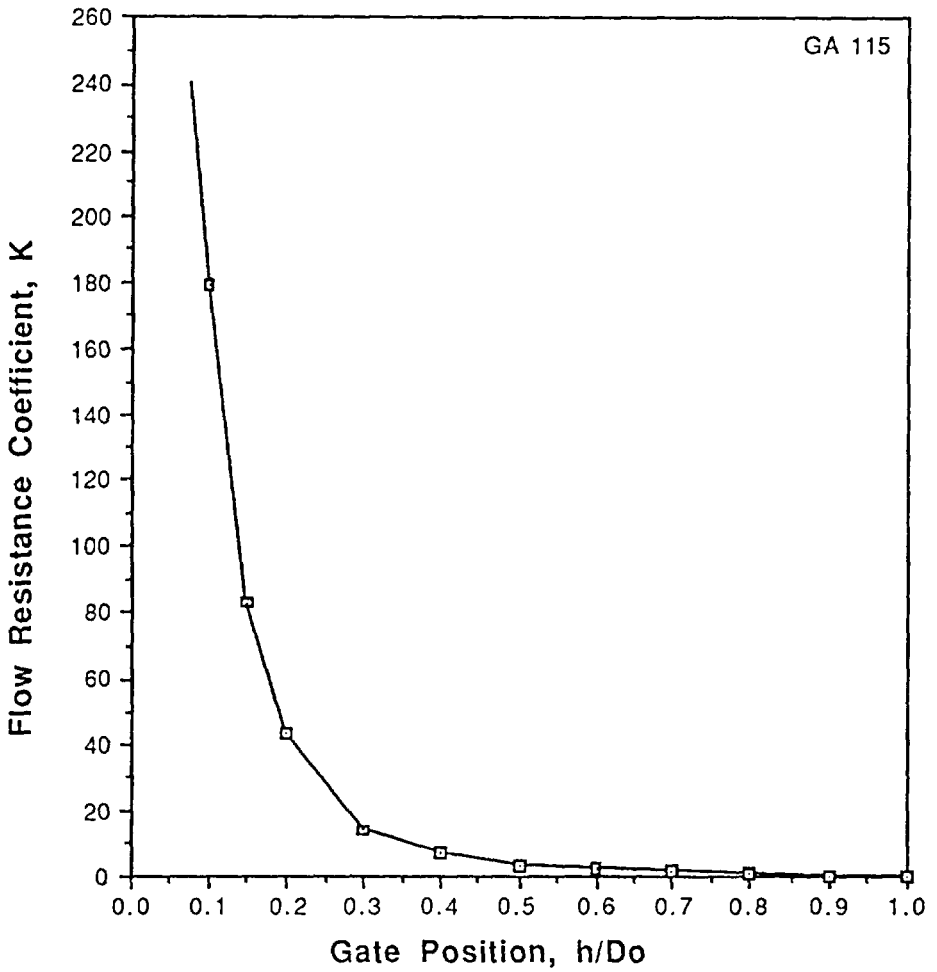

Figure 2.12
Flow Resistance Coefficient for Gate Valves Based
on an Average from Several Designs

The flow resistance decreases rapidly as the disc opens. At any disc opening, pressure drop across the disc can be estimated using the flow resistance coefficient and the fluid flow velocity by using the equation below:

$$\Delta P = K \rho \frac{V^2}{2} \qquad \text{(Eq. 2.13)}$$

where ΔP = differential pressure across the disc, lbs/ft^2

K = flow resistance coefficient at a given disc opening

ρ = mass density of the fluid, $slug/ft^3$

V = flow velocity, ft/sec

The fluid flow velocity in a piping system depends on the pump flow characteristics and the piping system resistance. As shown in Figure 2.13, the discharge pressure of a typical centrifugal pump decreases as the pump flow rate increases. On the other hand, pressure drop across the piping system increases as the flow rate increases. The intersection point of the two curves satisfies both the pump characteristics and the piping system flow resistance, and is the solution point for a given disc position.

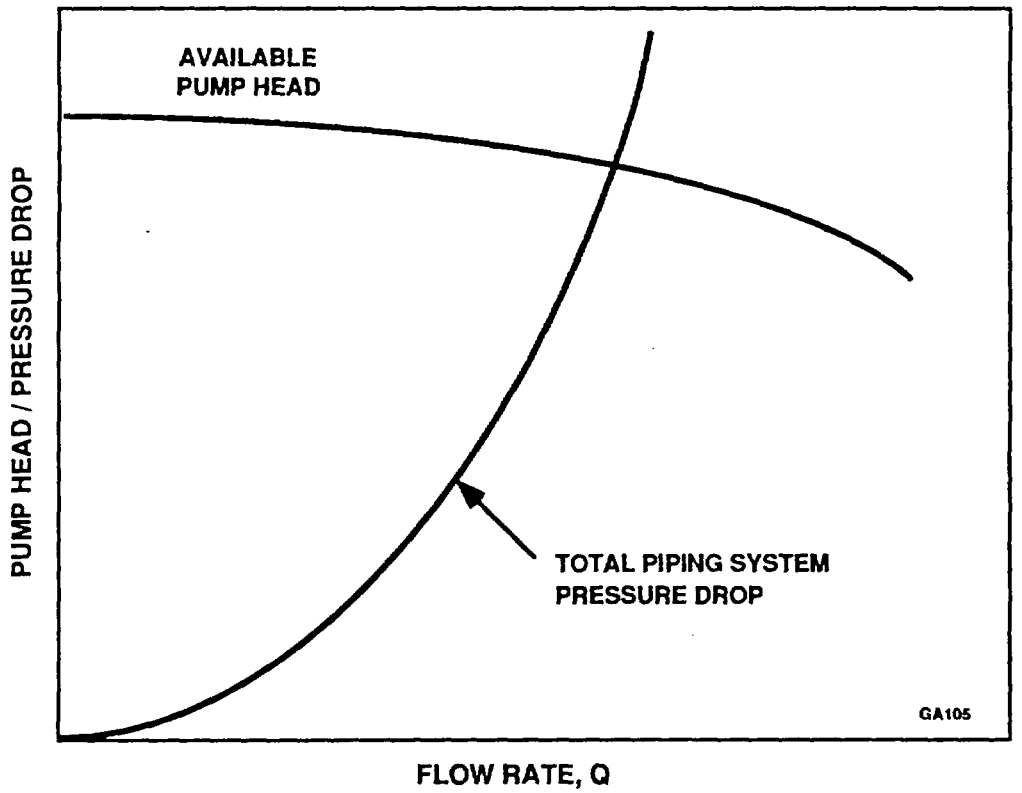

Figure 2.13
Balance of Available Pump Head and Piping System Pressure Drop

Using the above described approach, a typical change in the pressure drop across the disc as a function of disc opening in a pump flow system is shown in Figure 2.14. This figure is based upon test data for the 4-inch Borg-Warner valve tested at the Duke Power flow loop (see Footnote 1 on page 15). The pressure drop across the disc decreases rapidly as the valve opens, and after 30 percent of disc opening, the differential pressure drop across the disc is very low. This shows that the significant disc load in pumped flow systems is encountered during the final 30 percent of disc closing. The actual magnitude of the pressure drop across a disc will vary depending upon individual pump characteristics and system flow resistance.

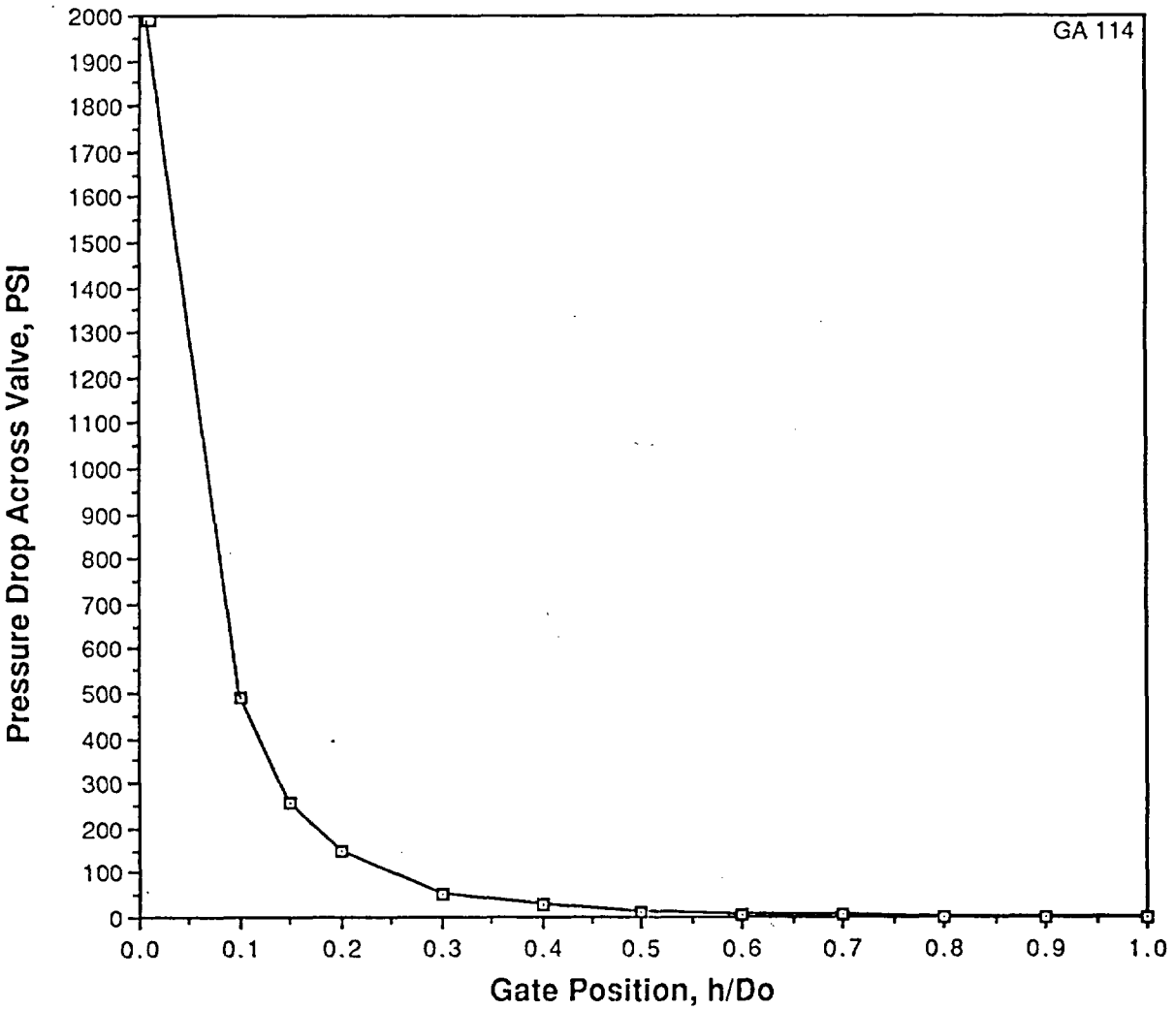

Figure 2.14
Typical Pressure Drop Across a Gate Valve as a Function of Gate Position In High Pressure Pumped Flow System

A comparison of ΔP versus the disc opening curve from the pump system in Figure 2.14 and blowdown tests performed by INEL [23,24] shows that the differential pressure across the disc, which directly affects the load on the disc, is significantly higher under blowdown conditions. For example, at 25 percent gate opening, the differential pressures ranged from 50 percent to 90 percent of the fully closed ΔP in various INEL tests as compared to approximately 5 percent predicted in the pumped flow results shown in Figure 2.14. Therefore, localized contact stresses and the propensity of galling damage to the valve internals is also much higher for valves subjected to blowdown conditions.

In order to make a preliminary estimate of the flow-induced load on the disc in mid-travel, it is assumed that the load on the disc is proportional to the differential pressure across the disc and the percentage of disc opening, as shown below:

$$F_p = \Delta P \times \left(\frac{100 - \% \text{ of disc opening}}{100} \right) \times \text{full disc area} \qquad \text{(Eq. 2.14)}$$

where F_p = pressure load on disc in mid-travel position

ΔP = differential pressure across the disc

Disc Area = $\frac{\pi}{4}$ (effective sealing dia)^2

The pressure loads across the disc calculated from this equation were used in the evaluation of localized contact stresses at the disc guide interface and disc-to-seat interface as detailed in Appendix C and discussed in Subsection 2.6.3.

2.6.2. *Disc Tilting and Its Interaction with Seats and Guides*

Figure 2.15 is a scaled drawing of a disc tilted in the mid-travel position due to forces imposed on it by the fluid flow. This figure was developed from actual design dimensions of a 4-inch ANSI Class 900 Borg-Warner flex wedge gate valve used in the Duke Power tests [15]. The geometrical interaction between the disc, seats, and guides was investigated in detail at several disc openings, and with the extreme combinations of tolerances of these components. In this figure, the disc is shown at an opening of approximately 25 percent. The disc guides in this valve design do not limit the disc tilting under fluid forces, thus allowing *point contact* to occur between the disc and the downstream seat face. High local stresses are developed at these points when disc tilting results in downstream seat contact. Also, the relative magnitude of these stresses is significantly higher than those encountered in a line contact that occurs when disc tilting is constrained by the guides. The actual magnitude of the contact stresses calculated for the 4-inch Borg-Warner gate valve are discussed in Subsection 2.6.3.

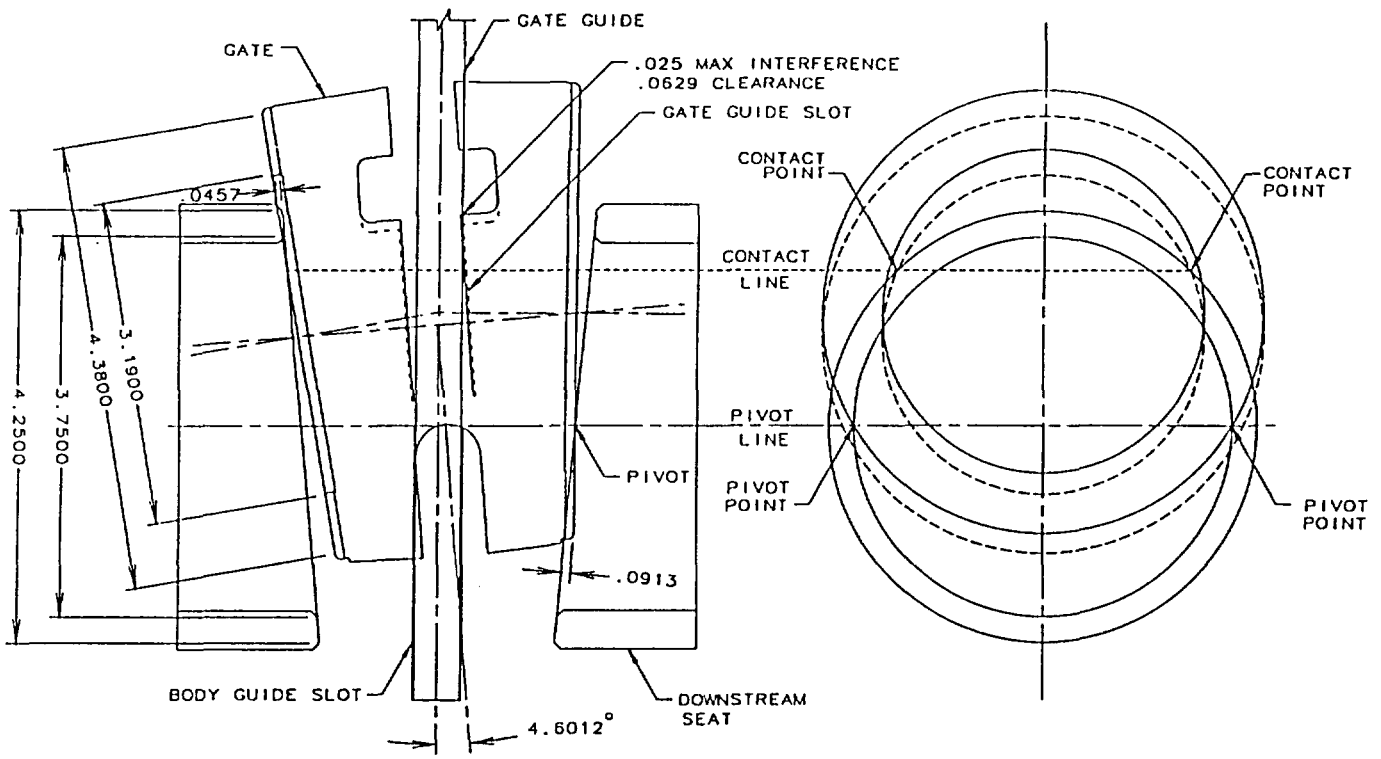

Figure 2.15*

Point Contact Against the Downstream Seat Due to Disc Tilting at a Typical Mid-Travel Position in 4", 1500# Borg-Warner Gate Valve

---

* See Footnote 1 on page 15. This figure is nonproprietary and is used by permission from Duke Power Company.

In general, the equilibrium position of the disc is defined by the resultant load vectors of the pressure load, stem thrust, seat contact force, and guide force as well as the geometry of the disc, guide, and seat area. The following three cases show the extreme variations that can occur between the disc guide and seat interaction:

1. Ideal disc slide

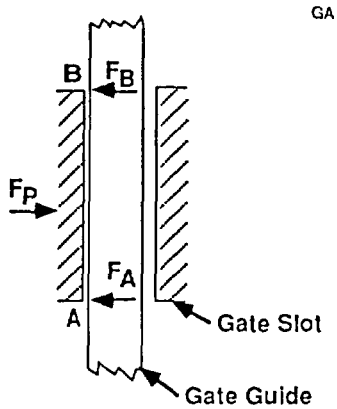

Figure 2.16
Ideal Gate Slide

As shown in Figure 2. 16, if the disc guide design is such that the resultant pressure load acts within the two extremes of the disc guide slots (Points A and B), full contact at the guide surface is achieved without tilting. This disc orientation results in the lowest contact stresses due to disc loads imposed in mid-travel. Sliding under a full-surface contact is the ideal disc guide design condition to withstand mid-travel pressure loads.

2. Tilted disc contacting guides

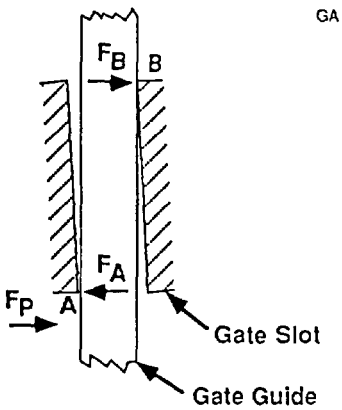

Figure 2.17
Tilted Gate Contacting Guides

If the resultant pressure load acts below the lower end of the guide contact point A, the disc will tilt, as shown in Figure 2.17. Depending on the guide clearance and other dimensions of the disc, guides, and seats, the disc may resist the resultant load by contacting the guides, thus preventing any disc-to-seat contact in mid-travel. From disc force equilibrium considerations along the flow axis, one can see that the contact load at Point A in this case will be at least as high as the pressure load F_p, and it may be higher depending upon the actual location of the resultant load vector F_p, below the guide. The location of F_p with respect to the disc will vary as the disc travels towards the closing position.

3. Tilted disc contacting seats

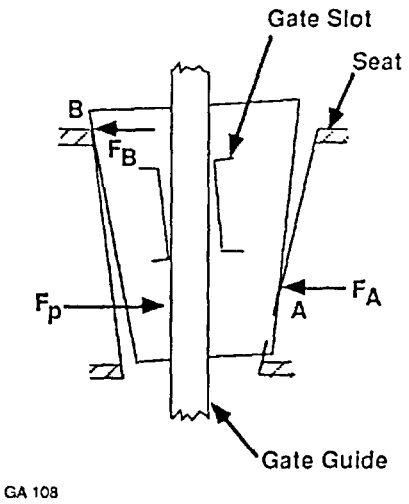

Figure 2.18
Tilted Gate Contacting Seat

In a valve design with large guide clearances and/or short guide length, disc tilting under the pressure load can result in point contact with the upstream and downstream seats as shown in Figure 2.18. As in the previous case of the disc contacting the guides, if the pressure load resultant acts below Point A, the contact load at *A* will be greater than the pressure load F_p. The actual load magnitude can be determined by force equilibrium along the flow axis. Contact stresses at Point A in this case can be very high because of point contact between two curved surfaces, as discussed in Section 2.6.3 and Appendix C.

The three extreme cases discussed above show that the pressure load magnitude, location, and dimensions of the disc guide and seats are essential in determining the actual configuration acquired by the disc in mid-travel. Reference 47 presents a mathematical model to facilitate the evaluation of disc-seat interference for a gate valve during valve closure. Better quantification of the pressure-induced load is needed to more accurately determine the disc equilibrium and quantitatively assess the adequacy of a valve to operate properly and without causing damage to valve internals in mid-travel position.

It should be noted that the disc equilibrium discussion in the above three cases was limited to pressure load acting along the flow axis only. Disc equilibrium along the stem axis can also be affected by the resultant pressure load and downstream seat friction load acting in the stem axis direction. The overall disc equilibrium equations can be further refined by including these load terms.

2.6.3. *Contact Stresses*

Gate tilting in mid-travel position can create high localized contact stresses in the disc, seat, and guide interfaces. The magnitude of contact stress depends on the geometrical shapes of the two contacting surfaces and their material properties. For simple, well-defined geometries such as spherical, elliptical, cylindrical, and plane surfaces, the contact stresses between the two surfaces can be calculated using the Hertzian general linear elastic solution for doubly curved surfaces as shown in Appendix C. For more complicated contact surfaces and loading situations, computer-aided numerical methods

such as finite element analysis can be used. Finite element analysis can also provide a more accurate assessment of the localized contact stresses by avoiding small displacement assumptions and accounting for elastic-plastic behavior.

In Appendix C, local contact stresses for the 4-inch Borg-Warner valve under pump flow conditions were investigated by using the closed-form Hertz contact stress equation for point and line contacts (the performance of this valve in Duke Power tests is discussed in Section 3.4). Localized contact stresses were calculated for two cases: (1) when the disc tilting causes a contact against the downstream seat, and (2) the case in which disc tilting causes a line contact at the guide surfaces. The results show that, based on linear elastic assumptions, the calculated contact stresses vary widely from near the material threshold of galling stress to an order of magnitude higher than that. As expected, highest localized stresses were found in the case of disc tilting which results in *point contact* against the downstream seat. With an assumption of 0.125-inch edge radii at both the disc outside diameter and seat inside diameter contacting surfaces, theoretical stresses based on the linear elastic assumption exceeded 300 ksi at the point contact. Local yielding, load redistribution, and localized material wear under repeated cycling are likely to occur, which will flatten or enlarge the contact area and reduce the contact stresses. However, these high stresses, which are significantly above the thresholds of galling for the sliding materials, will initially result in local galling. Depending upon the magnitude of the loads present and the local geometry, a stable frictional behavior without further galling can be attained after a progressive increase in the local contact area due to yielding as well as material removal by wear or galling occurs. On the other hand, if the loads are too high to be supported by area spreading achieved by local wear, continued galling and increase in frictional forces can be expected. Extensive testing is needed to quantify this mechanism for various load geometries and loading conditions.

It should be pointed out that the theoretical local contact stress based on simplifying assumptions cannot be used by itself to predict the valve performance. It can be used more as an *index of contact stress severity*, which can be related to *actual* performance, and to make relative comparisons to compare different local geometries and load magnitude

The contact stress analysis clearly shows that significant improvements can be made in the detailed design of valve components in possible contact areas by increasing local radii and resisting disc tilting by line contact instead of point contact, as shown in Appendix C. The ultimate goal of an improved gate valve design should be to incorporate a guide geometry that results in *ideal disc slide* (discussed earlier in Subsection 2.6.2), which eliminates high local contact stresses.

3. COEFFICIENT OF FRICTION AND THRESHOLD OF GALLING STRESS

Coefficient of friction between the disc and seats is the dominant factor in determining the operating thrust requirements for most gate valve applications. Valve manufacturers have standardized on Stellite hardfacing alloys for the disc and seat sliding surfaces because of their excellent resistance to corrosion, wear, and galling in the unlubricated state, even at elevated temperatures. In spite of the fact that Stellite has been in widespread use in gate valve applications for several decades, published data for Stellite vs. Stellite coefficient of friction show a significant lack of uniformity under seemingly similar test conditions. Reported data span, even under laboratory conditions, a wide range from 0.12 [44] to 0.48 [40], and sometimes even higher.

It should be pointed out that, even though several variables can affect the coefficient of friction results [29,42,43], the principal investigators have found that the most important factors responsible for the wide scatter in the reported data are (1) the differences between the size and geometry of the test specimen, (2) the presence, absence, or gradual removal of an absorbed layer of lubricant at the sliding surfaces, and (3) presence or absence of galling of various levels due to high localized contact stresses in some areas of contact. These factors should be kept in mind while reviewing test data and results reported by various sources.

During the 1970's, the principal investigators were involved in a gate valve development effort under which extensive testing and evaluation of coefficient of friction and galling data was done. A summary of the important results from these tests is presented in Section 3.2. This is followed by the recent results from the principal investigators' involvement in assisting Duke Power Company to perform a root cause analysis of the 4-inch Borg-Warner flexible wedge gate valves that failed to close under high differential pressure conditions in a pumped flow system [15]. Other recent test data for parallel slide gate valves reported by KWU-Siemens [26] and British National Power Division of the CEGB [21] are discussed next. Finally, the important results from the recent NRC-sponsored INEL blowdown tests [4,23] are also presented here for comparison, and for drawing overall conclusions from the presently available data.

Before proceeding with a discussion of the results from these sources, it is important to show the relationship between the commonly used term *disc factor*, sometimes called *valve factor*, to the coefficient of friction. This is presented in the next section.

3.1. Relationship Between Disc Factor and Coefficient of Friction

The common industry equation for determining valve thrust requirements for actuator sizing is:

Minimum stem thrust requirement = disc factor x differential pressure load across the disc
+ stem packing friction force
± stem rejection force

where the positive and negative signs apply to the closing and opening thrust requirements respectively. A disc factor of 0.3 has been commonly used in actuator sizing in the past. The *disc factor* used in the above equation exactly equals the coefficient of friction between the gate and seat for a *parallel slide* gate valve.

For a *conventional wedge gate valve* of solid, flexible, or split disc design, the disc factor is not exactly the same as the coefficient of friction. The relationship between the two, as derived in Section 2.1, is shown below:

$$\text{Disc Factor} = \frac{\mu}{\cos\theta \pm \mu \sin\theta}$$

where μ = coefficient of friction between disc and seat
θ = one-half of total included wedge angle
+ sign in the denominator applies to valve opening, and
– sign in the denominator applies to valve closing

The difference between disc factor and coefficient of friction for conventional wedge gate valves is usually small. Typical wedge gate valves use a wedge angle of ($\theta = 5°$), for which the ratio between disc factor and coefficient of friction over the typical range of coefficients of friction computed for the above equation is within ± 5 percent as shown in Table 3.1. For all practical purposes, the difference between the two is much smaller than variations in the coefficient of friction data, and can often be ignored without much impact on the overall conclusions. Some valves use higher wedge angles, for which the differences become more significant.

Stroke Direction	*Ratio* = $\frac{\textit{disc factor}}{\textit{coefficient of friction}}$			
	$\mu = 0.2$	$\mu = 0.3$	$\mu = 0.4$	$\mu = 0.5$
Open	0.99	0.98	0.97	0.96
Closing	1.02	1.03	1.04	1.05

Table 3.1
Relationship Between Disc Factor and Coefficient of Friction
for a 10° Wedge Gate

3.2. Data for Coefficient of Friction from Principal Investigators' Experience

3.2.1. *Background*

During the 1970's, the principal investigators worked in the research and development department of a major U.S. valve manufacturer. This valve manufacturer had been a dominant supplier of valves for oil field, pipeline, and petrochemical applications for several decades. In the early 1970's, this manufacturer decided to pursue the nuclear power, geothermal, coal gasification, and synthetic natural gas markets. In order to meet the technical challenges posed by the development of valves for these applications, major additions to the test facilities were made. Significant additions pertinent to the nuclear power valve development effort included a 1,500 psi air/water high energy blowdown system; a 600°F, 12,500 lbs/hr steam generator; an external pipe load simulator capable of applying bending moments of up to 2×10^6 ft-lbs; and a Falex friction/wear test machine. Additionally, the laboratory was equipped with a 100-channel strain gage data acquisition system, various load and torque cells, pressure transducers, and a tension/compression test machine. This environment provided an excellent opportunity to the principal investigators to be involved in a systematic research and development effort on gate valves for high temperature applications.

A common test frequently performed on a valve under development consisted of several hundred cycles (1,000 cycles was the usual goal) of opening and closing under maximum design differential pressure generated by small positive displacement pumps using room temperature city water as the flow medium. Stem thrust measurements using strain gage load cells were performed on several gate valves ranging in size from 2 inches to 16 inches during this developmental testing effort. Testing was also done on valves for high temperature service using saturated steam with pressures up to 1,500 psi and temperatures up to 600°F. Most of the test data were primarily used to support the in-house development of the new valve designs and were considered proprietary at that time; therefore, no data were published in the open technical literature. With the virtual disappearance of the nuclear power market in the early 1980's, this valve manufacturer stopped its nuclear valve production. Valuable technical data that had been developed were never published. The principal investigators have taken this opportunity to present highlights of the most significant results from these tests relating to the coefficient of friction, which are summarized below:

3.2.2. *Results from Room Temperature Water Tests*

Using room temperature, ordinary tap water as the test medium, the typical range of coefficient of friction for Stellite-6 overlaid gate and seats from a large number of tests on several different sizes of valves up to 16 inches was found to be between 0.15 and 0.25 over several hundred cycles of operation. These tests were performed on parallel expanding, through-conduit gate valves of the type shown in Figure 2.1b. As discussed below, two important features of this design are that the gate cannot physically tilt, and the contact stresses at the seat faces are well below the threshold of galling.

As can be seen in Figure 2.1b, the gate length in this type of through-conduit valve design is approximately twice as long as the ones used in the conventional solid wedge or flex wedge gate valves. The lower (extended) part of the gate has a bore through it, which lines up with the seat bore when the valve is in the fully open position. Under the action of fluid flow forces on the gate in the mid-travel position, this type of gate assembly is simply pushed down against the downstream seat face, thus providing a *surface* contact instead of the *point* contact that can occur in conventional wedge gates which have excessive guide clearance as discussed in Section 2.6. Thus, the through-conduit design of Figure 2.1b avoids high localized contact stresses at the gate-to-seat faces which have the potential to cause galling. Furthermore, the design of these valves was based on limiting the average seat face contact stress to 10,000 psi or less under maximum differential pressure. This is well below the threshold of galling as discussed in Section 3.3.1. The absence of galling at the seat faces was confirmed by many tests under high differential pressure conditions. *In these cycle tests, no extraordinary effort was spent to remove any residual lubricants used during assembly*, except what is automatically removed by normal abrasive wear due to sliding under high contact pressure. The coefficient of friction was calculated using mean seat diameter as the effective seating diameter.

In summary, coefficients of friction values for Stellite vs. Stellite were typically found to range between 0.15 and 0.25 for several hundred cycles of testing with gate valves using room temperature ordinary tap water, with average seat contact stress of 10,000 psi or less, and a gate design which prevented any galling at the seating surfaces. It is important to note that the valves were not exposed to high temperatures prior to these tests. As discussed later, this has been reported to be a factor that can cause an increase in the coefficient of friction (Sections 3.5 and 3.7).

3.2.3. *Results from High Temperature Water and Steam Tests*

An extensive series of tests using saturated steam and hot water in temperatures up to 600°F were performed on the same type of parallel expanding, through-conduit gate valves (Figure 2.1b) as used in the cold water tests discussed in Section 3.2.2. Valves up to 12 inches in size were tested with a maximum differential pressure of 1,500 psi. As mentioned in the previous section, this type of gate design prevents mid-travel gate tilting and maintains a surface area contact against the downstream seat. The total number of cycles under various levels of differential pressures during these steam tests ranged from 10 to 30 ; and not hundreds of cycles as in the cases of cold water tests. The highest value for the coefficient of friction between Stellite and Stellite during any of these tests was found to be 0.39 using water or steam at 600°F. This coefficient of friction evaluation was based on using the mean seat diameter as the effective seating diameter The calculated average seat contact stress in these test valves was less than 10,000 psi under the maximum differential pressure conditions, and no evidence of galling was found at the seat faces.

Based on these results performed on actual gate valves (not friction test specimens), the principal investigators have found the value of 0.4 for coefficient of friction for pure sliding between Stellite seat and Stellite disc faces for high temperature steam and water applications to be a reliable result *provided* it is ensured that the seat faces are free of galling.

Conversely, the principal investigators have also used this data successfully in root cause analyses of valves to identify potential galling, component interference, or other problems with the valve internals when the coefficient of friction, based on measured thrust, significantly exceeds 0.4 in steam or high temperature water application. The above results for the coefficient of friction are in agreement with the results reported in Sections 3.5 and 3.6 by others using actual gate valves of improved designs that are free of galling damage.

3.2.4. *Long-Term Surveillance Tests on SIS Valves Under Flow and ΔP*

In 1981, the principal investigators were involved in the root cause analysis investigation and modification of two safety injection system (SIS) gate valves at a PWR plant following their failure to open when challenged[1] [51]. The problem was attributed to an increase in the required thrust to open the valves due to galling of the seat faces (see Footnote 1). After the modifications proposed by the principal investigators and the utility were implemented and demonstrated to be successful, NRC required a periodic surveillance testing of these valves under differential pressure *and* flow. The objectives of these NRC-imposed long-term surveillance tests were to ensure that (1) the root cause of the failures is indeed understood and has been corrected, and (2) there is sufficient margin in the actuator force to account for degradation of the valve internals and possible increase in friction due to long-term set effect caused by constantly applied differential pressure across the disc.

A total of six dynamic tests were performed under hot standby conditions (plant operating Mode 3) with temperatures up to 330°F on each of the two valves between November 1981 and August 1985. During these surveillance tests, both the differential pressure across the valves and the actuator force required to open the valves were measured. The valves were operated by hydraulic actuators, and the actuator force was calculated from the pressure measured on both sides of the piston, plus the stem rejection force due to pressure inside the valve. All of the pressure measurements were done using calibrated pressure transducers in accordance with controlled test procedures. In 1986, the principal investigators performed a detailed evaluation of these surveillance test results[2]. It was concluded that both of the SIS valves had continued to perform consistently and successfully with sufficient margin below the maximum capabilities of the actuator.

---

[1] M. S. Kalsi. *Independent Review of Operability Failure Problems with the Safety Injection System Valves HV-851 A and B at SONGS 1*, Kalsi Engineering, Inc. proprietary report to Southern California Edison, KEI 3.2.0, September 1981.

[2] M. S. Kalsi and J. K. Wang. *Independent Evaluation of Safety Injection System Valve Surveillance Test Results and the Proposed Periodic Testing at Songs 1*, Kalsi Engineering proprietary report to Southern California Edison Company, KEI-919, May 1986.

One of the important conclusions drawn from these 12 tests performed on the two valves over a span of approximately four years is that the coefficient of friction between the Stellite disc and seats ranged from 0.17 to 0.34, including the long-term set and other degradation effects. Stem packing friction was not subtracted from the total opening thrust to obtain *conservative* estimates for the coefficient of friction. As stated earlier, these tests were performed under dynamic flow and differential pressure with temperatures up to 330°F during Mode 3 hot standby conditions. It should also be pointed out that the *average* seat contact stress for these modified valves under the maximum differential pressure was around 7,500 psi, well below the threshold of galling for Stellite against Stellite (as discussed in Section 3.3); and thrust measurements did not indicate a trend of continuing increase in friction.

3.3. Contact Stress and Threshold of Galling

As the contact stress between the sliding surfaces is increased, a *threshold* is reached beyond which the required sliding force between the mating materials increases rapidly due to significant material transfer through localized welding, tearing, and digging of the surfaces. The contact stress at which this behavior is initiated is called *threshold of galling stress*. Unlike normal wear, the damage to the materials due to galling goes well beyond the surface in just a few strokes. Under galling conditions, the coefficient of friction is unpredictable because sliding between the two surfaces involves significant shearing and tearing of the cold-welded junctions formed between the mating materials.

3.3.1. *Threshold of Galling for Stellite vs. Stellite and Other Valve Trim Materials*

The threshold of galling stress for Stellite against Stellite in the unlubricated condition is reported by some investigators to be *over* 50 ksi [42, 45, 46], and by others to be *over* 70 ksi [48, 49] based on the maximum limits of their respective test apparatuses. This is based on a single forward rotation of 360 degrees using block and button test specimens in which the load is gradually increased until first signs of galling appear. Using slightly larger specimens (0.5 inch diameter instead of 0.375 inch), and using one forward rotation of 360 degrees, one reverse rotation of 360 degrees, and another forward rotation of 360 degrees, Schumacher, the author of Reference [46], has found the threshold of galling stress for Stellite to be 47 ksi. This situation more nearly duplicates a valve cycling application rather than an unidirectional 360-degree test. In the experience of the principal investigators, the threshold of galling stress is somewhat subjective, and a reasonable margin should be provided against threshold values to achieve satisfactory performance. Stellite vs. Stellite was still found to rank in the category of materials having the best resistance to galling. Comparatively, the galling resistance of stainless steels and carbon steels without any hard surface treatment is much lower, as shown in Tables 3.2 and 3.3 reproduced from Reference 42.

TABLE 4.16 Galling Resistance of Stainless Steels

Block material	Condition and nominal hardness (BHN)	Button material: 410	416	430	440C	303	304	316	630 (17-4 PH)	Nitronic 32	Nitronic 60
Type 410	Hardened and stress relieved (352)	21	28	21	21	28	14	14	21	320	350+
Type 416	Hardened and stress relieved (342)	28	90	21	145	60	165	290	14	310	350+
Type 430	Annealed (159)	21	21	14	14	14	14	14	21	21	250
Type 440C	Hardened and stress relieved (560)	21	145	14	75	35	21	250	21	350+	350+
Type 303	Annealed (153)	28	60	14	35	14	14	21	21	350+	350+
Type 304	Annealed (140)	14	165	14	21	14	14	14	14	210	350+
Type 316	Annealed (150)	14	290	14	255	21	14	14	14	21	260
Type 630 (17-4 PH)	H 950 (415)	21	14	21	21	14	14	14	14	350+	350+
Nitronic 32	Annealed (235)	315	310	55	350+	350+	210	21	350+	210	350+
Nitronic 60	Annealed (205)	350+	350+	250	350+	350+	350+	260	350+	350+	350+

Note: Values shown are threshold galling stress (MPa); condition and hardness apply to both the button and the block material; tests were terminated at 350 MPa, so values given as 350+ indicate the samples did not gall.

Source: Adapted from Anonymous (1978d).

Table 3.2
Galling Resistance of Stainless Steels (1 MPa = 145.14 psi)

Handbook of Tribology; Bharat Bhushan and B. K. Gupta, 1991, McGraw-Hill, Inc.

TABLE 4.17 Galling Resistance of Alloys

Alloys in contact*	Threshold galling stress,† MPa
Silicon bronze (200) vs. silicon bronze (200)	28
Silicon bronze (200) vs. AISI 304 (140)	300
AISI 660 (A286) (270) vs. A286 (270)	21
AISI 4337 (484) vs. AISI 4337 (415)	14
AISI 1034 (415) vs. AISI 1034 (415)	14
Waukesha 88 (141) vs. AISI 303 (180)	350+
Waukesha 88 (141) vs. AISI 201 (202)	350+
Waukesha 88 (141) vs. AISI 316 (200)	350+
Waukesha 88 (141) vs. AISI 630 (405)	350+
Waukesha 88 (141) vs. 20Cr-80Ni (180)	350+
AISI 201 (202) vs. AISI 201 (202)	105
AISI 201 (202) vs. AISI 304 (140)	14
AISI 201 (202) vs. AISI 630 (17-4 PH) (382)	14
AISI 201 (202) vs. Nitronic 32 (231)	250
AISI 301 (169) vs. AISI 416 (342)	21
AISI 301 (169) vs. AISI 440C (560)	21
AISI 410 (322) vs. AISI 420 (472)	21
AISI 416 (342) vs. AISI 416 (372)	90
AISI 416 (372) vs. AISI 410 (322)	28
AISI 416 (342) vs. AISI 430 (190)	21
AISI 416 (342) vs. 20Cr-80Ni (180)	50
AISI 440C (560) vs. AISI 440C (604)	80
AISI 630 (17-4 PH) (311) vs. AISI 304 (140)	14
AISI 630 (17-4 PH) (380) vs. Nitronic 32 (401)	21
AISI 630 (435) vs. AISI 304 (140)	14
AISI 630 (400) vs. AISI 631 (400)	21
AISI 630 (435) vs. AISI 631 (435)	14
Nitronic 32 (235) vs. AISI 630 (380)	75
Nitronic 32 (401) vs. Nitronic 32 (401)	235
Nitronic 32 (235) vs. Nitronic 32 (401)	235
Nitronic 32 (235) vs. AISI 304 (140)	50
Nitronic 32 (401) vs. AISI 304 (140)	90
Nitronic 32 (205) vs. AISI 1034 (205)	14
Nitronic 50 (205) vs. Nitronic 50 (205)	14
Nitronic 50 (321) vs. Nitronic 50 (321)	14
Nitronic 50 (205) vs. Nitronic 32 (401)	90
Nitronic 50 (321) vs. Nitronic 32 (235)	55
Nitronic 50 (205) vs. AISI 304 (140)	28
Nitronic 60 (205) vs. AISI 301 (169)	350+
Nitronic 60 (205) vs. AISI 420 (472)	350-
Nitronic 60 (213) vs. AISI 630 (313)	350+
Nitronic 60 (205) vs. AISI 630 (332)	350+
Nitronic 60 (205) vs. Nitronic 50 (205)	350+
Nitronic 60 (205) vs. AISI 4337 (448)	350+
Nitronic 60 (205) vs. AISI 660 (A286) (270)	350+
Nitronic 60 (205) vs. 20Cr-80Ni (180)	250
Nitronic 60 (205) vs. Ti-6Al-4V (332)	350+
Nitronic 60 (205) vs. Stellite 6B (415)	350+
Stellite 6B (415) vs. AISI 304 (140)	240
Stellite 6B (415) vs. AISI 316 (140)	25
Stellite 6B (415) vs. Stellite 6B (415)	350+
Stellite 6B (415) vs. Tribaloy 400 (54 HRC)	350-
Stellite 6B (415) vs. Tribaloy 700 (47 HRC)	350+
Tribaloy 400 (54 HRC) vs. Tribaloy 400 (54 HRC)	350+
Tribaloy 700 (47 HRC) vs. Tribaloy 700 (47 HRC)	185

*Numbers in parentheses following alloy designations are nominal hardness (Brinell).
†Values given as 350- indicate the samples did not gall.
Source: Adapted from Anonymous (1978d) and Foroulis (1984).

Table 3.3.

Galling Resistance of Alloys (1 MPa = 145.14 psi)

Handbook of Tribology; Bharat Bhushan and B. K. Gupta, 1991, McGraw-Hill, Inc.
This material is reproduced with permission

3.3.2. *Average and Local Contact Stresses*

In the design of valve seating surface, the average contact stress based upon maximum differential pressure and full face contact should be kept well below the threshold of galling stress. A margin is necessary in practice to allow for the higher localized stresses that are caused by elastic displacement of the disc, body, and seats, resulting in a non-uniform distribution. Figure 3.1a qualitatively shows that the highest localized contact stresses occur in the gate valve seat faces around the 3 o'clock and 9 o'clock positions circumferentially, and near the seat inside diameter radially. It should be pointed out that this non-uniform distribution is *not* the result of disc tipping as discussed in Section 2.6, but is due to the uneven stiffness of a gate valve body and flexure of the gate. In Section 2.6 it is shown how disc tilting can also result in high localized stresses in the guide areas or at the downstream point contact. If the localized stresses exceed threshold of galling, galling in local areas is initiated. In our review of differences in various manufacturers' valve designs and their performance, we have found that the average *seat face* contact stress of 20 ksi should not be exceeded, and 15 ksi or less is preferred in order to achieve repeatable performance using Stellite hardfacing.

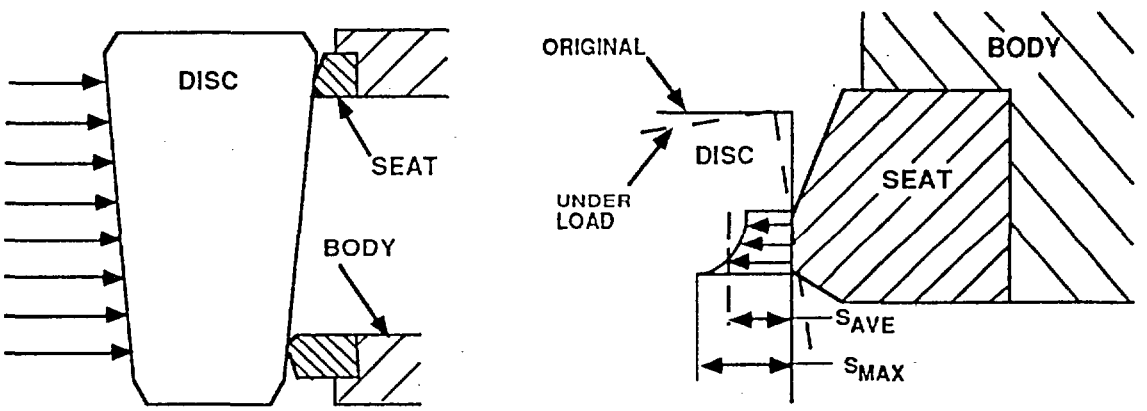

Figure 3.1a
Radial Seat Contact Stress Variation

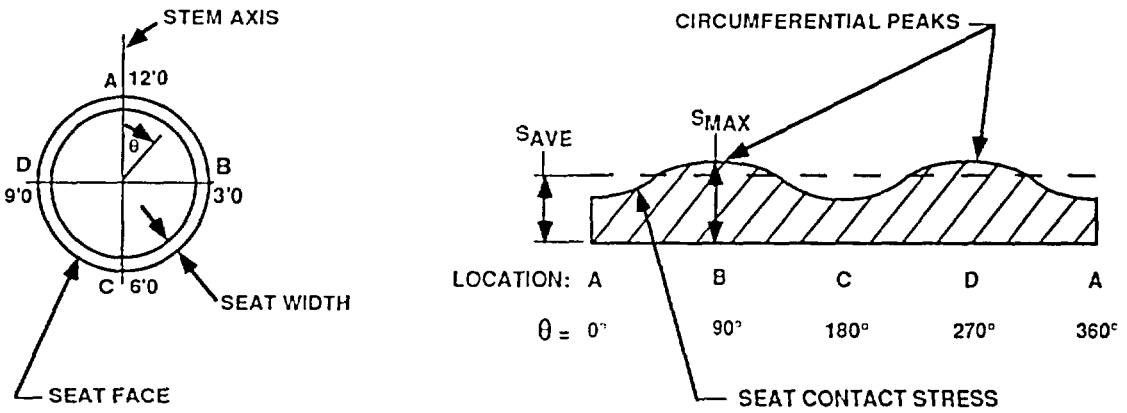

Figure 3.1b
Circumferential Seat Contact Stress Variation

Whether this local galling, once initiated, progresses continuously until seizure or heals itself by spreading the load over a larger area during successive cycling depends upon the load magnitude and the local geometry of the two contact solids. Actual testing of full-scale or near full-scale test specimens under realistic simulation of actual loading conditions has been found by the principal investigators to be the most reliable way to determine the limits of operation without galling.

When analyzing the test results from any valve to determine the applicable coefficient of friction, it is extremely important to establish that the surfaces are free of galling damage. Otherwise, "apparent" coefficient of friction values much higher than those obtained in pure sliding behavior can be erroneously concluded from the test results and applied to other valves that are of different, healthy designs.

3.4. Duke Power Data for 4-Inch Borg-Warner Flexible Wedge Gate Valve

Following the failure of a 4-inch Borg-Warner flexible wedge gate valve to fully close under a differential pressure of 1,800 psi at Catawba Nuclear Power Plant, Unit 2 in 1988 [14], Duke Power Company undertook a systematic root cause analysis investigation of the failure. The valve that failed was a 4-inch, ANSI 1500, flexible wedge, carbon steel gate with a U-shaped guide fitted into a milled slot in the body at the bottom and pinned to the bonnet at the top. Duke Power performed extensive differential pressure tests at their Riverbend Steam Station flow loop on another Borg-Warner carbon steel valve identical in design to the one that failed at Catawba. Tests were also performed on a stainless steel valve of the same size and design. The seat and disc faces were overlaid with Stellite in all of these valves. Stem force data were obtained in these tests using stem strain gages.

Kalsi Engineering, Inc. assisted Duke Power in the root cause evaluation of these valves which failed to perform under a manufacturer-specified valve factor of 0.3. With Duke Power's permission, the important results from this investigation (see Footnote 1 on page 15) are presented here.

The *coefficient of friction* extracted from the carbon steel valve tests is presented in Figure 3.2 for 24 consecutive cycles, starting with a newly refurbished valve. During cycle testing, the differential pressure was varied between nominal values of 500, 1,000, 1,500, and 2,000 psi. These tests spanned a period of four to five days during November 1988.

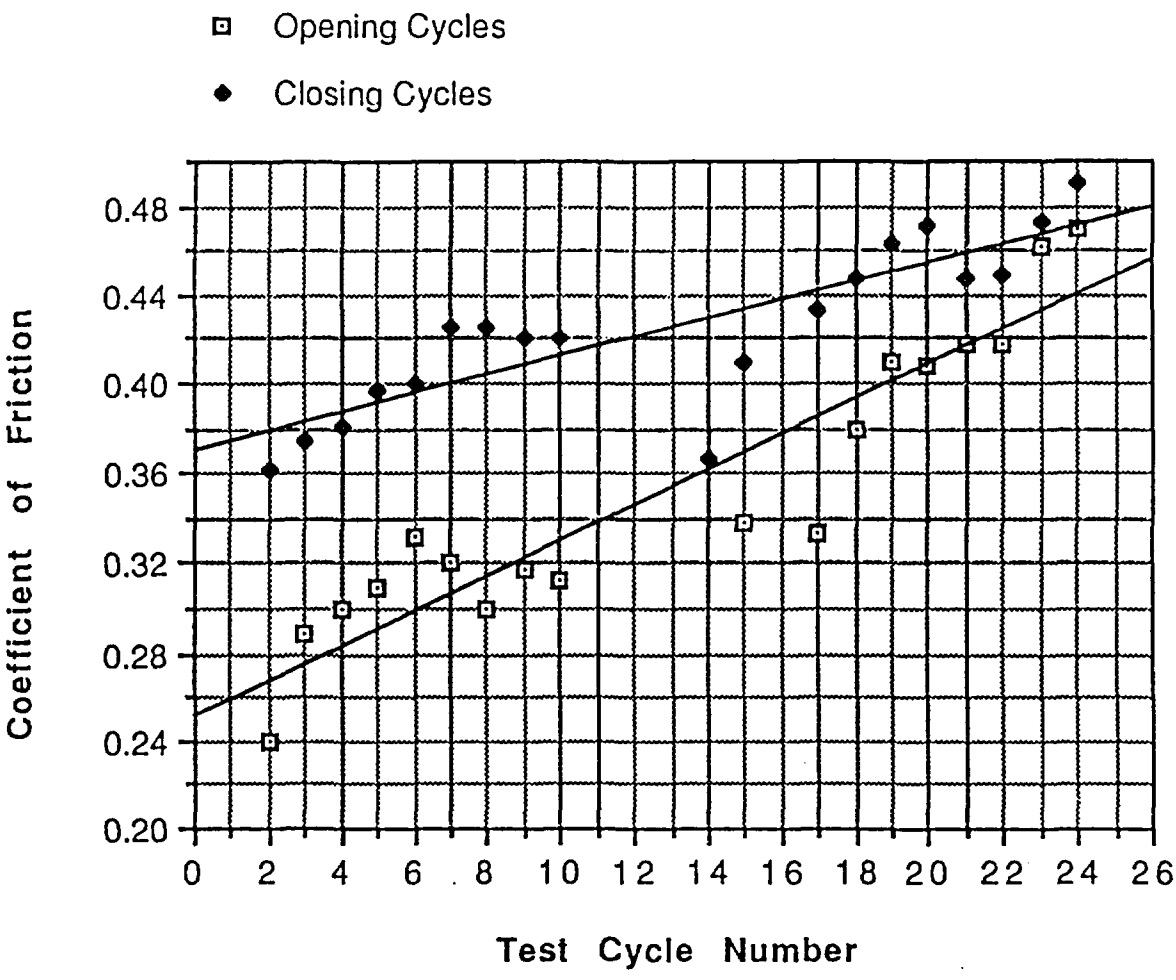

Figure 3.2*

Increasing Friction Trend During 4-inch Borg-Warner Gate Valve Cycle Testing by Duke Power, Reference

* See Footnote 1 on page 15. This figure is nonproprietary and is used by permission from Duke Power Company.

The plotted results shown are obvious overall central tendency of gradual increase in the coefficient of friction, along with the expected variation around the mean. Coefficient of friction magnitude increased from 0.36 to 0.49 in the closing direction, and 0.24 to 0.47 in the opening direction during cycling. As discussed in Section 2.6, the disc guide design of this valve has large clearances, and it allows the disc to make point contact against the downstream seat face. Inspection of the disc clearly shows evidence of contact against the downstream seat at 4 o'clock and 8 o'clock positions, and two localized areas of relatively minor wear that have spread to a width of about 1/16-inch at the outside edge of the disc. It is believed that the progressive wear of this area, even though minor, contributed to the removal of the contaminant layer and a gradual increase in friction aggravated by local galling.

It can be conjectured whether or not this trend of increasing friction would have continued until seizure occurs or stabilized at a certain value if the cycling had been continued.

Based on the magnitude of loads involved in this valve application under pump flow conditions, minor localized wear and the spreading of the load bearing area results in a substantial decrease in localized contact stress to below the threshold of galling stress. Once the localized areas have spread to an equilibrium condition below the threshold of galling stress, stable performance at some lower coefficient of friction value than that encountered at the end of this test can be expected from this valve under continued cycling under the same differential pressure and flow condition.

3.4.1. *Summary and Comparison of Duke Power Data for Carbon Steel vs. Stainless Steel Valves*

The average, minimum, and maximum values for the coefficient of friction for the first ten cycles for this carbon steel valve test (results plotted in Figure 3.2) are summarized in Table 3.4. It should be noted that two organizations that have performed extensive blowdown tests on isolation valves have typically specified five test cycles for their operability qualification [26,39].

Test Valve Disc and Seat Material	*Operation*	*Coefficient of Friction*	
		Average	*Minimum/Maximum*
Carbon Steel with Stellite	Closing	0.401	0.362/0.426
	Opening	0.302	0.239/0.338
Stainless Steel with Stellite	Closing	0.288	0.19/0.349
	Opening	0.256	0.12/0.348

Table 3.4*
Comparison of Coefficient of Friction Results for Carbon Steel and Stainless Steel Valves for First Ten Cycles

The results from another 4-inch Borg-Warner flexible wedge valve of the same design, but of stainless steel material, which was tested by Duke Power in their Riverbend flow loop, are also shown in this table for comparison. Both of these valves had Stellite hardfacing overlay on the disc and seat faces. The comparison shows that the results for the stainless steel valve are significantly lower than the carbon steel. Duke Power suspected that the differences in material of the overlay, due to the differences in the iron content, may be responsible for the differences in their coefficient of friction behavior. This seems plausible, especially since differences in the composition of various Stellite alloys (e.g., Stellite-1, -6, and -12) exhibit different coefficients of friction as reflected by Foroulis [40] and Rockwell Edwards [27].

Foroulis [40] has reported that the coefficient of friction under relatively light contact stress (approximately 50 psi) in clean water for Stellite-1, Stellite-6, and Stellite-12 materials in self-mated tests were 0.28, 0.48, and 0.24 respectively. In non-self-mated tests, when Stellite-6 was tested against Stellite-1 or Stellite-12, the coefficient of friction was 0.28. This is significantly lower than for the self-mated case of 0.48.

Rockwell Edwards has also reported significant differences in the coefficient of friction values for Stellite during their Equiwedge gate valve development program [27]. They selected Stellite-21 based on its overall performance, including lower coefficient of friction. However, they did not report actual values from their tests.

Based on the above comparisons, it is clear that further testing under controlled conditions, using an appropriate range of contact stresses, is needed to evaluate the effect of iron content and possibly other alloying elements in the cobalt-based Stellite alloys.

---

* See Footnote 1 on page 15. This table is nonproprietary and is used by permission from Duke Power Company.

3.5. KWU-Siemens Test Data

KWU-Siemens has recently reported results of their high pressure blowdown testing on a 6-inch parallel slide gate valve under cold water, hot water, and steam conditions. Friction coefficients were calculated for consecutive cycles and tabulated as shown in the following table [26].

Medium	*State*	*Max Coefficient of Friction during*		*Avg Coefficient of Friction during*	
		Opening (5)	*Closing (5)*	*Opening*	*Closing*
Water	t = 86°F P_O = 123 bar (1,784 psi) 112 bar (1,624 psi)		0.13 0.15 0.17 0.18 0.21		Rises continuously with the number of tests
Water	t = 290°C (556°F) P_O = 120 bar (1,740 psi) 112 bar (1,595 psi)	0.39 0.39 0.38 0.36 0.36	0.41 0.41 0.41 0.41	0.38	0.41
Steam	Sat. Steam P_O = 100 bar (1,450 psi) 90 bar (1,305 psi)	0.38 0.36 0.38 0.33 0.33	0.41 0.40 0.38 0.38 0.38	0.36	0.39

Table 3.5
Friction Coefficients of a Parallel Disc Gate Valve Subjected to High Pressure and High Flow Tests [26]

The above frictional coefficients were conservatively estimated by KWU-Siemens using the seat inside diameter for the pressure area calculation. The coefficients of friction ranged from 0.33 to 0.41 after the initial cold water cycles. Initial low friction coefficients for cold water cycles were attributed to the original good surface finish of the contact surfaces according to the authors of the paper [26]. After testing with hot water and steam, the coefficient of friction obtained from the subsequent cold water test remained high, and

approximately in the same range as measured during hot water or steam tests. The same phenomenon has been observed in the NRC-sponsored blowdown tests on 6-inch and 10-inch valves by INEL [4,23,24]. The differences in the coefficients of friction from KWU-Siemens tests for hot water and steam are insignificant, as reflected in Table 3.5. The highest stem thrust occurred just after the flow isolation, as expected.

3.6. UK PWR Valve Testing

Results of high energy line break tests on parallel slide gate valves at 2,275 psi and 620°F flow conditions have also been reported by National Power Division of the CEGB [21]. Conventional parallel slide gate valves of original design, which use a round disc, suffered severe galling damage and required higher thrust to close than predicted by the manufacturer [21,41]. The problem was caused by tilting of the disc by fluid flow forces which results in point contact against the downstream seat, much in the same fashion as experienced in the conventional wedge gates tested under NRC-sponsored INEL tests.

Subsequently, tests were performed on an improved valve design, in which the lower part of the disc is made rectangular to provide a *line* contact at the lower edge of the disc, thus eliminating disc tilting and the potential of galling. (Independently, the same approach had been recommended by the principal investigators to Duke Power (see Footnote 1 on page 15).) The new valves have been successfully tested under the U.K. PWR valve qualification program with repeatable performance and no galling damage. The coefficients of friction found during these tests with improved parallel slide gate valves have been reported to be around 0.35 at the MOV User's Group meeting in Jupiter, Florida in January 1991. These results are in general agreement with the KWU-Siemens results summarized in Section 3.5 as well as the principal investigators' experience summarized in Section 3.2.

3.7. NRC-Sponsored INEL Test Data

Results of NRC-sponsored testing by INEL on 6-inch and 10-inch valves under high energy pipe break conditions are reported in detail in References 4 and 23. Two 6-inch flexible wedge gate valve designs were tested under Phase I. Testing was extended to Phase II, which included three 6-inch valves and three 10-inch flexible wedge gate designs made by four different U.S. valve manufacturers. The overall conclusions from these tests were that disc friction factors required to close the disc and achieve flow isolation were higher than the 0.3 that had been used in the standard industry sizing equation used by most valve manufacturers. Significant differences in the performance and in the amount of damage to the valve internals were found, which were due to differences in the specific design features used by the four manufacturers. Two of the valves, made by the same manufacturer, were found to have the most severe galling damage to the disc and

seat faces because of excessive disc guide clearance. These two valves were concluded to have *unpredictable behavior*, and were not used by INEL in their coefficient of friction evaluation.

INEL presented results from their detailed review of the data obtained from Phase I and Phase II testing at the MOV User's Group meeting held in Jupiter, Florida in January 1991. The results were presented in the form of a ratio of Normalized Sliding Load/Normalized Normal Load, which is the same as the coefficient of sliding friction. The *average* coefficient of friction was reported to be 0.4 for less than 70°F subcooling and 0.5 for water that is subcooled by more than 70°F. However, usable data for the > 70° subcooled testing were available for only two valves, whereas data for < 70°F subcooling were from six different valves.

This dependency of the coefficient of friction of Stellite vs. Stellite on the degree of subcooling of the flow media has not been reported by others, and it requires confirmation by additional testing. This testing should be done using valves that are clearly free of problems that tend to affect the assessment of coefficient of friction at the disc-to-seat interface, i.e., disc-to-seat galling, disc-to-guide galling, insufficient clearances between the guides and disc, the inaccuracy of alignment between the seat wedge plane and the disc wedge plane, etc.

As reported by KWU-Siemens (see Section 3.5), INEL testing also showed that the coefficient of friction between seat faces tested with room temperature water shows an irreversible increase after the valves are exposed to high temperature water or steam tests.

A detailed review of the NRC-sponsored Phase I and Phase II blowdown test results was also performed by EPRI to determine the applicability and limitations of these results to other operating conditions [24]. The disc factor during closing from these test results under disc sliding conditions to achieve flow isolation was reported by EPRI to range from 0.28 to 0.48 for the different gate valve designs. For the opening direction, the coefficient of friction was reported to range from 0.25 to 0.52. It is also stated in the EPRI report that the highest values of 0.48 and 0.52, which were encountered with only one of the valves, may not be due to simple sliding friction. The overall condition of the seating faces in this valve was found to be excellent. Even though a possible mechanism for the higher values was proposed qualitatively in the report [24], no conclusive quantitative explanation was given. This valve design needs to be reviewed further to derive more definite conclusions regarding the reason for apparently higher-than-expected coefficient of friction values based on the overall condition of the valve.

3.8. Conclusions from Presently Available Friction and Galling Data

The discussion on coefficient of friction and galling for Stellite vs. Stellite materials for gate valve applications can be concluded with the following observations and conclusions:

1. In our experience, the coefficient of friction of Stellite for normal sliding behavior *without galling* of the surfaces can range from 0.12 to 0.5 based on the presence or absence of an absorbed layer of lubricant at the sliding surfaces. Based on our assessment of the test results in Section 3, the typical range using cold water (without prior exposure of specimens to high temperature) is from 0.15 to 0.25, and with high temperature water or steam is from 0.3 to 0.4.

   Based on our experience, we have found that it is necessary to perform testing on actual components that duplicate the geometry and size of the sliding contact to obtain applicable friction data. Test specimens that have markedly different geometries and size can produce significantly different results than valves in actual application.

2. The absorbed contaminant layer of lubricant is sometimes only a few molecular layers in thickness; however, it can significantly alter the surface traction. The absorbed layers can be removed by abrading the two surfaces against each other in distilled water or by exposing the surfaces to high temperatures. Chemical solvents are typically not effective in removing the absorbed layer of lubricant. In gate valve applications, the absorbed surface layer may be gradually removed during cycling under differential pressure which causes high enough pressure at the contact. This can result in a gradual increase in coefficient of friction approaching values obtained with clean unlubricated surfaces.

3. Even though we have stated in Conclusion 1 that the normal range of coefficient of friction for Stellite can be up to 0.5, in our experience values above 0.4 are usually associated with some type of surface damage such as galling, excessive localized wear, significant change in surface roughness due to scratches, etc.

4. Threshold of galling stress for Stellite vs. Stellite for cyclic sliding applications is reported to be around 47 ksi. The average contact stress under the contact should be kept well below this to allow for higher local peaks in the contact area since the stress distribution is rarely uniform. To obtain valid galling data, it is important to faithfully duplicate the actual geometry, loading, and cycling conditions.

5. The initiation of localized galling at the sliding contact surface can either (1) result in continued damage and deterioration of the sliding surfaces along with an increase in friction forces or (2) heal itself by spreading until the average contact

stress falls below the threshold of galling. Whether or not localized galling will continue to spread until seizure or stabilize to a repeatable sliding behavior depends upon the local geometry and the magnitudes of the loads involved.

6. Under relatively low contact stresses, there is a significant difference in the self-mated coefficient of friction values for different alloys of Stellite, i.e., Stellite-1, Stellite-6, Stellite-12, and Stellite 21. Stellite-6 in self-mated tests is reported to have the highest coefficient of friction, and Stellite-6 against any of the other Stellite alloys has a significantly lower value. However, under the higher contact stresses typically encountered in valve seats, there is not much difference in their coefficients of friction.

7. Duke Power tests showed significantly lower coefficient of friction performance when using stainless steel disc and seats with Stellite overlay, instead of carbon steel disc and seats with Stellite overlay. The difference in performance may be due to iron content in the overlay caused by dilution from the base metal. The effect of iron content or other significant alloying constituents should be investigated in controlled tests.

8. When comparing coefficient of friction data obtained from valve tests performed by different organizations, it is important to distinguish whether the seat inside diameter or mean diameter was used; and whether the valve factor or coefficient of friction is being reported. The combined effect of these variations can easily amount to as much as 10 percent difference in the reported results.

4. PREDICTION OF THRUST OVERSHOOT DUE TO INERTIA

This section presents an *analytical* methodology to predict inertial thrust overshoot in motor operated gate valves. The industry has relied on some rules of thumb, and mostly experience, to make estimates of thrust overshoot. Actual testing using MOV diagnostic devices is the only method used to reliably quantify the magnitude of the thrust overshoot at the present time. In some cases, this results in unexpectedly higher thrusts that exceed the manufacturers' ratings of the valve or actuator components.

The principal investigators have developed an analytical methodology from first principles that can be used to predict thrust overshoot due to inertia. The predictions using this methodology have been compared against actual test data for the 4-inch Borg-Warner flexible wedge gate valve obtained by Duke Power Company in their Riverbend Steam Station flow loop. The overall comparison between the predictions and the test results show very good agreement, thus confirming that the methodology is sound. Additional comparisons against test data should be made to further validate and/or refine the analytical approach presented here. In the meantime, an analytical tool has been developed which the industry can use to improve the MOV reliability and performance.

The following sections present the details of the methodology. Appendix D documents the detail calculations used in comparison against Duke Power test data.

4.1. Description of the Inertial Overshoot Phenomenon

Figure 4.1 taken from Reference [25] shows a typical wedge gate valve stem thrust versus time curves for closing sequences under pump generated flow and no flow conditions. The stem thrust during the running portion of the closing stroke is low and nearly constant for both full flow and no flow conditions. As the disc approaches the closed position, the disc friction force begins to increase because of differential pressure buildup across the disc. After flow interruption, the disc friction force remains high and relatively constant during the time that the disc is sliding against the downstream seat with differential pressure across the disc. Stem thrust builds up rapidly after the wedge makes solid contact with both upstream and downstream seats. During the gate wedging action, the torque switch trips at a preset value to de-energize the actuator motor.

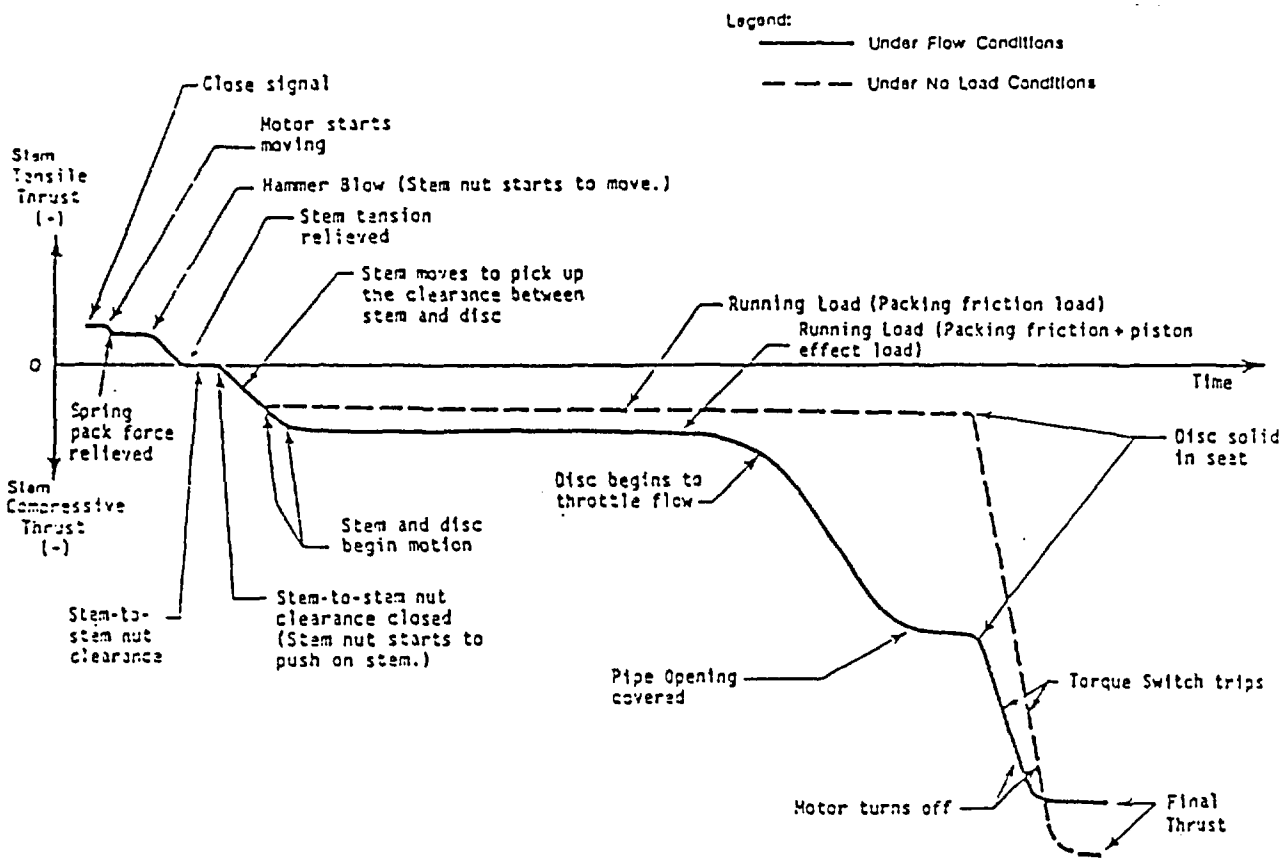

Notes:

1. Illustrated trace is for packing friction load exceeding piston effect load.
2. Not to scale.

Figure 4.1

Typical MOV Closing Sequence for Gate Valve-Stem Thrust Versus Time [25]

Inertia of the drive train between the motor through the worm gearing, stem nut, stem, and gate assembly can cause stem thrust overshoot after the torque switch trips and cuts off the current to the electric motor. Overshoot beyond the torque switch tripping point depends upon the kinetic energy of the system and the additional energy added to the MOV by the motor during the time delay of the contactor switch to cut off the electrical supply to the motor. The system energy available after the torque switch trips is used to overcome the disc frictional drag for the remainder of travel, and the excess is converted into strain energy in the system. The magnitude of stem thrust overshoot can be calculated considering the energy balance to account for various factors including inertia of the components, ΔP across the disc, component stiffness, and the distance of disc travel from torque switch trip point to final seating position, as shown in the following subsections. Appendix D documents the actual calculations for a 4-inch Borg-Warner flex wedge gate valve used in the Duke Power flow tests (see Footnote 1 on page 15).

4.2. Available Energy After Torque Switch Trip (TST)

After the torque switch trips, the motor continues to run for a short time due to time delay normally associated with the contactor dropout. Therefore, the energy available to wedge the disc further during the final stage of closing is the sum of motor work after the torque switch trips and the kinetic energy of the actuator and valve components at that instant. The method of estimating the available energy components are discussed in Sections 4.2.1 and 4.2.2.

4.2.1. *Motor Work After Torque Switch Trip*

The motor work after the torque switch trips can be estimated based on the time delay in contactor dropout and the motor running speed and torque at trip as:

$$W = \omega T \, \Delta\tau \qquad \text{(Eq. 4.1)}$$

where W = motor work after TST, in-lb

ω = motor shaft rotating speed at TST, rad/sec

T = motor running torque at TST, in-lb

$\Delta\tau$ = time delay in contactor dropout, sec

The motor work is calculated at the motor shaft location. Using the same method, the available work at the stem nut location can be estimated by replacing motor speed and torque with stem nut speed and torque. The available energy calculated at the stem nut location is expected to be lower than the available energy at the motor shaft location due to additional frictional loss from the motor shaft to the stem nut. The time delay in contactor dropout, depending on the specific motor design, can typically vary between 10 and 30 milliseconds.

4.2.2. *Kinetic Energy of Moving Components*

The kinetic energy stored in both actuator and valve components can be estimated using the following equations.

Rotating Components

The major rotating components in the valve assembly are the motor shaft, gears, worm, and worm gear assembly. The kinetic energy for the rotating components can be estimated as:

$$KE = \frac{1}{2} I\omega^2 \qquad \text{(Eq. 4.2)}$$

where I = mass moment of rotating inertia, in-lb-sec^2

ω = angular speed, rad/sec

Rectilinear Moving Components

Kinetic energy for rectilinear moving components such as stem and gate can be estimated as:

$$KE = \frac{1}{2} mV^2 \qquad \text{(Eq. 4.3)}$$

where m = mass of the disc and stem, lb-sec^2/in

V = disc velocity, in/sec

4.3. Stored Energy in Valve Components After Torque Switch Trip

Load-transmitting components from motor shaft to valve disc and seats experience different levels of stress and strain. The stored energy in the MOV components can be estimated using the following equations.

Axial Load

After torque switch trip (TST), the stored energy in an axially loaded valve component such as a stem is estimated as:

$$SE = SE_f - SE_t \qquad \text{(Eq. 4.4)}$$

where SE = stored energy in component after TST, in-lbs

SE_f = stored energy in component at final thrust, in-lbs

SE_t = stored energy in component at TST, in-lbs

or

$$SE = \frac{L}{2EA}\left(F_f^2 - F_t^2\right) \qquad \text{(Eq. 4.5)}$$

where L = effective component length, in.

E = elastic modulus, psi

A = cross-section area, in^2

F_f = final axial load, lb

F_t = axial load at TST, lb

Torsional Load

The stored energy for torsional load is estimated as:

$$SE = SE_f - SE_t \quad \text{(Eq. 4.6)}$$

$$= \frac{L}{2GJ}\left(T_f^2 - T_t^2\right) \quad \text{(Eq. 4.7)}$$

where L = effective component length, in.

G = modulus of rigidity

= $E/2(1 + \nu)$, psi

E = elastic modulus, psi

ν = Poisson's ratio

J = polar moment of inertia, in^4

T_f = final torque, in-lb

T_t = torque at TST, in-lb

Valve components such as motor shaft, worm, and stem are subjected to torsional loads during the final stage of valve closing.

General Spring Load

The axial load and torsional load cases can be considered as special cases of a general spring load case. Any linear elastic MOV component can be analyzed as a general spring as long as the component stiffness is known. This approach may be used in calculating the strain energy stored in the actuator spring pack, a disc spring, valve disc, or any other highly loaded/strained component of the MOV. The component stiffness may be derived from the available closed form solution, through experimental testing, or by performing detailed finite element analysis.

Stored energy in a linear elastic component is given by:

$$SE = \frac{1}{2} F_f \delta_f - \frac{1}{2} F_t \delta_t \quad \text{(Eq. 4.8)}$$

or

$$SE = \frac{1}{2K}\left(F_f^2 - F_t^2\right) \quad \text{(Eq. 4.9)}$$

where δ_f = final component deformation, in.

δ_t = component deformation at TST, in.

K = component stiffness, lb/in

4.4. Energy Dissipated After Torque Switch Trip

Other than the strain energy stored in the valve components, one of the major sources of energy consumption in the final stage of valve closing is the frictional loss between sliding components. The key areas where energy is dissipated after TST are summarized below:

Stem Packing Frictional Loss

Energy consumption due to stem packing friction is estimated as:

$$L_1 = F_1 \Delta d \qquad \text{(Eq. 4.10)}$$

where L_1 = stem packing frictional loss, in-lb

F_1 = stem packing frictional force, lb

Δd = distance of stem travel after TST, in.

The stem travel distance after TST, Δd, can be expressed in terms of stem thrust loads and gate stiffness and geometry as:

$$\Delta d = \frac{F_f - F_t}{2 K \sin\theta (\sin\theta + \mu \cos\theta)} \qquad \text{(Eq. 4.11)}$$

where F_f = final stem thrust, lb

F_t = stem thrust at TST, lb

K = disc and seat assembly stiffness (one side), lb/in.

θ = one-half wedge angle, deg

μ = coefficient of friction for disc and seat interface

Work Against Stem Rejection Force

During valve closing, the stem thrust is required to work against the stem rejection force. The energy loss after TST is:

$$L_2 = F_2 \Delta d = \frac{\pi}{4} d^2 P \Delta d \qquad \text{(Eq. 4.12)}$$

where d = stem diameter at packing, in.

P = pressure inside the valve body, psi

Frictional Loss Due to Disc Friction under ΔP

Energy loss due to the disc sliding against the downstream seat under ΔP is calculated as:

$$L_3 = F_3 \Delta d \qquad \text{(Eq. 4.13)}$$

where $$F_3 = \Delta P \times \frac{\pi}{4} d_s^2 \qquad \text{(Eq. 4.14)}$$

d_s = effective disc sealing diameter, in.

Frictional Loss Due to Disc Wedging

The disc frictional loss during final wedging can be estimated as:

$$L_4 = F_4 \Delta d \qquad \text{(Eq. 4.15)}$$

where $$F_4 = \frac{1}{2}(F_f + F_t) - (F_1 + F_2 + F_3) \qquad \text{(Eq. 4.16)}$$

Frictional Loss in Worm/Worm Gear and Stem/Stem Nut Connections

Energy loss due to friction between the worm/worm gear or stem/stem nut interfaces can be estimated by using the worm gear/threaded connection efficiency as shown below [36]:

Output Energy = e x input energy

where $$e = \frac{\cos\theta_n - \mu \tan\lambda}{\cos\theta_n + \mu \cot\lambda} \qquad \text{(Eq. 4.17)}$$

θ_n = one-half of the thread angle, deg

μ = coefficient of friction

λ = lead angle, deg

4.5. Energy Balance and Final Thrust Prediction

After all of the energy components are known, the final thrust, F_f, can be calculated by considering the overall energy balance after torque switch trip:

Total available energy = total stored energy + total dissipated energy

Total available energy is the combination of kinetic energy of the moving components and the motor work due to contactor dropout delay after torque switch trip, as described in Section 4.2. Stored and dissipated energies are calculated using the equations given in Sections 4.3 and 4.4. Appendix D documents detailed calculations using the above described energy balance approach to predict stem thrust overshoot. The overall results of this comparison are presented next.

4.6. Comparison of Predicted Final Thrust Against Test Results

The calculations along with the relevant assumptions documented in Appendix D show a predicted final thrust of 20,535 pounds for the 4-inch Borg-Warner flex wedge gate valve tested under a maximum differential pressure of 2,000 psi, with torque switch tripping at 17,615 pounds. This final thrust of 20,535 pounds is in good agreement with the actual final thrust that was measured to be 20,963 pounds using strain gages on the stem. The overall comparison over 31 test cycles and the corresponding analytical predictions was found to be within 9 percent for this valve.

From this comparison, it is concluded that the overall analytical methodology presented in this report to predict stem thrust overshoot is sound. Further comparison should be made against test results for valves of other sizes and other manufacturers to validate and refine the assumptions used in the inertia overshoot model. This model presents the analytical capability to predict final thrust due to inertia overshoot in the MOVs, for the first time. This predictive capability can be used to improve the sizing and avoid overthrusting of MOVs.

5. FACTORS AFFECTING OPENING THRUST REQUIREMENTS

Opening thrust requirements for gate valves to overcome the disc friction load were presented in Section 2 for different types of gate valve designs. Unlike in the case of closing operations, the disc friction load in the *opening* direction is not only dependent upon the differential pressure across the disc , but is also significantly affected by other factors. These factors are:

1. Wedging force the previous closing cycle, including the effect of inertia overshoot.
2. High body cavity pressure, resulting in the energization of both the upstream and the downstream discs.
3. External piping loads causing disc pinching/sticking.
4. Temperature transients causing thermal binding of the disc.

Even though all of these factors can have significant impact on the operability of the valve during opening, they do not lend themselves to reliable quantification and are therefore not used in actual sizing calculations. In practice, the effect of these variables on the operability performance has been *minimized* by bypassing the torque switch during the first portion of the opening stroke, which makes the *maximum* actuator output available to initiate opening. The problems caused by these factors, however, do surface when the magnitude of the disc friction force increase due to these effects exceeds the actuator output.

This section provides an insight into these problems and how they affect the gate valve operability in the opening direction. It also summarizes some analytical approaches that have been used by the principal investigators to quantitatively investigate the magnitude of these problems and assess design modifications or alternative valve designs to solve them. The method of analysis can assist the valve manufacturers in making design improvements.

5.1. Effect of Wedging Force From the Previous Closing Operation

The final wedging force, F_N, from the previous closing cycle, affects the magnitude of the opening force required. For the same switch settings on a MOV, the final wedging force can vary because the inertia overshoot is affected by the magnitude of the differential pressure across the disc. Typically, the highest wedging force is introduced when the valve is closed without any differential pressure. The equations given in Section 2 of this report can be used to quantify the unwedging force during opening if the wedging force is known. The inertia overshoot effect on the final wedging force can be quantitatively addressed by analytical techniques presented in Section 4, or by actual testing. Regardless of the approach used, the dependence of the opening thrust during unwedging on the wedging

force from the previous cycle should be assessed to ensure that the actuator output is sufficient. This is currently not a standard practice in MOV sizing.

5.2. Effect of Higher Bonnet Pressure on Some Gate Valve Designs

Gate valves of the types known as flexible wedge, spilt wedge and double disc (See figures 2..1 a , b and c) have the ability to seal against both seats at the same time. The problem is related to only these types of valves where the two disc seating surfaces can move independently of each other; therefore, solid wedge gates do not experience this problem. Two types of conditions can arise that lead to a higher pressure in the body cavity or bonnet area than in either upstream or downstream piping:

1. When the valve is closed, fluid may be entrapped in the body cavity, and if the system is then heated up, an uncontrollable rise in pressure in the body cavity can result. The reported effects of such pressure increase range from inability to open the valve, to the structural failure of the internal parts, or failure of the valve bonnet [50].

2. When the valve is in its closed position under a certain upstream pressure, and this upstream pressure is subsequently reduced, e.g. due to the tripping of an upstream pump, the original (higher) upstream pressure may remain trapped in the body cavity. This can result in an increase in the opening thrust requirements due to the energization of both the upstream and downstream disc seating faces. This condition is referred to as *double disc friction* or *double disc drag [16].*

Regardless of which of these two factors are responsible, the total disc friction force for a double drag condition can be expressed as:

$$F_{dt} = F_{d1} + F_{d2}$$
$$= \mu \frac{\pi}{4} d_S^2 (P_b - P_1) + \mu \frac{\pi}{4} d_S^2 (P_b - P_2)$$
$$= \mu \frac{\pi}{4} d_S^2 (2P_b - P_1 - P_2)$$

where F_{dt} = total disc drag force, lb
F_{d1} = upstream disc drag force, lb
F_{d2} = downstream disc drag force, lb
μ = coefficient of friction for the disc/seat interface
d_S = disc sealing diameter, in.
P_1 = upstream pressure, psi
P_2 = downstream pressure, psi
P_b = valve body cavity pressure, psi

The effect of lowering the upstream pressure before opening the gate on the stem thrust can be illustrated in the following example.

Let P_1 = 1,250 psi for the case of steady upstream pressure

P'_1 = 350 psi for the case of lowered upstream pressure before opening

P_b = 1,250 psi for valve body cavity pressure

P_2 = 0 psi for downstream pressure after closing

Then
$$\frac{F'_{dt}}{F_{dt}} = \frac{\text{Lowered upstream pressure case}}{\text{No change in upstream pressure case}} = \frac{2P_b - P'_1 - P_2}{2P_b - P_1 - P_2}$$
$$= \frac{2 \times 1{,}250 - 350 - 0}{2 \times 1{,}250 - 1{,}250 - 0} = \frac{2{,}150}{1{,}250} = 172\% \quad \leftarrow$$

In this example, the stem force required to overcome the disc drag is *increased* by 72 percent when the upstream pressure was *lowered* from 1,250 psi to 350 psi [16].

Provision must be made to eliminate the possibility of this excessive pressure build-up in the body cavity to avoid excessive disc drag as well as structural damage. Simple methods of mitigating body pressure increase to avoid double disc drag condition can be achieved by equalizing the body cavity and upstream pressures with a single drilled hole, an external by-pass piping, an internal or external relief valve, etc., as detailed in Reference 16. Each of these options have their advantages and limitations which must be carefully reviewed before selecting the one which is the most appropriate one for the specific application being considered.

5.3. Effect of External Piping Loads

Variations in pressure, temperature, and piping load in a nuclear power plant piping system can exert significant forces at the ends of the valve body, resulting in valve body and seat plane distortions. Normally the valve body is much stronger than the connecting pipe; therefore, external pipe loads on the valve are not of concern from the standpoint of the structural integrity of the valve. The main concern about external piping loads on a gate valve is the valve operability under these loads, especially for certain types of wedge gate and expanding gate valves. As a wedge gate valve is closed, the space between the seats is taken up by the relatively stiff gate with metal-to-metal contact on both upstream and downstream seats.

Any changes in external piping load that tend to reduce the distance between the seat faces after the valve is closed can cause gate "pinching" or "binding". Depending upon the magnitude of those external loads and the stiffness of the valve members, the stem thrust

required to open the valve may increase. Load components that have the most significant effect are the axial compressive loads, and bending moments. Torsional and shear loads have negligible effect on the seat face distortions and opening thrust requirements in gate valves.

The effect of these external piping loads is most pronounced on solid wedge type gate valves. Some of the parallel expending gate valve designs also have high gate stiffness and therefore exhibit high sensitivity to piping loads. The use of flexible wedge disc reduces the sensitivity of the valve to piping loads. However, it should be noted that the actual axial stiffness of the disc needs to be significantly less than that of the valve body to ensure that its sensitivity to piping loads is negligible. Appendix E compares the predictions in opening thrust increase for a relatively stiff gate design used in an 18-inch parallel expanding gate valve against a flexible wedge design. Based on the assumptions stated in that appendix, it is shown that the stiff gate design could experience approximately a 32 to 36 percent increase in opening stem thrust, whereas a flexible wedge gate opening thrust is predicted to increase by only 12 percent under the applied axial load.

In summary, it is important to know that even a flexible wedge disc will experience *some*, no matter how small, increase in opening thrust under compressive pipe load. Therefore, simply specifying a flexible wedge gate design does not ensure immunity from the effect of external piping loads. The valve manufacturers should *quantitatively* design the disc stiffness and body stiffness that ensures that resultant increase in opening stem thrust under anticipated pipe loads is less than a specified percentage of the normal operating load due to differential pressure. At least one of the U.S. valve manufacturers has published quantitative test results that show that increase in opening stem thrust is 5 percent or less in their valve design [27].

Another approach that eliminates the effect of external piping loads on opening stem thrust requirements is to close the valve with no wedging, if the seat leakage requirements permit it.

5.4. Effect of Temperature Changes on Opening Thrust

Some wedge gate valves exhibit "thermal binding" problems when they are closed hot, and then allowed to cool down with the disc in the wedged position. Thermal binding is caused by the body cooling down at the higher rate than the disc, thus causing an increase in the seat contact force. The magnitude of increase in the seat contact force depends upon the change in temperature, the difference in coefficient of thermal expansion between the body and gate, the stiffness of the valve body and gate, and the distance between the seat faces. Quantitatively, this increase in seat contact force, ΔF, can be evaluated from the following equation (see Appendix F for details):

$$\Delta F = L_o(\alpha_b - \alpha_g)\Delta T \frac{K_b K_g}{(K_b + K_g)}$$

where L_o = distance between seat faces

α_b = coefficient of thermal expansion for valve body material

αg = coefficient of thermal expansion for gate material

K_b = valve body stiffness along the flow axis

K_g = gate stiffness along the flow axis

The contact force increase can be negligible or high depending upon the actual materials, valve and gate stiffness, and temperature variations. The opening thrust increase is the product of ΔF and the coefficient of friction.

Another phenomenon related to the temperature effects that can also cause thermal binding is the net growth of stem length when the valve is closed. This is caused by a net increase in the overall length of the stem due to the previously exposed area of the stem being inserted into the higher temperature environment inside the body.

Appendix F shows a quantitative example of a 3-inch solid wedge gate valve subjected to temperature changes as described above. For the assumption stated in the appendix, an increase of 3,943 lbs, which is equivalent to 60 percent of the stem thrust needed to overcome the differential pressure load is predicted. The example also shows that gate stiffness, gate and seat materials, and temperature variations of the valve components have a significant influence on the calculated seat contact force. To reduce the thermal binding effects, one may consider the use of a flexible disc; favorable material combinations of disc, seat, and stem; and minimizing temperature changes in valve components. Actual testing of the valve designs to qualify their relative immunity to thermal binding effects is the most reliable approach to address these problems. Some of the valve manufacturers have performed such tests. In order to ensure freedom from thermal binding problems, the valve manufacturer should be requested to provide *quantitative* date to support their valve design.

It should be pointed out that parallel slide discs are relatively immune to the thermal binding problems, as well as gate pinching problem due to external loads.

6. CONCLUSIONS

All of the objectives stated for the SBIR Phase I effort have been fulfilled. Several improvements in the analytical models have been made, as discussed in Sections 2 through 5. A significant contribution has been made by the principal investigators by providing an analytical methodology to predict inertial thrust overshoot in an MOV gate valve. A comprehensive review of friction and galling data applicable to gate valves is provided. A preliminary analytical approach to quantify localized contact stresses due to disc tilting has been developed. The concept of an *index of contact stress severity* has been introduced which can be used to determine the potential for unpredictable behavior in gate valves. However, an extensive matrix of tests is needed to empirically correlate the index of contact stress severity to the actual performance of gate valves over a wide range of conditions.

It is concluded that the Phase I effort was successful in completing the *preliminary* development of improved analytical models to predict operability of the motor operated gate valves. This can serve as a good foundation for continued analytical and empirical development that is necessary to provide *reliable* and *proven* gate valve operability models to the nuclear power industry.

7. REFERENCES

1. U.S. NRC IE Bulletin 85-03: *Motor Operated Valve Common Mode Failures During Plant Transients Due to Improper Switch Settings*, November 11, 1985.

2. U.S. NRC Generic Letter 89-10: *Safety-Related Motor-Operated Valve Testing and Surveillance*, June 28, 1989.

3. T. G. Scarbrough. *Action Plan for Motor-Operated Valves and Check Valves*, U.S. NRC, NUREG-1352, June 1990.

4. K. G. DeWall and R. J. Steele. *BWR Reactor Water Cleanup System Flexible Wedge Gate Isolation Valve Qualification and High Energy Flow Interruption Test*, NUREG/CR5406 (Vols. 1, 2, & 3), U.S. Nuclear Regulatory Commission, October 1989.

5. Owen O. Rothberg. *In-Situ Testing of Motor Operated Valves in Nuclear Power Plants*, presented at 17th Water Reactor Safety Meeting, Rockville, MD, October 1989.

6. Jim Tills. *Motor-Operated Valve (MOV) Failure Trends in the Nuclear Industry*, EPRI Power Plant Valves Symposium, October 1988.

7. D. D. Reiff. *NRC Activities Related to Pump and Valve Operability*, ASME Paper No. 80-C2/PVP-31.

8. E. J. Brown and F. S. Ashe. *Survey of Valve Operator-Related Events Occurring During 1978, 1979, and 1980*, U.S. NRC, AEOD/C203, May 1982.

9. Earl J. Brown. *A Review of Motor-Operated Valve Performance*, U.S. NRC, AEOD/C603, December 1986.

10. W. L. Greenstreet, G. A. Murphy, and D. M. Eissenberg. *Aging and Service Wear of Electric Motor-Operated Valves Used in Engineered Safety-Feature Systems of Nuclear Power Plants*, U.S. NRC, NUREG/CR-4234, Vol. 1, June 1985.

11. H. D. Haynes. *Aging and Service Wear of Electric Motor-Operated Valves Used in Engineered Safety-Feature Systems of Nuclear Power Plants*, U.S. NRC, NUREG/CR-4234, Vol. 2, 1989.

12. *Investigation of Valve Failure Problems in LWR Power Plants*, DOE, Report No. ALO-73, April 1980.

13. *Guide for the Application and Use of Valves in Power Plant Systems*, EPRI Report No. NP-6516, August 1990.

14. *Failure of Borg-Warner Gate Valves to Close Against Differential Pressure*, NRC Information Notice No. 89-61, August 30, 1989.

15. Cancelled.

16. Cancelled.

17. Cancelled.

18. Cancelled.

19. M. S. Kalsi and D. C. Guerrero. *Finite Element Aids Non-Circular Valve Specification*, **Hydrocarbon Processing**, May 1982.

20. M. S. Kalsi and B. L. McDougal. *Moment Capability of Valves Using Semi-Analytical Finite Element Approach*, ASME Paper 76-PET-38.

21. P. T. George and S. Bryant. *Valve Testing for UK PWR Safety Application*, presented at 17th Water Reactor Safety Meeting, Rockville, MD, October 1989.

22. B. Zeigler et al. *Evolution of Test Requirements for Valves in PWR Power Plants (in France)*, presented at the International Conference on Operability of Nuclear Systems in Normal and Adverse Environments, Lyon, France, September 1989.

23. R. Steel, K. G. DeWall, and J. Watkins. *Flexible Wedge Gate Valve Testing Program Phase II Results and Analysis*, NUREG/CR-5558, U.S. Nuclear Regulatory Commission, 1990.

24. P. Damerell, T. Lubnow, and T. Walker. *Review of NRC/INEL Gate Valve Test Program Research Project 3343-03*, Electric Power Research Institute report, 1990.

25. W. Grant and R. Keating. *Application Guide for Motor-Operated Valves in Nuclear Power Plants*, NP-6660-D, Electric Power Research Institute , 1990.

26. U. Simon, N. Rauflmann, and H. Schafer. *Testing of Safety-Related Valves of PWR and BWR Power Plants*, **Pipeline Dynamics and Valves**, Vol. 180, American Society of Mechanical Engineers, 1989.

27. E. Bake. *Design Basis Qualification of Equiwedge Gate Valves for Safety-Related MOV Applications*, V-Rep-90-1, Edward Valves, Inc., 1990.

28. Baumeister and Marks. **Standard Handbook for Mechanical Engineers**, 7th Ed., McGraw-Hill, 1967.

29. E. Rabinowicz. **Friction and Wear of Materials**, John Wiley & Sons, 1965.

30. I. E. Idelchik. **Handbook of Hydraulic Resistance**, 2nd Ed., Hemisphere Publishing Company, 1986.

31. R. D. Blevins. **Applied Fluid Dynamics Handbook**, Van Nostrand Reinhold Co., 1984.

32. G. M. White and D. F. Denny. *The Sealing Mechanism of Flexible Packings*, (British) Ministry of Supply, Memorandum No. 3/47, 1967.

33. D. E. Turnbull. *The Sealing Action of a Conventional Stuffing Box*, British Hydromechanics Research Association, Research Report No. 592, 1958.

34. D. F. Denny and D. E. Turnbull. *Sealing Characteristics of Stuffing Box Seals for Rotating Shafts*, **Proceedings of Institution of Mechanical Engineers**, Vol. 54, No. 6, London, 1960.

35. J. A. Aikin. *Evaluation of a Composite Anti-Extrusion Ring*, Chalk River Laboratories, Ontario, September 1990.

36. J. Shigley. **Mechanical Engineering Design**, 4th Ed., McGraw-Hill, 1983.

37. Rourk and Young. **Formulas for Stress and Strain**, 5th Ed., McGraw-Hill, 1975.

38. R. C. Juvinall. **Stress, Strain, and Strength**, McGraw-Hill, 1967.

39. A. Bossier and G. Guillot. *Valve Tests at Electricite de France*, **Revue Generale Nucleaire**, September-October 1985.

40. Z. A. Foroulis. *Guidelines for the Selection of Hardfacing Alloys for Sliding Wear Resistant Applications*, **Wear**, Vol. 96, pp. 203-218, 1984.

41. NRC Information Notice No. 90-72: *Testing of Parallel Disc Gate Valves in Europe*, issued by U.S. Nuclear Regulatory Commission, November 28, 1990.

42. Bhushan and Gupta. **Handbook of Tribology**, McGraw-Hill, Inc., 1991.

43. I. V. Kragelsky, M. N. Dobychin, and V. S. Kombolov (USSR). **Friction and Wear Calculation Methods**, Pergamon Press, 1982.

44. **Haynes Wrought and Wear Resistant Alloys**, catalog, Cabot Corporation, Stellite Division (1977 data). [f = 0.119 for Stellite against Stellite].

45. *Product Data Bulletin S-56B*, ARMCO Steel, Advanced Materials Division, Middletown, Ohio.

46. W. J. Schumacher. *Wear and Galling Can Knock Out Equipment*, **Chemical Engineering**, May 9, 1977.

47. J. C. Moyers and D. M. Eissenberg. *A Gate Valve Closure Model to Investigate Disk-Seat Interference*, ORNL Letter Report, May 8, 1990.

48. K.J. Bhansali and A.E. Miller, *Role of Stacking Fault Energy on the Galling and Wear Behavior of a Cobalt Base Alloy*, **Wear of Material**, American Society of Mechanical Engineers, New York, N.Y., 1981.

49. P. Crook, *The Development of a Series of Wear Resistant Materials with Properties Akin to those of the Cobalt-Chromium Alloys*, **Wear of Materials**, American Society of Mechanical Engineers, New York, N. Y., 1981.

50. U. S. NRC IE Circular 77-05: *Fluid Entrapment in Valve Bonnets*, March 29, 1977.

51. NRC Licensee Event Report, San Onofre Nuclear Generating Station, Unit 1, September 11, 1981.

Appendix A
Opening and Closing Stem Thrusts for Variations in Disc Designs

Appendix A
Opening and Closing Stem Thrusts for Variations in Disc Designs

This appendix provides a detailed analysis of stem thrust required to close or open the disc in the gate valve designs shown in Section 2 of this report. The analysis is based on free body equilibrium considerations of the disc.

A.1. DISC FORCE EQUILIBRIUM: STEM LOAD FOR SOLID, FLEXIBLE, AND SPLIT WEDGE GATE VALVES

A.1.1. Stem load to overcome ΔP - Closing

$$\sum F_x = 0,$$

$$F_p \cos\theta - F_N \cos\theta + F_f \sin\theta = 0, \textit{ and}$$

$$F_f = \mu F_N$$

$$\therefore \quad F_N = \left(\frac{\cos\theta}{\cos\theta - \mu \sin\theta}\right) F_p \quad \leftarrow$$

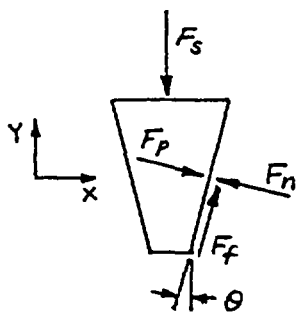

Figure A.1
Gate Equilibrium under ΔP Load During Closing

$$\Sigma F_y = 0,$$

$$F_s = F_f \cos\theta + F_N \sin\theta - F_p \sin\theta, \text{ and}$$

$$F_f = \mu F_N = \mu \left(\frac{\cos\theta}{\cos\theta - \mu \sin\theta}\right) F_p$$

$$\therefore \quad F_s = \left(\frac{\mu}{\cos\theta - \mu \sin\theta}\right) F_p \quad \leftarrow$$

where
- F_p = disc pressure load, lb = differential pressure x area
- F_s = stem load, lb
- F_N = seat normal load, lb
- F_f = seat frictional load, lb
- μ = coefficient of friction between disc and seat
- θ = one-half of wedge angle, deg

A.1.2. Stem load to overcome ΔP - Opening

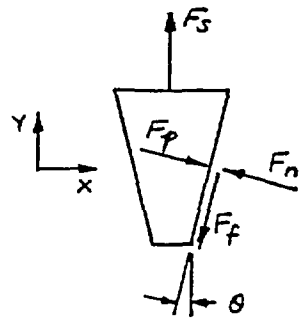

Figure A.2
Gate Equilibrium under
ΔP Load During Opening

$$\sum F_x = 0,$$

$$F_p \cos\theta - F_N \cos\theta - F_f \sin\theta = 0, \text{ and}$$

$$F_f = \mu F_M$$

$$\therefore \quad F_N = \left(\frac{\cos\theta}{\cos\theta + \mu \sin\theta}\right) F_p \qquad \leftarrow$$

$$\sum F_y = 0,$$

$$F_s = F_p \sin\theta - F_N \sin\theta + F_p \cos\theta, \text{ and}$$

$$F_f = \mu F_N = \mu \left(\frac{\cos\theta}{\cos\theta + \mu \sin\theta}\right) F_p$$

$$\therefore \quad F_s = \left(\frac{\mu}{\cos\theta + \mu \sin\theta}\right) F_p \qquad \leftarrow$$

A.1.3. Stem wedging load - Closing

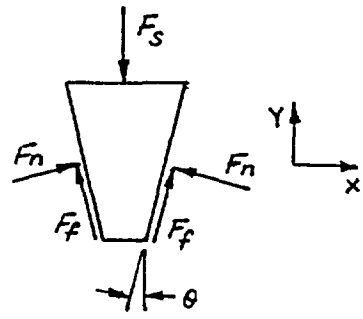

Figure A.3
Gate Equilibrium under Wedging Load
During Closing

The stem wedging load is the required stem thrust to overcome the seat frictional resistance of a wedge gate.

$$\sum F_y = 0,$$

$$F_s = 2\left(F_N \sin\theta + F_f \cos\theta\right), \text{ and}$$

$$F_f = \mu F_N$$

$$\therefore \quad F_N = \frac{1}{2(\sin\theta + \mu \cos\theta)} F_s \qquad \leftarrow$$

$$\text{or} \quad F_s = 2\ (\sin\theta + \mu \cos\theta)\, F_N$$

A.1.4. Stem unwedging load - Opening

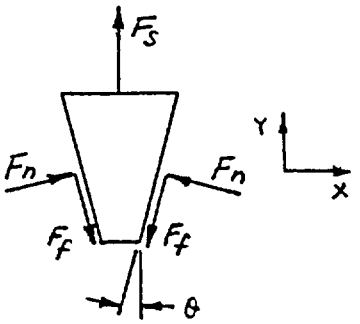

$$\sum F_y = 0,$$

$$F_s = 2\left(F_f \cos\theta - F_N \sin\theta\right), \textit{ and}$$

$$F_f = \mu F_N$$

$$\therefore \quad F_N = \frac{1}{2\left(\mu \cos\theta - \sin\theta\right)} F_s \qquad \leftarrow$$

$$\text{or} \quad F_s = 2\left(\mu \cos\theta - \sin\theta\right) F_N$$

Figure A.4
Gate Equilibrium under Unwedging Load During Opening

A.2. STEM LOAD FOR PARALLEL EXPANDING GATE VALVES — THROUGH CONDUIT AND DOUBLE DISC

A.2.1. Stem load to overcome ΔP - Closing and Opening

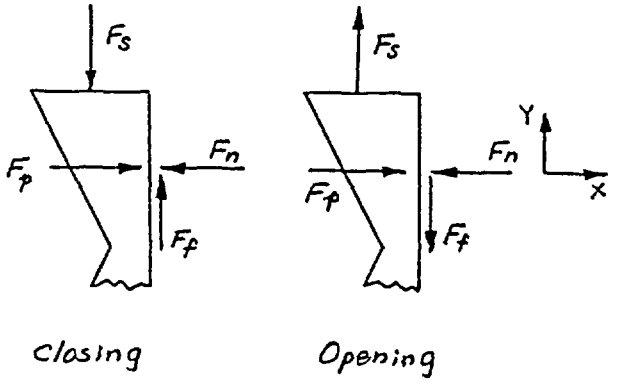

Figure A.5
Gate Equilibrium under ΔP Load During Closing/Opening

$$\sum F_x = 0,$$

$$F_p = F_N$$

$$\sum F_y = 0$$

$$F_s = F_f - \mu F_N = \mu F_p$$

$$\therefore \quad F_s = \mu F_p \qquad \leftarrow$$

This equation applies to both gate closing *and* opening conditions.

A.2.2. Stem wedging load - Closing

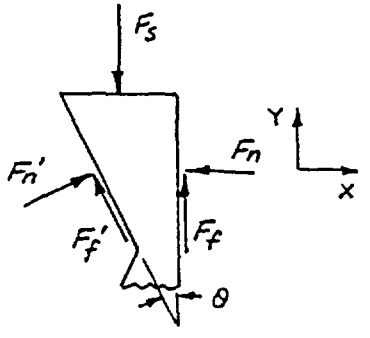

Figure A.6
Gate Equilibrium under Wedging Load During Closing

$$\sum F_x = 0,$$

$$F'_N \cos\theta - F'_f \sin\theta = F_N, \text{ and}$$

$$F'_f = \mu' F'_N$$

$$\therefore \quad F'_N = \frac{1}{\cos\theta - \mu' \sin\theta} F_N$$

$$\sum F_y = 0,$$

$$F_s = F'_N \sin\theta + F'_f \cos\theta + F_f \text{ and}$$

$$F_f = \mu F_N, F'_f = \mu' F'_N$$

$$\therefore \quad F_s = \frac{(1 - \mu\mu')\sin\theta + (\mu + \mu')\cos\theta}{\cos\theta - \mu' \sin\theta} F_N \qquad \leftarrow$$

For $\mu = \mu'$, this equation becomes:

$$F_s = \left(\frac{\sin\theta\left(1 - \mu^2\right) + 2\mu\cos\theta}{\cos\theta - \mu\sin\theta} \right) F_n$$

A.2.3. Stem unwedging force - Opening

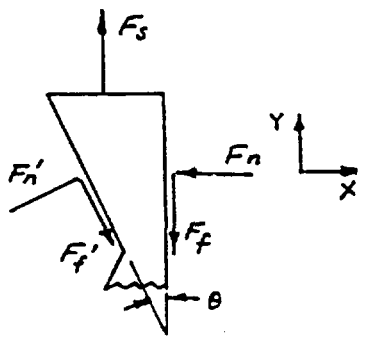

Figure A.7
Gate Equilibrium under Unwedging Load During Opening

$$\sum F_x = 0,$$

$$F_N' \cos\theta + F_f' \sin\theta = F_N, \text{ and}$$

$$F_f' = \mu' F_N'$$

$$\therefore \quad F_N' = \frac{1}{\cos\theta + \mu' \sin\theta} F_N \qquad \leftarrow$$

$$\sum F_y = 0,$$

$$F_s = F_f' \cos\theta - F_N' \sin\theta + F_f \text{ and}$$

$$F_f = \mu F_N, \; F_f' = \mu' F_N'$$

$$\therefore \quad F_s = \frac{(\mu\mu' - 1)\sin\theta + (\mu + \mu')\cos\theta}{\cos\theta + \mu' \sin\theta} F_N \qquad \leftarrow$$

For $\mu = \mu'$, this equation becomes:

$$F_s = \left(\frac{(\mu^2 - 1)\sin\theta + 2\mu\cos\theta}{\cos\theta + \mu\sin\theta} \right) F_n$$

A.3. STEM LOAD FOR PARALLEL SLIDING GATE VALVES

A.3.1. Stem load to overcome ΔP - Closing and Opening

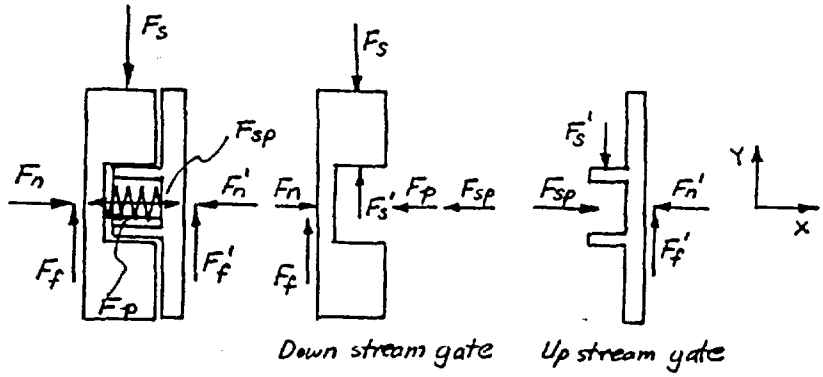

Figure A.8
Gate Equilibrium under ΔP Load During Closing

Assume that the coefficient of friction on both sides of the seats are the same; then for the downstream disc, we obtain

$$\Sigma F_x = 0,$$

$$F_N = F_p + F_{sp}$$

where

F_{sp} = spring load between parallel gates, lb

$$\Sigma F_y = 0$$

$$F_s = F_f + F_s'$$

where F_s' = upstream gate resisting force, lb

And for the upstream disc, we obtain

$$\Sigma F_x = 0,$$

$$F'_N = F_{sp}$$

$$\Sigma F_y = 0$$

$$F'_s = F'_f$$

$$\therefore \quad F_s = F_f + F'_s = F_f + F'_f = \mu (F_N + F'_N)$$

$$F_s = 2\mu F_{sp} + \mu F_p \qquad \leftarrow$$

This equation applies to both opening and closing directions.

Appendix B
Disc Load Calculations for a Gate Valve In a Pump Flow System

Appendix B
Disc Load Calculations for a Gate Valve
In a Pump Flow System

Based on available test data for a 4-inch Borg-Warner flexible wedge gate valve tested under typical pump flow conditions at Duke Power Company's flow loop (see Footnote 1 on page 15 of main text), a simple analysis is presented in this Appendix to approximately quantify the forces acting on the disc in mid-travel. Section 2.6 and 3.4 describe test results and their analysis for this valve.

The pressure drop across the disc is estimated by using the gate valve flow resistance data from References [30] and [31]. The flow velocity used in the pressure drop calculations depends on pump characteristics and the overall piping system design. Finally, the pressure load is computed based on the calculated pressure drop and the gate opening position.

B.1. GATE VALVE FLOW RESISTANCE COEFFICIENT

The flow resistance coefficient as defined in Section 2 is given by:

$$K = \frac{2\,\Delta P}{\rho\, V^2}$$

where K = flow resistance coefficient

ΔP = differential pressure across the valve, lb/ft^2

ρ = mass density of the fluid, $slug/ft^3$

V = flow velocity, ft/sec

Flow resistance coefficient data available from References [30] and [31] for gate valves are summarized in Table B.1. Overall average values from these data are plotted in Figure B.1 for reference.

Gate Valve Description	*Gate Position, h/Do**										
	0.1	*0.15*	*0.2*	*0.3*	*0.4*	*0.5*	*0.6*	*0.7*	*0.8*	*0.9*	*1.0*
Gate valve in straight pipe without a recess for the disc	150	62	35	10	4.6	2.06	0.98	0.44	0.17	0.06	0
Gate valve in straight pipe with a recess for the disc	200	77	33	11	4.7	2.35	1.23	0.67	0.31	0.11	0.05
Gate valve at the exit	200	64	36	14.2	7.1	3.85	2.3	1.4	0.75	0.21	0.11
Gate valve with reduced port	200	77	34	12.5	6.5	3.65	2.15	1.35	0.71	0.24	0.07
Gate valve tested at U. of Wisconsin**	212	155	90	23	15	4.5	4	3.5	2.5	1.5	0.38
Conventional gate valve	100	72	43	15	7.5	3.5	2	1.5	0.6	0.4	0.25
Disc type gate valve**	190	72.9	35.7	12.7	5.7	2.7	1.34	0.6	0.24	0.07	0
Total Average	**179**	**82.8**	**43.8**	**14.1**	**7.3**	**3.23**	**2.0**	**1.35**	**0.75**	**0.37**	**0.12**

* Gate position is represented by h (gate opening) and Do (pipe inside diameter at gate)

** Average flow resistance coefficient for the valve type. Data may be interpolated/extrapolated to other gate positions without specific test data.

Table B.1

A Comparison of Gate Valve Flow Resistance Coefficients
(Data from References 30 and 31)

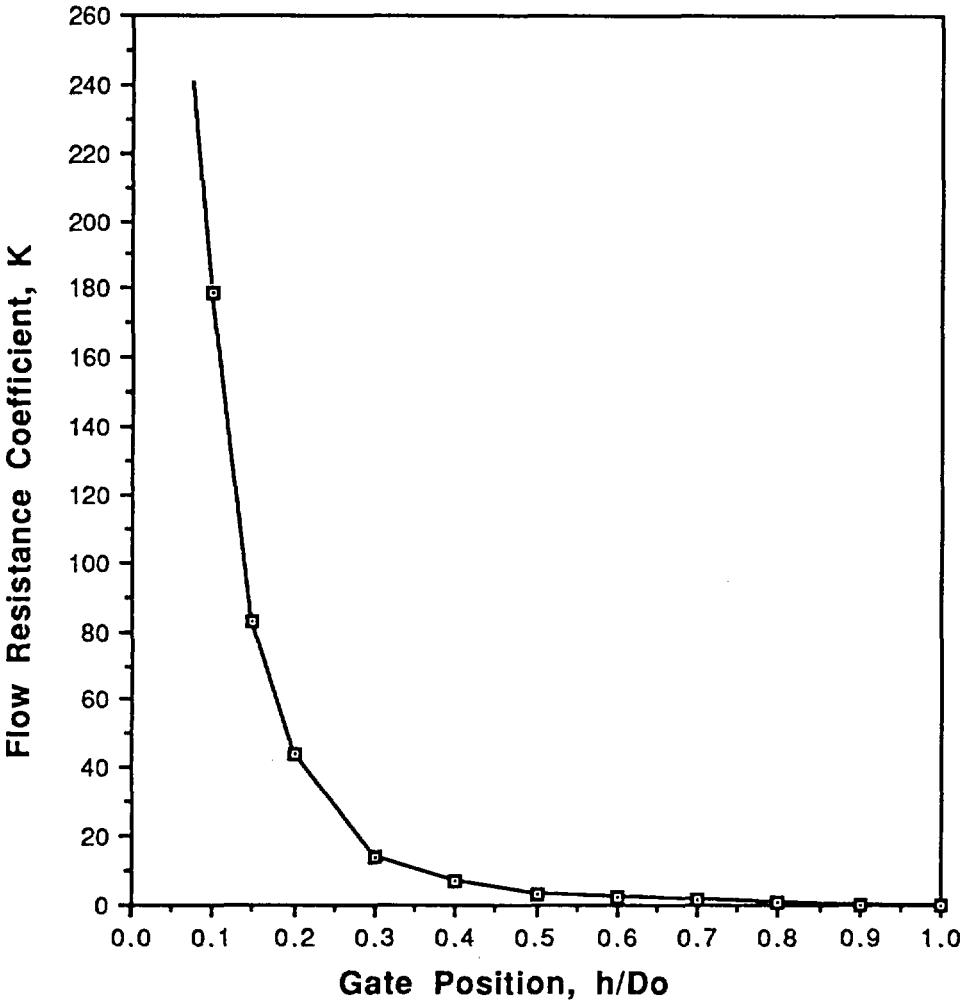

Figure B.1

Average Flow Resistance Coefficient Variation as a Function of Disc Travel for Gate Valves

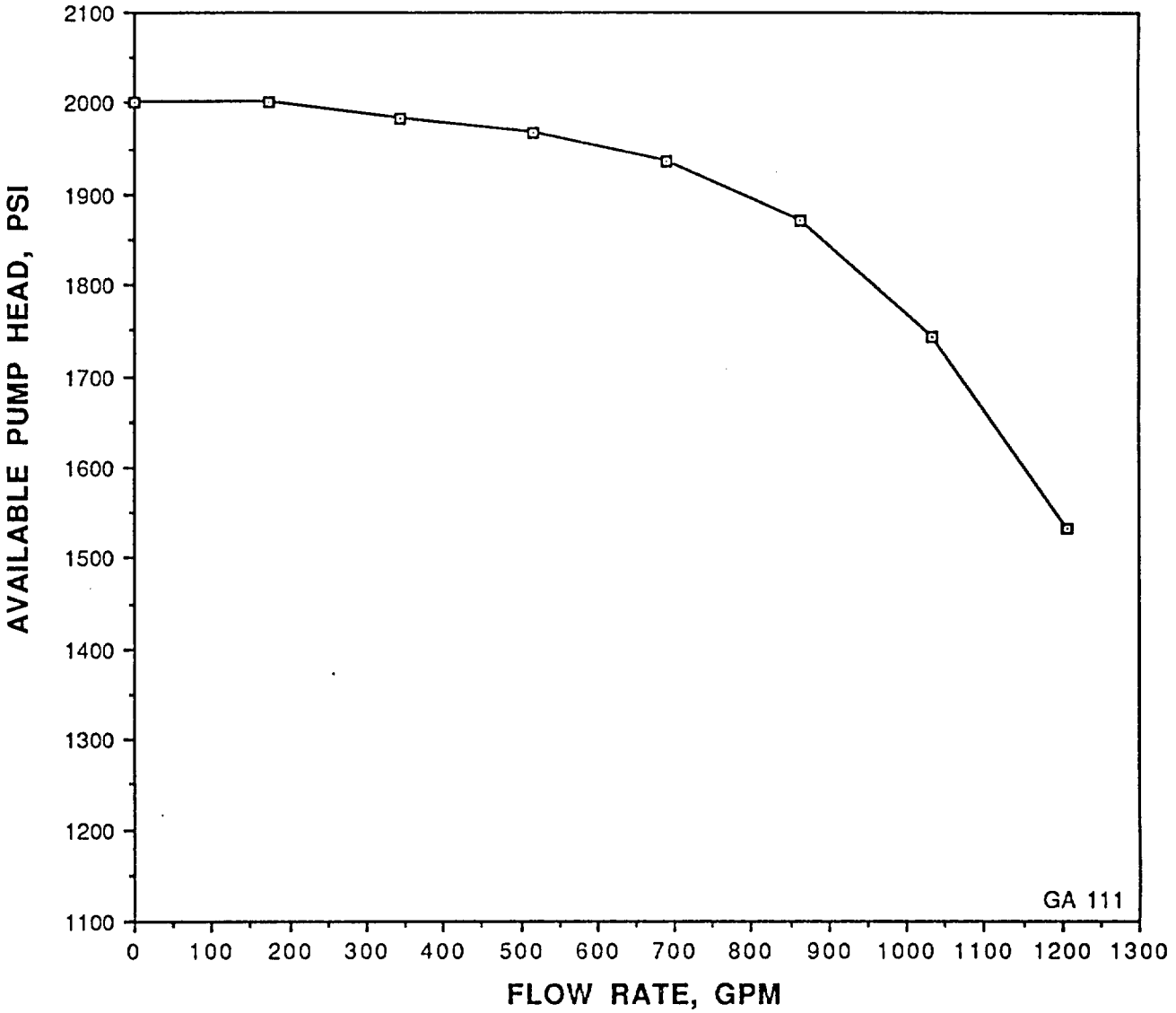

Figure B.2

Estimated Pump Performance Curve Used in

Gate Valve Pressure Drop Calculations

B.2. PRESSURE DROP ACROSS GATE VALVE IN PUMP FLOW SYSTEM

Pressure drop across a gate valve in a pump driven flow system was computed using an example case for 4-inch flexible gate valve tested at Duke Power Company's flow loop (see Footnote 1 on page 15 of main text).

In a pump driven flow system, the overall piping system pressure drop should equal the available pump head in a steady flow condition. Therefore, the system pressure drop can be expressed as:

$$\Delta P_{pump} = \Delta P_{system} = K_{total}\,\rho\,\frac{V^2}{2}$$

where ΔP_{pump} = available pump head at a specific flow rate, psi

ΔP_{system} = total system pressure drop at a specific flow rate, psi

K_{total} = total system flow resistance coefficient

= $K_{valve} + K_{others}$

K_{valve} = valve flow resistance coefficient

K_{other} = other components' flow resistance coefficient

$\cong$ 518 (estimated from Duke Power flow loop data)

Based on a given pump flow characteristics curve, as shown in Figure B.2, the pressure drop across a gate can be estimated as:

$$\Delta P_{pipe} = \Delta P_{system} = (K_{valve} + 518)\,\rho\,\frac{V^2}{2}$$

where K_{valve} and ρ are known for a given gate position and fluid. Using a numerical iterative solution approach, the system flow rate and pressure drop across the gate valve can be calculated. Iterative solutions may be started with a low estimated value of flow rate for the piping system to calculate the system pressure drop. If the system pressure drop is lower than the available pump head given in Figure B.2 for the same system flow rate, then the estimated flow rate should be increased to match the available pump pressure head. This process is repeated until the pump head and system pressure drop are equal. Table B.2 summarizes the results for the 4-inch Borg Warner valve tested in Duke Power flow loop, using the above described procedure.

Gate Position, L/D_o	*System Flow Rate, gpm*	*Gate Valve Pressure Drop,psi*
0	0	2,000
0.1	778	487
0.15	843	258
0.2	870	145
0.3	890	49
0.4	895	25.6
0.5	899	11.5
0.6	900	7.1
0.7	900	4.8
0.8	900	2.7
0.9	901	1.3
1.0	901	0.4

Table B.2
Estimated Flow Induced Pressure Drop Across a 4-Inch Gate Valve at Different Valve Openings

B.3. PRESSURE LOAD ON DISC

A simple and maybe conservative way of estimating the pressure load on a gate disc is by assuming that the pressure load on the gate is proportional to the pressure drop across the valve and the percentage of gate closing as:

$$F_p = \Delta P \left(\frac{100 \text{ - } \% \text{ of gate opening}}{100} \right) \times A_{disc}$$

where F_p = pressure load on gate in mid-travel position, lbs

ΔP = pressure drop across the valve, psi

A_{disc} = disc area

$= \frac{\pi}{4} \times$ (disc sealing dia)^2

Using a nominal disc sealing diameter of four inches, the pressure loads at different valve opening positions are summarized in Table B.3. These loads can be used to calculate localized contact stresses between the disc and guide or disc and seat to determine the potential for galling damage (as shown in Appendix C).

Percent of Gate Opening, %	*Pressure Drop Across Gate, psi*	*Pressure Load lb*
0	2,000	25,133
10	487	5,508
15	258	2,756
20	145	1,458
30	49	431
40	25.6	193
50	11.5	72
60	7.1	36
70	4.8	18
80	2.7	7
90	1.3	2
100	0.4	0

Table B.3

Estimated Flow InducedLoad on a 4-Inch Gate at Different Valve Openings

Appendix C
Analysis of Local Contact Stresses

Appendix C
Analysis of Local Contact Stresses

Contact stresses between two surfaces can be estimated using closed-form linear elastic solution for single, well-defined geometries such as spherical, elliptical, cylindrical, and plane surfaces. In this section, two contact stress cases are investigated using Hertz contact stress equation for point and line contacts. The contact loads used in the analysis are the estimated pressure loads caused by disc tilting as shown in Appendix B, and Section 2.6. The results of contact stress analysis are compared with material threshold of galling stresses for the study of disc tilting effect in mid-travel position in Section 3.4. It should be pointed out that this contact stress analysis is based on linear elastic, small displacement assumptions using original (unworn) geometry of contact.

Contact stresses based on these simplifying assumptions should be used as an *index of contact stress severity* and used as design guides for comparison against actual test data or to make design improvements.

Hertz equations for contact stress distribution

The intensity of *contact* stress, p, over the surface of contact between two *general curved surfaces* can be calculated from the following equation derived by Hertz [38]:

$$p = p_o \sqrt{1 - \frac{x^2}{a^2} - \frac{y^2}{b^2}} \qquad (C.1)$$

where p = contact stress at a selected location (x, y)
p_o = peak contact stress, psi
x = X axis coordinate, in
y = Y axis coordinate, in
a = major semiaxis, in
b = minor semiaxis, in

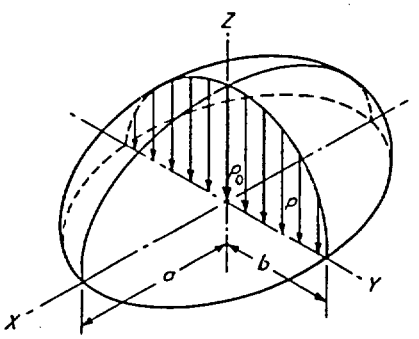

Figure C.1: Contact stress distribution between two general curved surfaces [38[

$$P = \frac{2\pi a b p_o}{3} \qquad (C.2)$$

where P = total load, lb
$\pi a b$ = contact area (ellipse), in^2

$$a = m\sqrt[3]{\frac{3P\Delta}{4A}} \tag{C.3}$$

$$b = n\sqrt[3]{\frac{3P\Delta}{4A}} \tag{C.4}$$

where $$\Delta = \frac{1-\nu_1^2}{E_1} + \frac{1-\nu_2^2}{E_2} \tag{C.5}$$

$$A = \frac{1}{2}\left(\frac{1}{R_1} + \frac{1}{R_1'} + \frac{1}{R_2} + \frac{1}{R_2'}\right) \tag{C.6}$$

$$B = \frac{1}{2}\left[\left(\frac{1}{R_1} - \frac{1}{R_1'}\right)^2 + \left(\frac{1}{R_2} - \frac{1}{R_2'}\right)^2 + 2\left(\frac{1}{R_1} - \frac{1}{R_1'}\right)\left(\frac{1}{R_2} - \frac{1}{R_2'}\right)\cos 2\Psi\right]^{1/2} \tag{C.7}$$

$$m = f\left(\cos^{-1}(B/A)\right) \qquad \text{(see Table C.4 below)} \tag{C.8}$$

$$n = f'\left(\cos^{-1}(B/A)\right) \qquad \text{(see Table C.4 below)} \tag{C.9}$$

Also, ν, E, R, and R' denote Poisson's ratio, Young's modulus, and minimum and maximum radii of curvature of the unloaded contact surfaces. Subscripts 1 and 2 denote contacting bodies 1 and 2. ψ is the angle between the planes containing curvatures $1/R_1$ and $1/R_2$.

cos-1 (B/A)	*30°*	*35°*	*40°*	*45°*	*50°*	*55°*	*60°*
m	2.731	2.397	2.136	1.926	1.754	1.611	1.486
n	0.493	0.530	0.567	0.604	0.641	0.678	0.717

cos-1 (B/A)	*65°*	*70°*	*75°*	*80°*	*85°*	*90°*
m	1.378	1.284	1.202	1.128	1.061	1.000
n	0.759	0.802	0.846	0.893	0.944	1.000

Table C.4
Values of *m* and *n* for Hertz Equations [38]

Example 1: Point Contact Between Disc and Downstream Seat

This example simulates a tilted gate contacting the edge of the seat inside diameter with two point contact, as shown in Figure C.2.

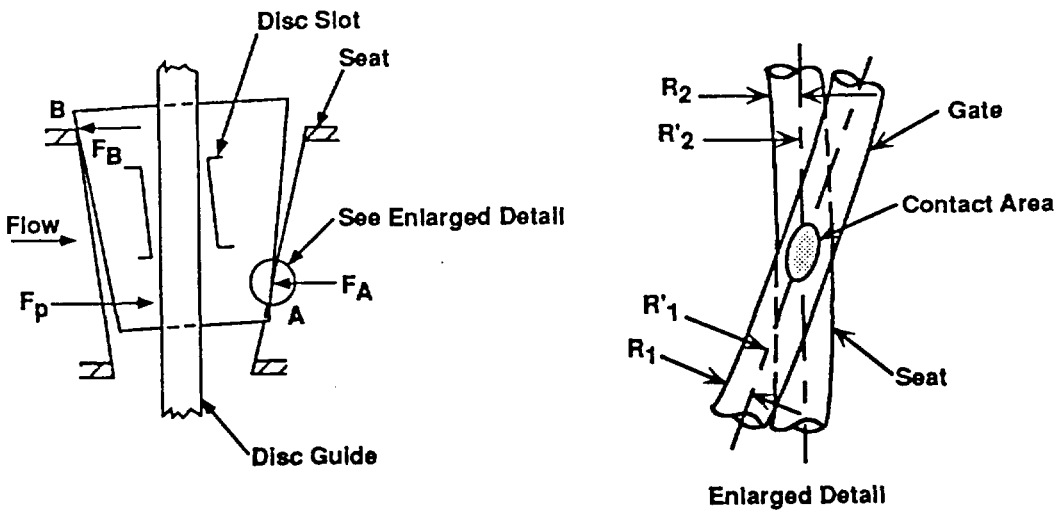

Figure C.2
Tilted Disc Contacting Seat

The following data case was used for contact stress calculations:

$R_1 = R_2 = 0.125$ in.

$R_1' = 2$ in., $R_2' = -2$ in. (concave)

$P = \frac{431}{2} = 215.5$ lb (from Appendix B @ 30% opening)

$E_1 = E_2 = 30 \times 10^6$ psi

$\nu_1 = \nu_2 = 0.3$

The actual angle, ψ, between the curved surfaces present at the radiused edge of the disc outside diameter and the radiused edge of the seat inside diameter with the gate in the tilted position is somewhat difficult to calculate. However, it can be seen from Equation C.7 that, for values of ψ between 0° and 15° (or 2ψ = 0° to 30°), the magnitude of B does not significantly change. Therefore, ψ = 15° is used in the following calculations.

Applying the Hertz equation, we have

$$\Delta = 2 \times \frac{1 - 0.09}{30 \times 10^6} = 6.067 \times 10^{-8}$$

$$A = \frac{1}{2}\left(\frac{2}{0.125} + \frac{2}{2}\right) = 8$$

$$B = \frac{1}{2}\left[(8 - 0.5)^2 + (8 - 0.5)^2 + 2(8 - 0.5)^2 + \cos 30°\right]^{1/2} = 7.728$$

$$\cos^{-1}(B/A) = 15°$$

$m = 4.2$ *(extrapolated from Table C.4)*

$n = 0.39$ *(extrapolated from Table C.4)*

$$a = 4.2\sqrt[3]{\frac{3 \times 215.5 \times 6.067 \times 10^{-8}}{4 \times 8}} = 0.04495 \text{ inch}$$

$$b = 0.39\sqrt[3]{\frac{3 \times 215.5 \times 6.067 \times 10^{-8}}{4 \times 8}} = 0.004174 \text{ inch}$$

$$p_o = \frac{3 \times 215.5}{2\pi \times 0.04495 \times 0.04174} = 548{,}411 \text{ psi} \quad \leftarrow$$

$$p_{ave} = \frac{p_o}{1.5} = 365{,}608 \text{ psi} \quad \leftarrow$$

The estimated local contact stress at the downstream disc-to-seat point contact is almost one order of magnitude higher than the Stellite material threshold of galling stress of 47 ksi as discussed in Section 3.4, based on linear elastic, small displacement, and original unworn geometry assumptions elastic stress analysis. The calculated results a and b, which are .045 inch and .0042 inch respectively, are the dimensions of the elliptical contact at the seat to disc interface under load at 30 percent mid-travel disc position. Local yielding, load redistribution, and material wear are likely to occur before the contact stress actually reaches this level.

Example 2: Line Contact Between Disc and Guide

In some gate valve designs, line contact between the disc guide and disc guide slot resists the flow-induced load imposed on the disc during mid-travel. This example presents an estimate of contact stresses based on the following design and material data assumptions:

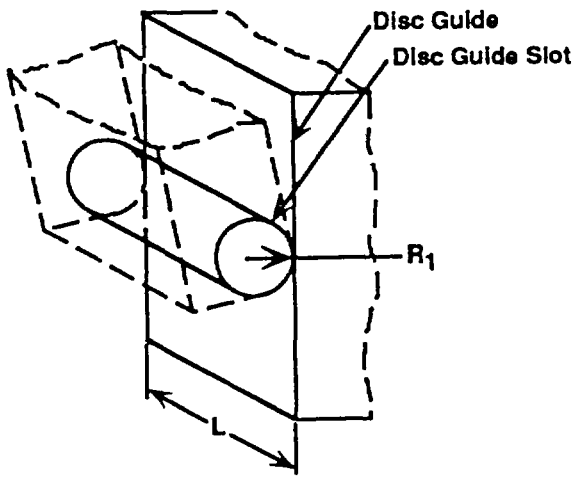

$R_1 = 0.1875$ in.

$R_2 = R_1' = R_2' = \infty$

$L = 0.375$ (contact width) in.

$\psi = 0$

$P = \frac{431}{2} = 215.5$ lbs

$E_1 = E_2 = 30 \times 10^6$ psi

$\nu_1 = \nu_2 = 0.3$

Figure C.3
Math Model for
Line Contact between Disc and Guide

Applying the Hertz equations for parallel cylinders ([38], p. 374):

$$\Delta = 6.067 \times 10^{-8}$$

$$b = 1.13\sqrt{\frac{P\Delta}{L\left(\frac{1}{R_1}+\frac{1}{R_2}\right)}} = 1.13\sqrt{\frac{215.5 \times 6.067 \times 10^{-8}}{0.375\left(\frac{1}{0.1875}\right)}} = 0.002889 \text{ in.}$$

$$p_o = \frac{2P}{\pi L b} = \frac{2 \times 215.5}{\pi \times 0.375 \times 0.002889} = 126{,}633 \text{ psi} \quad \leftarrow$$

$$p_{ave} = \frac{P}{2Lb} = 99{,}458 \text{ psi} \quad \leftarrow$$

This estimated contact stress with line contact between the disc guide slot and the guide surface is an order of magnitude lower than in the case of disc making a point contact against the downstream seat. Also, it is in the same order of magnitude as the material threshold of galling stress for Stellite. As mentioned at the beginning of this appendix, the contact stresses based on simplifying assumptions used in the analysis can be used as an *index of contact stress severity*. Comparisons against actual tests under controlled conditions should be used to obtain an empirical correlation between these theoretical values and actual performance.

Appendix D
Analysis of Stem Thrust Overshoot for 4-Inch Borg-Warner Valve Tested at Duke Power Flow Loop

Appendix D

Analysis of Stem Thrust Overshoot for 4-Inch Borg-Warner Valve Tested at Duke Power Flow Loop

This appendix documents the analysis performed for stem thrust overshoot estimation using the energy balance method described in Section 4 of the main report. The actuator and valve data selected for the calculations are Rotork 16NAX1, 57 rpm actuator and Borg-Warner 4-inch flex wedge gate valve used in Duke Power Company's flow loop tests. The analysis results compare well with the actual test data, as shown in this appendix.

D.1. AVAILABLE ENERGY AT TORQUE SWITCH TRIP

D.1.1. Motor Work After Torque Switch Trip

Motor work for Rotork 16NAX1 actuator is estimated as

$$W_1 = \omega T \, \Delta\tau$$

ω = motor speed = 3,600 rpm x 0.9 = 3,240 rpm

T = motor torque = 8 ft-lb = 96 in-lb

$\Delta\tau$ = contactor dropout delay = 10 ms = 0.01 sec

$$\therefore \quad W_1 = 3{,}240 \times \frac{2\pi}{60} \times 96 \times 0.01 = 326 \text{ in - lb}$$

D.1.2. Kinetic Energy of Moving Components

1. *Rotor*

Based on the estimated rotor dimensions shown in Figure D.1, the rotor kinetic energy is:

$$KE_1 = \frac{1}{2}\left(3{,}600 \times \frac{2\pi}{60}\right)^2 \times \frac{1}{4}\left(\frac{8.3}{386.4} \times 1.55^2 + \frac{2.46}{386.4} \times 0.533^2\right)$$

$$= 1{,}911 \text{ in - lb}$$

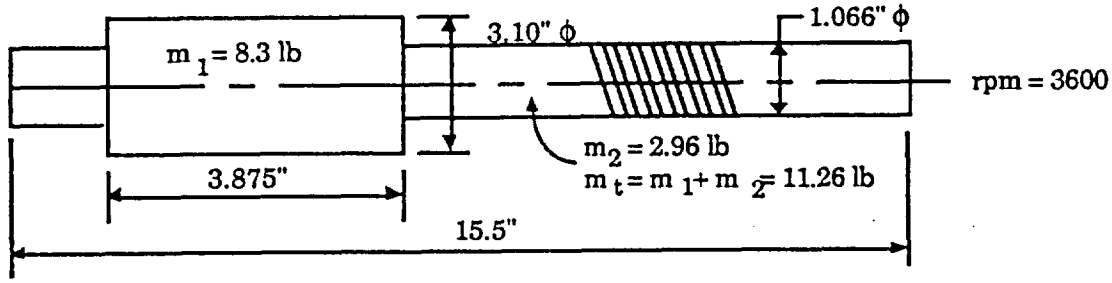

Figure D.1

Worm Shaft Weight and Dimensions

2. *Worm gear/stem nut assembly*

Based on the estimated dimensions shown in Figure D.2, the kinetic energy for the assembly is:

$$KE_2 = \left(\frac{57}{60} \times 2\pi\right)^2 \times \frac{1}{4}\left(\frac{1.2}{386.4} \times 1.75^2 + \frac{5.7}{386.4} \times 1.25^2\right)$$

$$= 0.29 \text{ in - lb} \quad \leftarrow \text{ small}$$

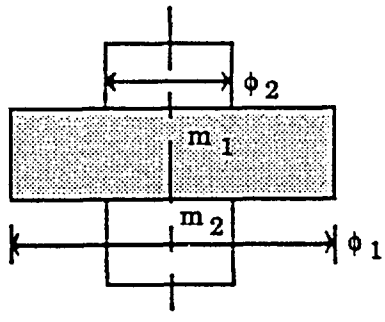

Estimated Weight & Dimensions:

$\phi_1 = 3.5\ \phi$

$\phi_2 = 2.5\ \phi$

$m_1 = 1.2$ lb

$m_2 = 5.7$ lb

rpm = 57

Figure D.2

Worm Gear/Stem Nut Assembly Weight and Dimensions

3. *Valve stem and gate assembly*

The estimated valve stem and gate dimensions and weight are:

Stem Dimensions	=	32" x 1.375"ϕ
Stem Weight	=	$32 \times 1.375^2 \times 0.7854 \times 0.283 = 13.45$ lbs
Gate Dimensions	=	2.7" thk x 4.5" ϕ
Gate Weight	=	$0.7854 \times 4.5^2 \times 2.7 \times 0.283 = 12.2$ lbs

The estimated valve closing speed is 0.5 in/sec. Therefore, the kinetic energy for the stem and gate assembly is:

$$KE_3 = \frac{1}{2}\left(\frac{13.45 + 12.2}{386.4}\right) \times 0.5^2$$

$$= 0.0083 \text{ in - lbs} \quad \leftarrow \text{ very small}$$

D.2. STORED ENERGY IN VALVE COMPONENTS AFTER TORQUE SWITCH TRIP

Theoretically, all of the load transmitting components store some strain energy. For this example case, only the three members (stem, disc, and spring pack) that have significant strain energy stored during valve closing are considered here.

D.2.1. Stem

The stored stem energy under axial load is:

$$SE_1 = \frac{L}{2EA}\left(F_f^2 - F_t^2\right)$$

for

F_t = 17,615 lbs thrust at TST

L = 32 in.

E = 30×10^6 psi

d = 1.375 in.

$$SE_1 = 3.5917 \times 10^{-7}\left(F_f^2 - 310.288 \times 10^6\right)$$

The stored energy in torsion is:

$$SE_2 = \frac{L}{2GJ}\left(T_f^2 - T_t^2\right)$$

for $G = 1.15 \times 10^7$ psi

$$J = \frac{\pi}{32}(1.375)^4 = 0.3509 \text{ in}^4$$

T_t = 200 ft-lbs = 2,400 in-lbs

$$SE_2 = 3.965 \times 10^{-6}\left(T_f^2 - 2{,}400^2\right)$$

$$= 3.965 \times 10^{-6}\left[\left(\frac{2{,}400}{17{,}615}\right)^2 F_f^2 - 2{,}400^2\right]$$

D.2.2. Disc

The stiffness of the Borg-Warner flex wedge disc may be estimated using the following simplified mathematical model.

Assume the gate (one side) is a circular disc with the outer diameter uniformly loaded and the central circular area fixed or free as the two extremes.

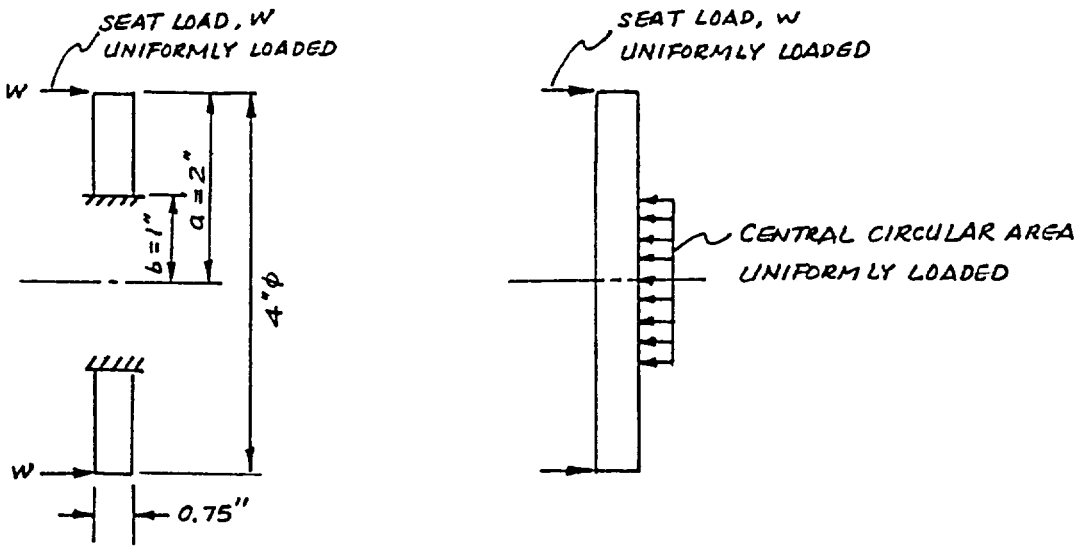

Model 1 Model 2

Figure D.3
Simplified Math Models for Gate Disc Flexibility Calculations

Based on the above disc dimensions, disc stiffness is estimated using closed-form equations as given in Reference [37], pages 338 and 366:

K_1 = 2.0525 x 10^6 lb/in (Model 1)

K_2 = 1.434 x 10^6 lb/in (Model 2)

The lower stiffness of 1.43×10^6 lb/in is selected for the stem thrust overshoot calculations. More precise gate stiffness may be obtained through the finite element analysis or testing.

The stored energy in the gate is:

$$SE_2 = 2 \times \frac{\left(F_f'^2 - F_t'^2\right)}{2K_2}$$

$$= \frac{F_f'^2 - F_t'^2}{K_2}$$

where $F_f' = \frac{F_f - (F_1 + F_2 + F_3)}{2(\sin\theta + \mu\cos\theta)}$ = final gate lateral load due to wedging

$$= \frac{F_f - 3,935}{0.92146}$$

$F_t' = \frac{F_t - (F_1 + F_2 + F_3)}{2(\sin\theta + \mu\cos\theta)}$ = gate lateral load at TST

$$= \frac{17,615 - (891 + 2,970 + 9,819)}{2(\sin 5° + 0.375\cos 5°)}$$

$$= 14,846 \text{ lbs}$$

$$\therefore \quad SE_3 = \frac{1}{1.434 \times 10^6}\left[(1.0852\,F_f - 4,270)^2 - 14,846^2\right]$$

D.2.3. Spring Pack

The stored energy in the spring pack after torque switch trip is:

$$SE_4 = \frac{1}{2K_s}\left(S_f^2 - S_t^2\right)$$

where K_s = spring pack stiffness, lb/in

S_f = final spring pack load, lb

S_t = spring pack load at TST, lb

The estimated spring pack stiffness and load at torque switch trip are:

K_s = 6,000 lb/in

S_f = 600 lbs

$$\therefore \quad SE_4 = \frac{1}{12,000}\left[\left(\frac{600}{17,615}F_f\right)^2 - 600^2\right]$$

D.3. ENERGY DISSIPATED IN VALVE COMPONENTS

The energy dissipated in valve components after torque switch trip is estimated as follows:

D.3.1. Stem Packing Frictional Loss

$$L_1 = F_1 \Delta d$$

where

$$F_1 = \frac{\mu K \rho (\pi d \ell)}{2}$$

$$= \frac{0.1 \times 1.5 \times 2{,}000 (\pi \times 1.375 \times 1.375)}{2}$$

$$= 891 \text{ lbs}$$

$$\Delta d = \frac{F_f - F_t}{2K \sin\theta (\sin\theta + \mu \cos\theta)}$$

$$= \frac{F_f - 17{,}615}{2 \times 1.434 \times 10^6 \sin 5° (\sin 5° + 0.375 \cos 5°)}$$

$$\therefore \quad L_1 = 7.737 \times 10^{-3} (F_f - 17{,}615)$$

D.3.2. Work Against Stem Rejection Force

$$L_2 = F_2 \Delta d$$

where

$$F_2 \frac{\pi}{4} d^2 p = \frac{\pi}{4} \times 1.375^2 \times 2{,}000 = 2{,}970 \text{ lbs}$$

$$\therefore \quad L_2 = 2{,}970 \times 8.683 \times 10^{-6} (F_f - 17{,}615)$$

$$= 0.01875 (F_f - 17{,}615)$$

D.3.3. Frictional Loss Due to Disc Friction Under ΔP

$$L_3 = F_3 \Delta d$$

where

$$F_3 = \frac{\frac{\pi}{4} D^2}{\cos\theta} p \left(\frac{\mu}{\cos\theta - \mu \sin\theta} \right)$$

$$= \frac{\frac{\pi}{4} \times 4^2}{\cos 5°} \times 2{,}000 \times \left(\frac{0.375}{\cos 5° - 0.375 \sin 5°} \right)$$

$$= 8{,}919 \text{ lbs}$$

$$\therefore \quad L_3 = 8{,}919 \times 8.683 \times 10^{-6} (F_f - 17{,}615)$$

$$= 8.5258 \times 10^{-2} (F_f - 17{,}615)$$

D.3.4. Frictional Loss Due to Disc Wedging

$$L_4 = F_4 \, \Delta d$$

where $$F_4 = \frac{1}{2}(F_f + F_t) - (F_1 + F_2 + F_3)$$

$$= \frac{1}{2}(F_f + 17{,}615) - (891 + 2{,}970 + 9{,}819)$$

$$= 0.5\, F_f - 4{,}873$$

$$\therefore \quad L_4 = (0.5\, F_f - 4{,}873) \times 8.683 \times 10^{-6} (F_f - 17{,}615)$$

D.3.5. Efficiency of Worm/Worm Gear

$$e_1 = \frac{\cos \theta_n - \mu \tan \lambda}{\cos \theta_n + \mu \cot \lambda}$$

Using the following design data:

$$\theta_n = 14.5°$$

$$\mu = 0.08$$

$$\lambda = 4°$$

$$\therefore \quad e_1 = \frac{\cos 14.5° - 0.08 \tan 4°}{\cos 14.5° + 0.08 \cot 4°} = 46\%$$

Therefore, rotor kinetic energy and motor work are reduced to 46 percent of the original magnitudes when they pass through the worm/worm gear connection.

D.3.6. Efficiency of Stem/Stem Nut

$$e_2 = \frac{\cos \theta_n - \mu \tan \lambda}{\cos \theta_n + \mu \cot \lambda}$$

For the stem design of:

$$\theta_n = 14.5°$$

$$\mu = 0.08$$

$$\lambda = \tan^{-1} \frac{\ell}{\pi dm} = \tan^{-1} \frac{0.5}{\pi \times 1.28} = 7.088°$$

$$\therefore \quad e_2 = \frac{\cos 14.5° - 0.08 \tan 7.088°}{\cos 14.5° + 0.08 \cot 7.088°} = 59\%$$

D.4. ENERGY BALANCE AND FINAL THRUST PREDICTION

The overall energy balance for the example problem can be summarized as:

$$\left[(W_1 + KE_1 - SE_4)\, e_1 + KE_2\right] e_2 + KE_3 = SE_1 + SE_2 + SE_3 + L_1 + L_2 + L_3 + L_4$$

Solving the above equation, we have

$$F_f = 20{,}535 \text{ lbs}$$

The calculated stored energy and losses in the valve and actuator components are:

SE_1 = 40 in-lb
SE_2 = 8 in-lb
SE_3 = 73 in-lb
SE_4 = 10 in-lb
L_1 = 23 in-lb
L_2 = 75 in-lb
L_3 = 249 in-lb
L_4 = 137 in-lb

The calculated final stem thrust of 20,535 pounds is in good agreement with the measured stem thrust of 20,963 pounds. Thrust predictions were compared for 31 test cycles, and the average deviation was found to be within 9 percent.

Appendix E
Analysis of Piping Load Effect on Opening Thrust

Appendix E

Analysis of Piping Load Effect on Opening Thrust

The piping load effect on opening stem thrust is illustrated using a through-conduit 18 x 16 x 18 parallel expanding gate valve as an example. This type of valve design has a relatively stiff gate assembly, similar to *solid* wedge gate valves which tend to be particularly sensitive to gate pinching under external pipe loads. Moreover, valve bodies tend to be less stiff in larger sizes, which accentuates the gate pinching problem in larger valves. Calculations are also performed for *flexible* wedge gate design to show the relative improvement. Even though bending moment in the plane of the valve stem and flow axis has the worst potential for affecting the valve performance from the standpoint of gate pinching, the example shown here addresses the effect of axial compressive load only to keep the illustrations simple.

Body Stiffness

As discussed in Section 4, the magnitude of gate *pinching* can be estimated through the valve body and gate stiffness calculations. For this 18 inch valve example case, the valve body stiffness along the flow axis is known through a detailed 3-D finite element analysis as documented in a report[1] by Kalsi Engineering to W-K-M.

$$Kb = 5.757 \times 10^7 \text{ lb/in}$$

The overall valve assembly stiffness can be expressed by a simple math model as shown in Figure E.1.

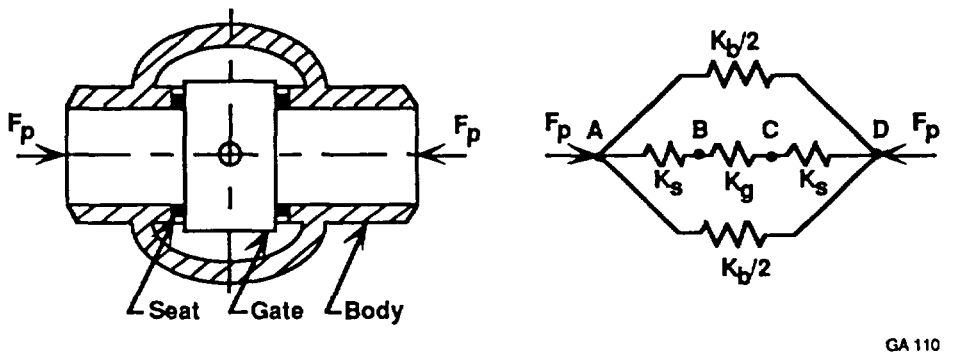

Valve Section Plot Simplified Valve Stiffness Math Model

Figure E.1
Simplified Math Model for Gate Valve Stiffness

---

1 J. K. Wang and M. S. Kalsi. *Finite Element Analysis of the 18" x 16" x 18" ANSI 900 Feedwater Isolation Valve Under Faulted Condition Nozzle Loads*, Kalsi Engineering, Inc. proprietary report to W-K-M, KEI 8.4.3, February 23, 1981.

The valve body stiffness obtained from the 3-D finite element analysis represents the valve body stiffness without the seat and gate in place. The overall valve stiffness for a gate valve at the closed position can be estimated based on the combined stiffness of body, seat, and gate as shown in the following calculations.

Gate Stiffness

The gate type is a parallel expanding gate valve (Figure 2.1B). When this gate assembly is wedged closed, all of the space between the seat faces is taken up by two relatively stiff pieces of wedges, in the same fashion as in a conventional solid wedge design. Stiffness for the two-piece expandable gate assembly can be estimated by using equivalent stiffness of a pipe section with two assumed pipe thicknesses. More precise estimation would require detailed finite element analysis or actual testing.

Case 1.

Gate Stiffness approximated by a pipe thickness equal to the seat contact width:

$$K_g = \frac{AE}{\ell}$$

$$= \frac{\frac{\pi}{4}\left(17^2 - 14.625^2\right) \times 30 \times 10^6}{10.25}$$

$$= 1.727 \times 10^8 \text{ lb/in}$$

Case 2.

Gate stiffness approximated by a pipe of thickness equal to twice the seat contact width:

$$K'_g = \frac{AE}{\ell}$$

$$= 2 \times 1.727 \times 10^8$$

$$= 3.453 \times 10^8 \text{ lb/in}$$

Seat Stiffness

Seat stiffness is also estimated using the dimensional data from KEI 8.4.3 (referenced in Footnote 1 on page E.1), which can be approximated as an equivalent pipe section:

$$K_s = \frac{AE}{\ell}$$

$$= \frac{\frac{\pi}{4}\left(17^2 - 14.625^2\right) \times 30 \times 10^6}{\frac{1}{2}(19.5 - 14.625)}$$

$$= 7.26 \times 10^8 \text{ lb/in}$$

Combined Stiffness of Gate and Seats

Overall stiffness through the gate and seats is:

$$\frac{1}{K_{gs}} = \frac{1}{K_s} + \frac{1}{K_g} + \frac{1}{K_s}$$

$$= \frac{2}{7.26 \times 10^8} + \frac{1}{1.727 \times 10^8}$$

$$K_{gs} = 1.17 \times 10^8 \text{ lb/in}$$

$$\frac{1}{K'_{gs}} = \frac{1}{K_s} + \frac{1}{K'_g} + \frac{1}{K_s}$$

$$= \frac{2}{7.26 \times 10^8} + \frac{1}{3.453 \times 10^8}$$

$$K'_{gs} = 1.77 \times 10^8 \text{ lb/in}$$

Valve Stiffness

The overall valve stiffness is the sum of body stiffness and combined disc/seat stiffness:

$$K_{total} = K_b + K_{gs}$$

$$= 1.746 \times 10^8 \text{ lb/in (using Case 1 gate stiffness)}$$

$$K_{total} = K_b + K'_{gs}$$

$$= 2.346 \times 10^8 \text{ lb/in (using Case 2 gate stiffness)}$$

Gate Pinching Force

Force through the gate assembly under a compressive external piping load can be expressed as:

$$F_{gs} = \frac{K_{gs}}{K_{total}} F_p$$

where F_{gs} = force through gate assembly, lb

F_p = external piping load, lb

Based on this estimated gate and valve stiffness, the gate pinching force is:

$$F_{gs} = \frac{117}{174.6} F_p$$

$= 0.67\ F_p$ for Case 1 gate stiffness, and

$$F'_{gs} = \frac{177}{234.6} F_p$$

$= 0.754\ F_p$ for Case 2 gate stiffness

The above estimate shows that 67 to 75 percent of the compressive external pipe load passes through the gate assembly. This increases the gate/seat contact load, thus resulting in higher stem thrust requirement. The amount of stem thrust increase depends directly on the magnitude of the compressive external piping load. The following assumed piping load and valve differential pressure are used in illustrating the external piping load effect on stem thrust increase.

Assuming that for this 18 inch gate valve:

Compressive external pipe = 100,000 lb (approximately 23 percent of the maximum estimated axial pipe load under transient pipe rupture condition (reference Footnote 1 on page E.3). This corresponds to approximately 2,200 psi axial compressive stress in the piping connected to the valve end.)

Maximum differential pressure = 1,250 psi

Then the gate pinching force is:

$F_{gs} = 0.67 \times 100{,}000 = 67{,}000$ lb for Case 1, and

$F'_{gs} = 0.765 \times 100{,}000 = 75{,}400$ lb for Case 2.

Gate/seat contact force due to maximum differential pressure is:

$$F_{\Delta P} = \frac{\pi}{4}(15)^2 \times 1,250 = 212,058 \text{ lbs}$$

Therefore, the stem thrust increase due to external pipe load can be expressed as a percentage of the required stem thrust to overcome the gate drag due to differential pressure load as:

$$R = \frac{F_{gs}}{F_{\Delta P}} = 31.6\% \qquad \leftarrow$$

$$R' = \frac{F'_{gs}}{F_{\Delta P}} = 35.6\% \qquad \leftarrow$$

Reduction in Gate Pinching Effect by Flexible Wedge Gate

The above example used a parallel expanding gate valve with high disc stiffness. Many gate valve designs employ flexible gate concept to reduce disc pinching effect under external pipe loads. The following calculations show the effect of gate flexibility on the stem thrust by replacing the parallel expanding disc with a flexible disc having the following assumed dimensions shown in the math model:

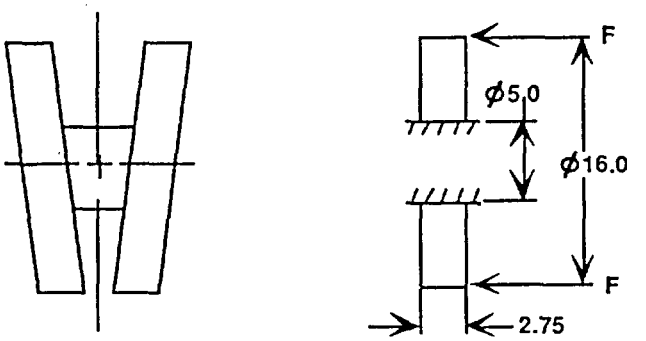

Flexible Gate Math Model for 1/2 Flexible Gate GA 112

Figure E.2
Flexible Gate Math Model

The gate assembly stiffness can be estimated using a closed-form solution as given in Reference 37, page 338:

$$K_g = 2.127 \times 10^7 \text{ lb/in}$$

Using the same approach as given in the parallel expanding gate case, we have

$$K_{gs} = 2.1146 \times 10^7 \text{ lb/in}$$

Note that the stiffness magnitude of the flexible disc and seat assembly is less than 1/8th the stiffness (1.77×10^8 lb/in) of the relatively stiff gate assembly used in the first example.

$$K_{total} = 7.8716 \times 10^7 \text{ lb/in}$$

$$F_{gs} = 0.2686\, F_p$$

$$= 26{,}860 \text{ lbs (for 100,000 lbs of external pipe load)}$$

$$R = \frac{26{,}860}{212{,}058}$$

$$= 12.7\%$$

Therefore, the stem thrust increase is approximately 12.7 percent of the required stem thrust to overcome disc drag under differential pressure load, instead of 31.6 to 35.6 percent stem thrust increase calculated for the high stiffness parallel expanding disc case.

Appendix F
Analysis of Temperature Effect on Opening Thrust

Appendix F

Analysis of Temperature Effect on Opening Thrust

This appendix provides the derivation of the seat contact force equation used in Section 5 discussions and an example case of the temperature effect on operating thrust. This example is based on a root cause analysis performed by Kalsi Engineering, Inc. The main purpose of the example is to show how to quantify various contributing factors that effect the opening stem thrust due to temperature changes.

F.1. EFFECT OF TEMPERATURE CHANGES ON SEAT CONTACT FORCE

As shown in the following simplified math model, the valve body and gate expansions (or contractions) due to temperature changes can be estimated as:

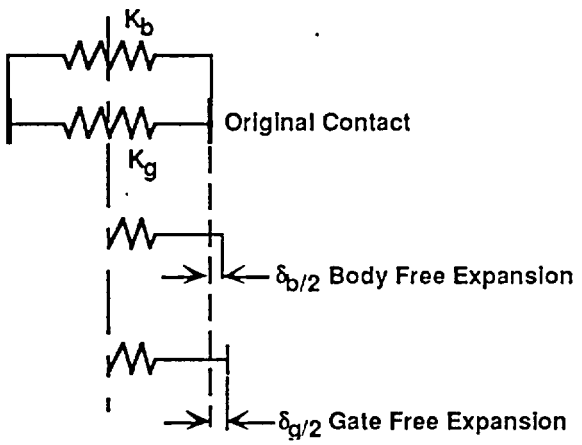

Figure F.1
Math Model for Body and Seat Stiffness

$$\delta_b = L_O \alpha_b \Delta T \quad \text{(F.1)}$$

$$\delta_g = L_O \alpha_g \Delta T \quad \text{(F.2)}$$

where δ_b = body expansion, in

δ_g = gate expansion, in

L_O = distance between seat faces, in.

α_b = thermal expansion coefficient for valve body, in/in/°F

α_g = thermal expansion coefficient for gate, in/in/°F

ΔT = temperature change, °F

Therefore, the net difference in valve body and gate expansion is:

$$\Delta\delta = \delta_g - \delta_b \text{ (positive for interference)}$$

$$= L_O \Delta T (\alpha_g - \alpha_b) \quad \text{(F.3)}$$

The differences in body and gate expansion will generate a seat contact force if $\Delta\delta$ is positive. Its magnitude can be calculated using the following relationships:

Valve body and gate deformations under seat contact force are:

$$\Delta\delta_b = \frac{\Delta F}{K_b}$$

$$\Delta\delta_g = \frac{\Delta F}{K_g}$$

where $\Delta\delta_b$ = valve body deformation under a seat contact force of ΔF, in.

$\Delta\delta_g$ = gate deformation under a seat contact force of ΔF, in.

ΔF = seat contact force, lb

K_b = valve body stiffness, lb/in

K_g = Gate assembly stiffness, lb/in (including seat stiffness)

$$\Delta\delta = \left(\delta_g - \delta_b\right) = \frac{\Delta F}{K_b} + \frac{\Delta F}{K_g} = \Delta F\left(\frac{K_b + K_g}{K_b K_g}\right)$$

Therefore,

$$\Delta F = \left(\delta_g - \delta_b\right)\left(\frac{K_b K_g}{K_b + K_g}\right)$$

$$= L_O \Delta T \left(\delta_g - \delta_b\right)\left(\frac{K_b K_g}{K_b + K_g}\right) \quad \leftarrow \qquad \text{(F.4)}$$

F.2. EFFECT OF STEM GROWTH

For a wedge gate valve, the average stem temperature before closing may be lower than the valve body temperature. After the valve is closed, the seat contact force may be increased by either of two possible conditions:

F.2.1. *Increasing stem temperature.*

If the valve temperature remains the same after closing, then the stem growth may be estimated as:

$$\delta_s = \ell_s \alpha_s \Delta T_s \qquad \text{(F.5)}$$

where δ_s = stem growth, in.

ℓ_s = the stem length which is subject to an average stem temperature change of ΔT_s after the valve is closed,in.

α_s = stem thermal expansion coefficient, in/in°F

ΔT_s = average stem temperature change, °F

F.2.2. ***Decreasing both stem and body temperature.***

If both the valve and stem temperatures decrease after closing and the valve body contraction is greater than the stem contraction, then the seat contact force may be increased due to this differential body and stem contraction. The relative stem *growth* may be estimated as:

$$\delta_s = \ell_b \alpha_b \Delta T_b - \ell_s \alpha_s \Delta T_s \qquad \text{(F.6)}$$

where ℓ_b = body length with average temperature change of ΔT_b, in.
α_b = body thermal expansion coefficient, in/in/°F
ΔT_b = average body temperature change, °F
ℓ_s = stem length with average temperature change of ΔT_s, in.
α_s = stem thermal expansion coefficient, in/in/°F
ΔT_s = average stem temperature change, °F

The calculated stem growth, δ_s, can be converted into disc lateral interference as

$$\delta_g = \delta_s \sin\theta \qquad \text{(F.7)}$$

where δ_g = disc lateral interference (one side) due to stem growth, in.
θ = one-half of the disc wedge angle, deg

It should be noted that the above equation does not include stem or valve topworks flexibility in the stem growth calculations. If the stem and valve flexibilities are considered, only a fraction of the stem growth due to differential valve component expansion/contraction will be converted into disc lateral interference. Net stem growth that can be converted into disc lateral interference, including the structural flexibility, may be expressed as:

$$\delta'_s = \delta_s - \delta_{sk}$$

where δ'_s = net stem growth including structural flexibility, in.
δ_s = stem growth excluding structural flexibility, in.
δ_{sk} = structural deformation (stem and body) due to stem compression, in.

F.3. EXAMPLE CASE

To illustrate the temperature effect on valve operating thrust, a simplified case from one of our root cause analysis investigations is used in the following calculations.

L_1 = 1.84 in. (gate width)

L_2 = 1.25 in. (seat length, one side)

ℓ_{s1} = stem length outside valve body = 21 in.

ℓ_{s2} = stem length inside valve body = 3.375 in.

$\alpha_b = 8.9 \times 10^{-6}$ in/in/°F (SA-182)

$\alpha_g = 9.7 \times 10^{-6}$ in/in/°F (SA-351)

$\alpha_s = 6 \times 10^{-6}$ in/in/°F (SA-564-630)

$K_b = 71 \times 10^6$ lb/in

$K'_g = 19 \times 10^6$ lb/in (gate stiffness only)

$K_{seat} = 78 \times 10^6$ lb/in

$\Delta T_b = 650 - 70 = 580°F$

$\Delta T_g = 635 - 70 = 565°F$

$\Delta T_{s1} = 175 - 70 = 105°F$ (outside valve body)

$\Delta T_{s2} = 450 - 70 = 380°F$ (inside valve body)

F.3.1 Combined Gate and Seat Contraction

Using the dimensions and coefficients of thermal expansion for the gate and the two seats, we can calculate the combined thermal contraction from Equation F.2:

$$\delta_g = 1.84 \times 9.7 \times 10^6 \times (635 - 70) + 2 \times 1.25 \times 9.7 \times 10^{-6} \times (650 - 70)$$
$$= 0.02415 \text{ in.}$$

F.3.2 Body Contraction

$$\delta_b = (1.84 + 2 \times 1.25) \times (650 - 70) \times 8.9 \times 10^{-6}$$
$$= 0.0224 \text{ in.}$$

F.3.3 Net Gate Expansion

$$\Delta\delta = 0.0224 - 0.02415 = -0.00175 \text{ in.}$$

Since, in this example case,the net expansion of the gate and the over the body dimensional changes is negative, no seat contact load is generated due to differential thermal contraction between valve body and gate alone.

F.3.4 Net Stem Growth

Using equation (F.6):

$$\begin{aligned}\delta_S \equiv\ & [21 \times 8.9 \times 10^{-6} \times (175 - 70) + 3.375 \times 8.9 \times 10^{-6} \times (650 - 70)] \\ & + [21 \times 6.0 \times 10^{-6} (175 - 70) + 3.375 \times 6.0 \times 10^{-6} \times (450 - 70)] \\ =\ & 0.02093 - 0.03705 = 0.01612 \text{ in.}\end{aligned}$$

To account for the net gate width contraction from F.3.3 and F.3.4, the net stem growth is

$$\delta_s = 0.01612 - \frac{0.00175}{2} \times \frac{1}{\tan 5^\circ} = 0.00612 \text{ in.}$$

F.3.5 Stem and Valve Topworks Stiffness

$$K = \frac{AE}{L}$$

where

$$A = \frac{\pi}{4} d^2 = \frac{\pi}{4} \times 1.125^2 \text{ in}^2$$

$$E = 30 \times 10^6, \text{ psi}$$

L ≈ equivalent length (including estimated valve topworks flexibility) ≈ 30 in.

$$\therefore \quad K = 9.94 \times 10^5 \text{ lb/in}$$

Based on the above estimated stem stiffness, the adjusted net stem growth using the result in F.3.4 and equation (F.8), is

$$\delta_s' = 0.00612 - \frac{F_s}{K}$$

where F_S = stem force = 2 ΔF (sin θ + μ cos θ) (see Appendix A, Section A.1.3)

ΔF = seat contact force

For a typical wedge angle of 5° and an estimated value of μ of 0.4, the above equation gives

$$F_S = 2 (\sin 5^\circ + 0.4 \cos 5^\circ) \Delta F = 0.97 \Delta F$$

Therefore, the adjusted net stem growth is

$$\delta_s' = 0.00612 - \frac{0.97\,\Delta F}{9.94 \times 10^5} = 0.00612 - 9.76 \times 10^{-7}\,\Delta F$$

From this, the equivalent disc lateral interference caused by the adjusted net stem growth can be calculated using equation (F.7) and is

$$\Delta\delta = 2\,\delta_s' \sin\alpha = 2 \times \left(0.00612 - 9.76 \times 10^{-7}\,\Delta F\right) \times \sin 5°$$

F.3.6 Seat Contact Force

Using the same approach as in Appendix E, the combined gate and seat stiffness is

$$\frac{1}{K_g} = \frac{1}{K_g'} + \frac{2}{K_{seat}} = \frac{1}{19 \times 10^6} + \frac{2}{78 \times 10^6} = 7.83 \times 10^{-8}$$

$$\therefore \quad K_g = 12.8 \times 10^6 \text{ lb/in}$$

The seat contact force, using the equation (F.4) derived in Section F.1, is

$$\Delta F = 0.1743\left(0.00612 - 9.76 \times 10^{-7}\,\Delta F\right)\left(\frac{71 \times 10^6 \times 12.8 \times 10^6}{71 \times 10^6 + 12.8 \times 10^6}\right)$$

$$= 11{,}553 - 1.842\,\Delta F$$

$$\therefore \quad \Delta F = 4{,}065 \text{ lbs}$$

$$\therefore \quad F_s = 0.97 \times \Delta F = 3{,}943 \text{ lb} \quad \leftarrow$$

This can be compared to the disc friction load of 6,505 lbs which is based on a coefficient of friction of 0.4 and a pressure of 2,100 psi across a mean seat diameter of 2.85 inches. The seat force increase of 3,943 lbs represents 61% of this disc friction load.

It should be pointed out that, the estimated stem thrust is very sensitive to the temperature and stiffnesses of the valve components. The estimated thrust can vary significantly based on a specific valve temperature profile and the actual stiffness of the flexible wedge. The main purpose of this appendix was to show how to quantify the effect of temperature changes on the opening thrust.

NRC FORM 335 (2-89) NRCM 1102, 3201, 3202

U.S. NUCLEAR REGULATORY COMMISSION

BIBLIOGRAPHIC DATA SHEET

(See instructions on the reverse)

1. REPORT NUMBER (Assigned by NRC, Add Vol., Supp., Rev., and Addendum Numbers, If any.)
NUREG/CR-5807
KEI 1721

2. TITLE AND SUBTITLE
Improvements in Motor Operated Gate Valve Design and Prediction Models for Nuclear Power Plant Systems

SBIR Phase I Final Report
September 1990–April 1991

3. DATE REPORT PUBLISHED
MONTH: May
YEAR: 1992

4. FIN OR GRANT NUMBER
L1667

5. AUTHOR(S)
J.K. Wang, M.S. Kalsi

6. TYPE OF REPORT
Technical

7. PERIOD COVERED *(Inclusive Dates)*

8. PERFORMING ORGANIZATION – NAME AND ADDRESS *(If NRC, provide Division, Office or Region, U.S. Nuclear Regulatory Commission, and mailing address; if contractor, provide name and mailing address.)*
Kalsi Engineering, Inc.
745 Park Two Drive
Sugar Land, TX 77478

9. SPONSORING ORGANIZATION – NAME AND ADDRESS *(If NRC, type "Same as above"; if contractor, provide NRC Division, Office or Region, U.S. Nuclear Regulatory Commission, and mailing address.)*
Division of Engineering
Office of Nuclear Regulatory Research
U. S. Nuclear Regulatory Commission
Washington, DC 20555

10. SUPPLEMENTARY NOTES

11. ABSTRACT *(200 words or less)*

This research is aimed at improving the performance of gate valves at nuclear power plants (1) by developing improved models for operability prediction and (2) by identifying improvements that overcome problems/limitations of the current designs. Phase I research is aimed at developing improved operating thrust models for the most common types of gate valves in use at U.S. nuclear power plants. Instrumented valve test data provided by Duke Power Company will be used to develop/compare the analytical predictions. Specifically, Phase I research will address shortcomings in the current techniques by investigating localized contact stresses under disc tilting caused by fluid flow, by predicting inertial thrust overshoot, and by providing a comprehensive review of friction/galling data for gate valves.

12. KEY WORDS/DESCRIPTORS *(List words or phrases that will assist researchers in locating the report.)*
gate valves
prediction models
valve test data
friction/galling data

13. AVAILABILITY STATEMENT
unlimited

14. SECURITY CLASSIFICATION
(This Page)
unclassified
(This Report)
unclassified

15. NUMBER OF PAGES

16. PRICE

THIS DOCUMENT WAS PRINTED USING RECYCLED PAPER

UNITED STATES
NUCLEAR REGULATORY COMMISSION
WASHINGTON, D.C. 20555-0001

OFFICIAL BUSINESS
PENALTY FOR PRIVATE USE, $300

SPECIAL FOURTH-CLASS RATE
POSTAGE AND FEES PAID
USNRC
PERMIT NO. G-67